

FEASIBILITY OF REMOTE NUCLEAR REACTOR ANTINEUTRINO
DIRECTIONALITY VIA ELASTIC ELECTRON SCATTERING IN THE
WATER CHERENKOV MONITOR OF ANTINEUTRINOS (WATCHMAN)

A Thesis

by

DANIEL HELLFELD

Submitted to the Office of Graduate and Professional Studies of
Texas A&M University
in partial fulfillment of the requirements for the degree of
MASTER OF SCIENCE

Chair of Committee, Craig Marianno
Committee Members, William Charlton
Robert Webb
Head of Department, Yassin Hassan

May 2015

Major Subject: Nuclear Engineering

Copyright 2015 Daniel Hellfeld

ABSTRACT

Cubic meter sized liquid scintillator detectors have demonstrated that the operational status, power level, and changes in fuel composition of a critical nuclear reactor system can be remotely measured with the antineutrino signal. With the success of these detectors, research has been pursued in the scaling of the detector size to increase sensitivity and standoff distance. One such detector is the WATER CHerenkov Monitor of ANTineutrinos (WATCHMAN). WATCHMAN is a kiloton-scale gadolinium-doped water Cherenkov detector, surrounded by approximately 4300 30.48 cm (12 inch) photomultiplier tubes (PMTs). The detector will utilize the inverse beta decay (IBD) interaction to measure the antineutrino rate and energy spectrum approximately 13 km away from a 3.758 GW(th) nuclear reactor. WATCHMAN will be the first to demonstrate the potential of gadolinium-doped water Cherenkov detectors for future nuclear reactor monitoring and safeguards applications.

While IBD will enable WATCHMAN to measure the antineutrino rate and energy spectrum, the detector will not be sensitive enough to extract the direction of the incident antineutrinos from this process. Antineutrino directionality would be useful if multiple reactors are located near the detector, or if it is used to search for and locate clandestine reactors. This research investigated the potential of an alternative interaction, elastic antineutrino-electron scattering, to determine the direction of the incident antineutrino flux in WATCHMAN. Calculations were done to determine the expected scattering rate and Monte Carlo simulations were performed with GEANT4 to model detector response. Event reconstruction software was then used to reconstruct the directions of the scattered electrons based on the triggered

PMT times, locations, and charge intensities. Estimated background rates were incorporated into the scattering signal by scaling reported measurements from similar detectors. Many potential sources of background were considered, including solar neutrinos and misidentified IBD interactions, gamma rays from the PMTs, detector walls, and surrounding rock, as well as the decays of cosmogenic radionuclides and water-borne radon. Preliminary results indicate that while most of the sources of background can be adequately controlled with strict detector component cleanliness and low radioactivity PMTs, radon levels consistent with other existing detectors are likely to exceed the acceptable limit for directional sensitivity in WATCHMAN.

ACKNOWLEDGEMENTS

I would first like to acknowledge my advisor, Dr. Craig Marianno, for all his support throughout this work. Although the project was not aligned with his research interests, he stood behind the project at all times, allowing me to pursue my own interests. I would also like to thank Dr. Adam Bernstein of Lawrence Livermore National Laboratory (LLNL), for without him I would not have had the opportunity to take part in this project. Also to Dr. Steven Dazeley of LLNL, for his consistent help with this research and for assisting me towards my decision to pursue a doctorate degree after the completion of my master's degree. Acknowledgments are also due to my committee members, Dr. William Charlton and Dr. Robert Webb.

I would like to thank my parents for supporting me throughout my academic career and specifically my father for giving me the drive to pursue graduate education. Also to my beautiful fiancé, Kalie, for your unconditional love and support.

This material is based upon work supported by the Department of Energy National Nuclear Security Administration under Award Number: DE-NA0000979 through the Nuclear Science and Security Consortium.

This report was prepared as an account of work sponsored by an agency of the United States Government. Neither the United States Government nor any agency thereof, nor any of their employees, makes any warranty, express or limited, or assumes any legal liability or responsibility for the accuracy, completeness, or usefulness of any information, apparatus, product, or process disclosed, or represents that its use would not infringe privately owned rights. Reference herein to any specific commercial product, process, or service by trade name, trademark, manufacturer, or otherwise does not necessarily constitute or imply its endorsement, recommendation,

or favoring by the United States Government or any agency thereof. The views and opinions of authors expressed herein do not necessarily state or reflect those of the United States Government or any agency thereof.

NOMENCLATURE

IAEA	International Atomic Energy Agency
INFCIRC	Information Circular
NPT	Nuclear Nonproliferation Treaty
WATCHMAN	WATER CHerenkov Monitor of ANtineutrinos
wt%	Percent by Weight
PMTs	Photomultiplier Tubes
IBD	Inverse Beta Decay
Gd	Gadolinium
MeV	Megaelectron Volt
m.w.e.	Meters of Water Equivalent
m	Meters
km	Kilometers
GW(th)	Gigawatt Thermal
RMSim	Reactor Monitoring Simulation
BONSAI	Branching Optimization Navigating Successive Annealing Iterations
VVER	Water-Water Energetic Reactor (Russian)
PWR	Pressurized Water Reactor
SONGS	San Onofre Nuclear Generating Station
kg	Kilogram
U	Uranium
KamLAND	Kamioka Liquid scintillator AntiNeutrino Detector
MW(th)	Megawatt Thermal

Super-K	Super Kamiokande
$\bar{\nu}_e$	Electron Antineutrino
E	Energy
Pu	Plutonium
Am	Americium
IsoDAR	Isotope Decay At Rest
Be	Beryllium
Li	Lithium
NSIs	NonStandard Interactions
e^-	Electron
n	Neutron
p	Proton
e^+	Positron
barn	10^{-24} cm ²
H	Hydrogen
C	Carbon
μ s	Microseconds
NC	Neutral Current
CC	Charged Current
ES	Electron Scattering
s	Second
Tl	Thallium
K	Potassium
Rn	Radon
FLUKA	FLUktuierende KAskade (German)

N	Nitrogen
B	Boron
γ	Gamma
μ	Muon
α	Alpha Particle
π	Pion
Hz	Hertz (s^{-1})
yr	Year
PDF	Probability Density Function
GEANT4	Geometry and Tracking
RMS	Root Mean Square
QQ	Quantile-Quantile
SNO	Sudbury Neutrino Observatory
ETL	Electron Tubes Limited
D ₂ O	Heavy Water
Bq	Becquerel ($\text{decays} \cdot s^{-1}$)

TABLE OF CONTENTS

	Page
ABSTRACT	ii
ACKNOWLEDGEMENTS	iv
NOMENCLATURE	vi
TABLE OF CONTENTS	ix
LIST OF FIGURES	xi
LIST OF TABLES	xv
1. INTRODUCTION	1
1.1 The International Atomic Energy Agency and Nuclear Reactor Safe- guards	1
1.2 Remote Monitoring	2
1.3 Antineutrino Detection	2
1.4 WATCHMAN	3
1.5 Antineutrino Directionality	5
1.6 Research Objective	7
2. PREVIOUS WORK	10
2.1 Near Field Detectors	10
2.2 Kiloton Scale and Directionality	12
2.3 Reactor Antineutrino Energy Spectrum	14
2.4 Physics Experiments	20
3. THEORY	22
3.1 Antineutrinos	22
3.2 Detection Methods	23
3.2.1 Inverse Beta Decay	24
3.2.2 Elastic Electron Scattering	26
3.3 Directionality	29
3.4 Event Reconstruction	34

	Page
4. BACKGROUNDS	36
4.1 Inverse Beta Decay Backgrounds	36
4.2 Electron Scattering Backgrounds	37
4.2.1 WATCHMAN Estimation	38
5. CALCULATIONS AND SIMULATIONS	45
5.1 Expected Number of Events	45
5.2 Event Generator	47
5.2.1 Comparison to IsoDAR	52
5.3 Monte Carlo Simulations	53
5.3.1 Event Reconstruction with BONSAI	56
5.3.2 Reactor Antineutrino-Electron Scattering	62
6. RESULTS AND DISCUSSION	65
6.1 One-Year Directional Reconstruction	65
6.1.1 Analysis and Statistical Significance Calculations	66
6.2 Multiple One-Year Directional Reconstruction	72
6.3 Directional Reconstruction for Various Acquisition Times	74
6.4 PMT and Radon Backgrounds	77
7. SUMMARY AND CONCLUSIONS	83
REFERENCES	86
APPENDIX A. EXPECTED EVENTS CALCULATION IN ROOT	92
APPENDIX B. EVENT GENERATOR IN ROOT	97
APPENDIX C. SIGNAL/BACKGROUND FITTING IN ROOT	108
APPENDIX D. MULTIPLE YEAR FITTING IN ROOT	113

LIST OF FIGURES

FIGURE	Page
1	Proposed design of WATCHMAN. Note the person in the left hand corner for scale [16]. 5
2	Cut away diagram of the SONGS antineutrino detector [19]. 11
3	Demonstration of the antineutrino rate measurement to determine the operational status of a nuclear reactor [20]. 12
4	Plot of the antineutrino rate measurement to determine the isotopic evolution of the fuel [20]. 12
5	Antineutrino energy spectrum from fissions occurring in ^{235}U , ^{239}Pu , ^{238}U , and ^{241}Pu . The black line represents a summation of the four isotopes with typical fission percentages of 49.6% ^{235}U , 35.1% ^{239}Pu , 8.7% ^{238}U , and 6.6% ^{241}Pu 15
6	Antineutrino energy spectrum below 1 MeV for the fission of ^{235}U [26]. 17
7	Comparison of the extension of Eq. (1) to the values calculated in Table 2. 18
8	Reactor antineutrino energy spectrum from fissions occurring in ^{235}U , ^{239}Pu , ^{238}U , and ^{241}Pu using Eq. (1) extended to 0 MeV. 18
9	Plot of the expected antineutrino spectrum from IsoDAR as well as the expected measured spectrum (incident flux folded with the total scattering cross section) [29]. 21
10	Schematic of the IsoDAR antineutrino generator. The red dots represent antineutrino production points within the ^7Li sleeve [29]. 21
11	Tree level Feynman diagrams of charged current (CC) and neutral current (NC) antineutrino-electron scattering [17]. 27
12	Plot of the inverse beta decay (IBD) and electron scattering (ES) cross-sections as function of the incident antineutrino energy. IBD possesses an energy threshold of 1.8 MeV. 27

FIGURE	Page
13 Inverse beta decay (IBD) and electron scattering (ES) cross-sections as function of the incident antineutrino energy folded with the reactor antineutrino energy spectrum.	28
14 Plot of the differential cross-section for antineutrino-electron scattering for several antineutrino energies.	30
15 Plot of the differential cross-section for antineutrino-electron scattering as a function of the cosine of the scattering angle for several incident antineutrino energies.	32
16 Cosine of the scattering angle with respect to the Sun for the directionality experiment at the Super-K detector [24].	34
17 Picture demonstrating the Cherenkov cone imparting a ring shape on an antineutrino detector [34].	35
18 Plot of the number of photoelectrons produced for each simulated source of background in WATCHMAN over one year [16].	43
19 Diagram of antineutrino-electron elastic scattering.	48
20 Diagram of antineutrinos travelling in the $+Z$ direction, such that electron scattering angle corresponds to the polar angle.	49
21 Plot of the sampled antineutrino energies from the event generator.	50
22 (a) Plot of the sampled scattered electron kinetic energies. (b) Plot of the cosine of the scattering angles.	51
23 Plot of the sampled antineutrino energy distribution from the IsoDAR spectrum using the IsoDAR generator (black) and the generator created for the WATCHMAN detector (blue). The distribution represents the antineutrinos that interacted (the energy spectrum folded with the scattering cross-section).	52
24 Plot of (a) the scattering angle distribution and (b) the electron energy distribution from the IsoDAR spectrum using the IsoDAR generator (black) and the generator created for the WATCHMAN detector (blue). Notice the 3 MeV threshold in the electron energy distribution.	53
25 (a) Plot of the starting positions for electrons evenly distributed throughout the detector volume. (b) Plot of the initial electron directions where the points represent unit vectors from the origin.	55

FIGURE	Page
26 (a) Histogram of the total photoelectrons produced per event. (b) Histogram of total number of PMTs hit per event.	56
27 Visualization of an electron scattering event in WATCHMAN using RMSim. The blue lines represent Cherenkov light and the yellow, orange, and red dots correspond to the hit PMT times.	56
28 Plots of the differences between the reconstructed and true x , y , and z vertex coordinates in cm (shown in (a), (c), and (e)). Plots of the reconstructed vs. true x , y , and z vertex coordinates in cm (shown in (b), (d), and (f)).	58
29 Plot of the directional reconstructions (cosine of the polar angle) from BONSAI (shown in blue) compared to the true directions (shown in red).	59
30 Plot of the reconstructed cosine of the scattering angle for electrons generated uniformly within the detector volume all travelling in the $+Z$ direction.	60
31 Plot of the photoelectron production for electrons at various energies.	61
32 Plot of the 1 MeV electron directional reconstructions before (a) and after (b) the trigger mechanism is applied. Although the trigger discards 96% of the events, the directional reconstruction improves. . . .	62
33 Plot of the directional reconstruction for reactor antineutrino-electron scattering in WATCHMAN for one year with (a) and without (b) a 65 photoelectron cut.	65
34 Total signal (background plus scattering) in the WATCHMAN detector over one year.	66
35 Plot of the total one-year scattering signal with background and fits included.	68
36 Plot of the signal significance as a function of the left integral bound used in Eq. (19).	69
37 Plot of directional reconstructions assuming a calibration source at WATCHMAN.	71

FIGURE	Page
38 Distributions of the signal significances for 64 one-year simulations calculated by with (a) and without (b) calibration.	73
39 QQ plots for the 64 signal significances with (a) and without (b) calibration.	73
40 Distributions of the signal significances for (a) six-month acquisitions, (b) two-year acquisitions, and (c) three-year acquisitions.	75
41 Plot of the signal significances as a function of the acquisition time. The blue and green lines represent the typical 3σ and 5σ detection thresholds.	76
42 Plot of the distance from the reconstructed event vertex to the nearest PMT.	78

LIST OF TABLES

TABLE	Page	
1	Parameter values for Eq. (1). The values reported for ^{235}U , ^{239}Pu , and ^{241}Pu are for thermal neutrons and the value for ^{238}U is for 0.5 MeV neutrons [26].	15
2	Calculated antineutrino fluxes for energies below 2 MeV [26].	16
3	De-excitation energies associated with neutron captures in antineutrino detectors [33].	25
4	Cosmogenic radionuclide yields generated from a Super-K FLUKA simulation [37].	39
5	Estimated background contributions to the WATCHMAN detector for one year.	42
6	Signal significances for various acquisition times with and without the use of calibration.	77
7	Total estimated background levels for two different fiducial volumes and two different PMTs for a 5 year run time including the 82% live-time. For each PMT, the backgrounds are estimated assuming both the single exponential function (denoted by Low) as well as the double exponential distribution (denoted by High).	80
8	Average antineutrino-electron scattering signal significances for various fiducial volume sizes and PMT types for a 5 year acquisition time. As in Table 7, each PMT was given a low and high background estimate.	80

1. INTRODUCTION

1.1 The International Atomic Energy Agency and Nuclear Reactor Safeguards

The International Atomic Energy Agency (IAEA) has set forth a safeguards regime to monitor the activities of nuclear reactors since the deployment of Information Circular 26 (INFCIRC/26) in 1961 and the updated INFCIRC/66 in 1965 [1,2]. With the introduction of the Nuclear Nonproliferation Treaty (NPT), INFCIRC/153, and INFCIRC/540 in 1970, 1972, and 1991, respectively, the IAEA has focused its core objectives to the timely detection of the diversion of significant quantities of nuclear material from peaceful nuclear activities to the manufacture of nuclear weapons or of other nuclear explosive devices or for purposes unknown, and the deterrence of such diversion by the risk of early detection [3,4,5]. To accomplish this task, the IAEA has implemented safeguards techniques such as item and bulk nuclear material accountancy, containment, and surveillance in a variety of reactors spread across the world [6]. The current safeguards regime has been largely successful in carrying out its objectives, but several problems still exist. For example, accountancy techniques such as serial number checking of fresh and spent fuel assemblies as well as isotopic verification via radiation detection are performed onsite, requiring IAEA inspectors to have access to certain areas within the reactor facility. However, in order to protect trade secrets, facilities in the past have been reluctant to grant complete access to inspectors [7,8,9]. Performing accountancy measures onsite also means that IAEA inspectors must physically travel to these reactors every month, every three months, or every year according to the timeliness detection goals of the facility [6]. With over 185 countries party to the NPT and over 380 nuclear reactors under safeguards agreements, these inspections can require sizable effort and manpower to conduct

[10,11]. Moreover, to determine if diversion has occurred, techniques such as isotopic verification require information from the reactor that inspectors are unable to measure directly, such as the power level history of the core [12]. This requires the facility to declare all pertinent activities as well as truthfully declare all information needed by the IAEA. Finally, containment and surveillance equipment such as seals, locks, motion detectors, and video cameras are used to ensure continuity of knowledge and to deter diversions between inspection periods [6]. However, these techniques can only inform the IAEA that suspect behavior may have occurred, requiring inspectors to travel to the site to take samples and measurements in order to confirm suspicions.

1.2 Remote Monitoring

To resolve the issues involved with IAEA safeguards, remote unattended monitoring systems have been developed to take measurements at facilities without having an inspector physically present, to take measurements in areas where inspectors do not have access, and to make measurements of parameters that would otherwise need to be declared by the facility. Such equipment includes integrated fuel flow monitors, core discharge monitors, and reactor power monitors [13]. Due to the appeal of remote monitoring systems, research has been conducted in several fields in order to produce new and innovative equipment that can be used to remotely monitor nuclear reactors. One such piece of new equipment is an antineutrino detector.

1.3 Antineutrino Detection

Antineutrinos are fundamental particles produced in the beta decays that occur inside of all critical nuclear reactor systems. Antineutrinos possess small interaction cross-sections, for example the inverse beta decay (antineutrino collides with a proton to produce a positron and neutron) cross-section is on the order of 10^{-43} cm².

Therefore, antineutrinos are essentially unaffected by any amount of reactor containment or shielding [14]. Thus antineutrinos emitted directly from the reactor core can be measured outside of containment, up to tens or even hundreds of kilometers away from the reactor. The antineutrino flux and energy spectrum can also provide information such as the operational status of the reactor, the power output of the core, and the isotopic evolution of the fissile material in the fuel [14,15]. Since antineutrinos can be measured remotely and can provide key information on the activities inside the reactor containment vessel, antineutrino detectors have the potential to be a significant complement to the current safeguards regime. Due to the unique and sometimes costly detection methods however, antineutrino detectors have been widely overlooked as a safeguards tool. But in recent years, significant work has been done in the fields of neutrino and antineutrino detection, specifically with respect to nuclear reactor safeguards, demonstrating that antineutrino detectors can serve as a functional tool in future IAEA safeguards [14].

1.4 WATCHMAN

The WATER Cherenkov Monitor of ANTineutrinos (WATCHMAN) is a new water Cherenkov antineutrino detector currently being proposed. Collaborators on the project include staff and faculty from Lawrence Livermore National Laboratory, Sandia National Laboratory, University of California, Berkeley, University of California, Davis, University of California, Irvine, University of Hawaii, and Virginia Tech University. WATCHMAN is a kiloton-scale detector filled with 0.1 wt% gadolinium-doped water and surrounded by approximately 4300 high quantum efficiency photomultiplier tubes (PMTs) [16]. The detector will measure the antineutrino rate and energy spectrum using inverse beta decay (IBD) and coincident detection methods.

Following an IBD interaction, the emitted positron will produce a Cherenkov

light cone that will be detected by the PMTs. The emitted neutron will thermalize and capture on a ^{157}Gd nucleus, resulting in a detectable ~ 8 MeV gamma ray cascade. The coincident detection of the positron and neutron in both space and time will constitute an antineutrino signal in WATCHMAN. Because the detector is very large, it will be buried deep below the Earth's surface to reduce background events induced by cosmic rays (backgrounds will be discussed further in Section 4). The detector is proposed to be placed in the 1500 meters of water equivalent (m.w.e) deep Morton salt mine in Fairport, OH, approximately 13 km away from a single-core 3.758 GW(th) boiling light water reactor in Perry, OH [16]. WATCHMAN aims to be the first kiloton-scale water Cherenkov detector to demonstrate mid- to far-field (> 10 km) remote reactor monitoring for nuclear safeguards purposes [16].

The WATCHMAN detector is a large cylindrical stainless steel tank, designed to fit in the allocated space within the Morton salt mine (24.4 m by 18.3 m by 23.8 m) [16]. The diameter and height of the cylinder are 15.8 m with a total water volume of 3.54 kilotons. The detector will be divided into two regions by a cylindrical PMT support structure 12.8 m in diameter [16]. The outer region will serve as a veto region and the inner region as the target region. There will be 1.81 kilotons of Gd-doped water in the target region and 1.73 kilotons of Gd-doped water in the veto region. In the PMT support structure, there will be 4328 30.48 cm high quantum efficiency Hamamatsu PMTs facing towards the inner target region and 482 PMTs facing the outer veto region, equivalent to a PMT coverage of 40% and 4% for the target and veto regions, respectively. Within the target region, a virtual fiducial volume boundary will be defined with a diameter and height of 10.82 m (~ 1000 m³ volume) [16]. Only events arising in this volume are considered as signal. Providing a space between the PMT support structure and the fiducial volume (known as the buffer region) will allow for better reduction of backgrounds from the PMTs and ex-

ternal radiation [16]. Fig. 1 shows the design and scale of the WATCHMAN detector.

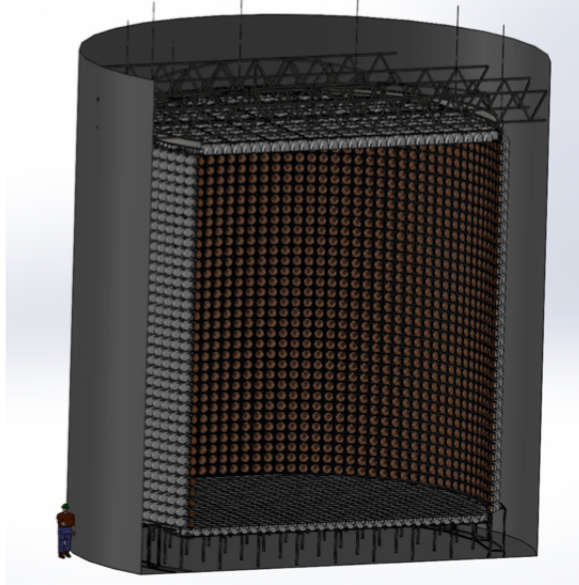


Fig. 1. Proposed design of WATCHMAN. Note the person in the left hand corner for scale [16].

1.5 Antineutrino Directionality

While IBD will allow for the monitoring of the antineutrino rate and energy spectrum from reactors in the local area, WATCHMAN will not be sensitive enough to extract the direction of the incident antineutrinos from this process (the neutron direction is highly correlated with the antineutrino direction, however it quickly diffuses and loses its original direction by the time of capture) [16]. This can thus cause problems if multiple reactors are near the detector. Without directionality, the detector would not be able to discern which reactor the antineutrinos were emerging from and would thus contribute to another source of background. Also, directional-

ity would be useful in a WATCHMAN-like detector if it were used to search for and locate clandestine nuclear reactors. Excluding terrestrial and cosmic induced backgrounds, antineutrinos are seldom produced anywhere else besides critical nuclear reactor systems. Therefore, if the detector is placed in an area where an undeclared nuclear reactor is thought to be operating, the IBD antineutrino signal can serve as physical evidence to either exclude or confirm the presence of a nearby reactor. If a reactor were thought to be operating near the detector, antineutrino directionality would be able to determine the direction in which the reactor is located.

Fortunately, in addition to IBD, antineutrinos can also participate in the directional elastic electron scattering interaction. The interaction cross-section as a function of incident antineutrino energy and the electron scattering angle reveals that the interaction is favored in the forward direction, meaning the electron is primarily scattered in the direction of the incident antineutrino [17]. The scattered electrons will possess enough energy to produce Cherenkov cones in the water in the direction of travel. Therefore, if WATCHMAN is able to detect and reconstruct the directions of the Cherenkov cones produced by the scattered electrons, it will be able to extract information about the direction of the incident antineutrinos.

Coincident detection methods cannot be used in antineutrino-electron scattering because there is only one detectable daughter product (the electron). Therefore, more background will be present. The scattering cross-section is also on the order of 10^{-45} cm², roughly two orders of magnitude smaller than the IBD cross-section, thus the primary concern is whether enough events can be detected for the detection statistics to be significant. However, when considerations such as the reactor antineutrino energy spectrum and the available interaction targets in WATCHMAN for both processes are accounted for (IBD can only occur on two out of the ten protons in each water molecule while scattering can occur on all ten of the electrons),

the total electron scattering cross-section is only approximately 5.4 times smaller than IBD. Therefore, this research aims to characterize the expected antineutrino-electron scattering signal and background in WATCHMAN in order to determine the feasibility of antineutrino directionality.

1.6 Research Objective

This project will investigate the feasibility of remote nuclear reactor antineutrino directionality using elastic antineutrino-electron scattering in the WATCHMAN detector. In order to accomplish this task, an event generator will be written in the CERN-based mathematical and data analysis C++ interpreter software, ROOT, to calculate the scattered electron energies and scattering angles resulting from antineutrino scattering interactions in WATCHMAN. Due to their small cross-sections, simulating antineutrinos in WATCHMAN would take an excessive amount of computational time. Alternatively, in this thesis, scattering cross-sections and kinematical equations will be used to calculate the electron energies and directions as if some number of antineutrino scattering interactions have already occurred. These electrons will then be used to simulate antineutrino scattering interactions in the detector. The expected number of events given over a specific period of time will be estimated with an understanding of the antineutrino flux and energies emerging from the reactor, the distance to the detector, the detector composition, and the cross-section for the scattering interaction. Once the event generator is completed, it will be compared against event generators constructed by other experiments to ensure functionality.

As a first step, this research will use the event generator to determine the electron scattering angle distribution resulting from antineutrinos emitted from a 3.758 GW(th) nuclear reactor located approximately 13 km away from the WATCHMAN

detector over the course of one year (assuming 365 effective full power days and constant fuel isotopics). Background rates will then be estimated by scaling from background measurements performed at other antineutrino and neutrino detection experiments. First, only background events due to misidentified IBD events, steel detector components, surrounding rock, ^{208}Tl in the water, solar neutrinos, and cosmogenic radionuclides will be considered. This will assume that the background events due to the PMTs and water-borne radon are insignificant.

This project will simulate the reactor antineutrinos (produced from the event generator) and background events in the C++ based Monte Carlo particle transport toolkit, GEANT4, to model the WATCHMAN detector response on the expected one-year scattering signal. An existing GEANT4 simulation package named Reactor Monitor Simulation (RMSim), maintained by the University of California, Davis, will be used. The simulation includes all relevant physics such as particle transport, Cherenkov physics, optical photon production and transport, PMT sensitivity, digitization, and timing, as well as all the current detector geometry specifications and optical properties. The simulation output will be fed into an existing event reconstruction software named BONSAI (Branching Optimization Navigating Successive Annealing Iterations), maintained by the University of California, Irvine. The software was originally developed for the Super Kamiokande neutrino experiment in Japan to reconstruct the direction of the scattered electrons based off the triggered PMT timings, locations, and charge intensities. It has since been developed to be used with WATCHMAN. A plot of the cosine of the reconstructed scattering angles, θ , will be produced with background included. Due to the forward peaked nature of electron scattering and the assumption that background will be isotropic, the signal should be visible as a peak near $\cos(\theta) = 1$ (scattering angle $\theta = 0$) above a flat background from -1 to 1. The signal and background will be fit using ROOT and a

statistical analysis will be performed to determine the signal significance. To comply with the standards of particle physics experiments, the WATCHMAN detector will be deemed capable of antineutrino directionality if the signal significance is at least 5σ . In the safeguards regime however, additional measures will be used in conjunction with WATCHMAN (such as satellite imaging and field inspections) and thus a 5σ significance may be unnecessarily high. In this thesis, the possibility of directionality with a 3σ significance will also be presented in the instance WATCHMAN is used cooperatively with other safeguards measurements.

Because of the ability to estimate the number of scattering events and background in the detector as a function of time, this research will also assess the temporal behavior of the signal significance. An analysis of WATCHMAN's directional capability as a function of time will be carried out to determine the required data acquisition time until the signal is statistically significant.

Finally, preliminary background estimates due to the PMTs and water-borne radon will be incorporated into the results. The directional sensitivity of WATCHMAN will then be reassessed. Although this research is specific to WATCHMAN, once completed, it can be applied to future directionality analyses for larger scaled detectors, larger standoff distances, varied detector depths, and smaller nuclear reactors.

2. PREVIOUS WORK

2.1 Near Field Detectors

The first detector used to monitor nuclear reactor operations via antineutrino detection was put into place at the Rovno Atomic Energy Station in Kuzentsovsk, Ukraine starting in 1982 [15]. The detector consisted of 1050 liters of gadolinium-doped organic liquid scintillator with 84 PMTs. It was placed 18 m below a Russian VVER-440 reactor loaded with low-enriched uranium. Utilizing the IBD interaction, the detector demonstrated sensitivity to both the power output and isotopic content of the core based on antineutrino rate and spectral measurements [15].

Another antineutrino detector used for remote nuclear reactor monitoring was deployed near the pressurized water reactor (PWR) at the Unit 2 San Onofre Nuclear Generating Station (SONGS) in San Onofre, California starting in 2002 [14,18,19]. The cubic meter sized detector consisted of 0.64 tons of gadolinium-doped liquid scintillator surrounded with eight PMTs and was placed approximately 25 m away from the core. Due to its shallow depth, a water and polyethylene shield as well as muon veto detectors were used to shield and discriminate background events (see Fig. 2) [14,18,19].

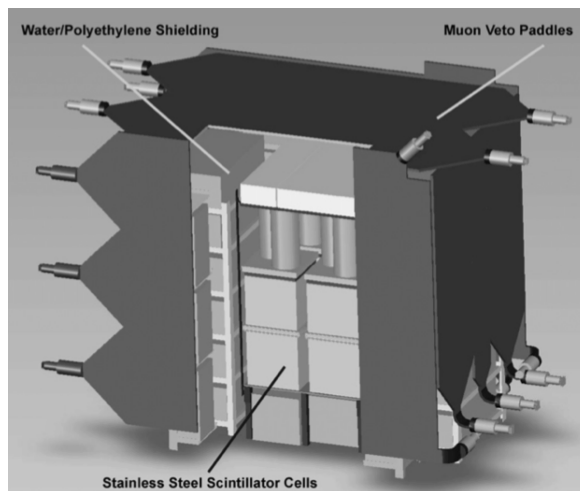


Fig. 2. Cut away diagram of the SONGS antineutrino detector [19].

The detector was able to demonstrate sensitivity to the operational status of the reactor within five hours of shutdown or startup with 99% confidence. Fig. 3 shows the detected antineutrino rate as a function of time with the vertical line representing the time in which the reactor shut down. The detected antineutrino rate significantly decreases from an hourly count rate of about 35 to about 20 following the shutdown of the reactor.

The SONGS detector also displayed the ability to measure fissile content evolution corresponding to the burnout of 500 kg of ^{235}U and build-in of ~ 80 kg of plutonium in about four months [20]. ^{239}Pu produces about 12% less antineutrinos per fission than ^{235}U on average (this will be discussed in the next section). Therefore, as the reactor fuel is burned and ^{239}Pu starts to contribute to the total number of fissions in the core, the antineutrino rate will decrease. Fig. 4 shows data from the SONGS detector demonstrating this effect with the solid blue line representing the expected antineutrino rate change due to isotopic evolution in the core. Lastly, the detector also measured the reactor power output, relative to an initial value, with 3% accuracy

in one week [20]. These small detectors were the first of their kind, thus the results can be expected to improve with further work.

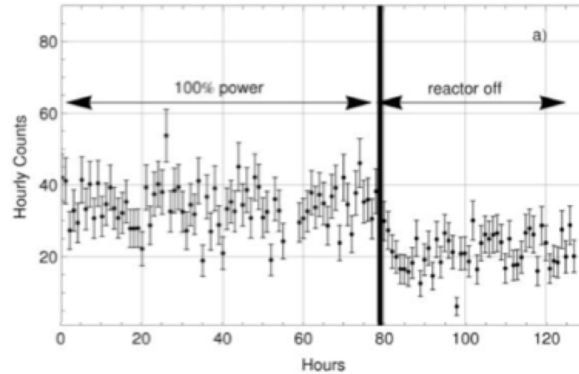


Fig. 3. Demonstration of the antineutrino rate measurement to determine the operational status of a nuclear reactor [20].

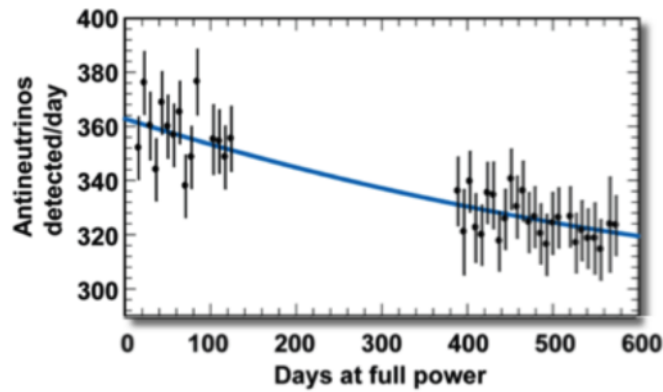


Fig. 4. Plot of the antineutrino rate measurement to determine the isotopic evolution of the fuel [20].

2.2 Kiloton Scale and Directionality

Large scale (kiloton) liquid scintillator antineutrino detectors have also been built such as the Kamioka Liquid scintillator AntiNeutrino Detector (KamLAND) near

Toyama, Japan and the CHOOZ detector in Chooz, France [21,22]. Both detectors were designed and deployed with the task of measuring the antineutrino oscillation phenomenon from antineutrinos produced from nearby nuclear reactors. KamLAND is currently the largest operational reactor antineutrino detector. It is located under 2700 m.w.e of rock and surrounded by multiple power reactors with an average standoff distance of ~ 180 km [21]. Results from KamLAND demonstrated that the operation of a 10 MW(th) reactor can be confirmed in a 10 km radius with a 1 kiloton sized detector in three months at a 95% confidence level [20].

The CHOOZ detector was located underground with 300 m.w.e. overburden and approximately 1 km away from two nuclear reactors producing a total of about 4.4 GW of thermal power [22]. The CHOOZ detector was the first nonsegmented scintillator detector to demonstrate antineutrino directionality from the IBD interaction. CHOOZ was able to locate the antineutrino source within a cone of half-aperture of about 18 degrees with a 1σ confidence, however it required approximately 2700 antineutrino events [22]. Due to the weak correlation between the positron location and neutron capture location to the antineutrino direction, directionality from IBD is quite difficult.

In addition to liquid scintillator detectors, there also exists WATCHMAN-like water-based Cherenkov detectors such as the large 50 kiloton Super Kamiokande (Super-K) detector [23]. Super-K is located in the Kamioka mine in Hida, Gifu prefecture, Japan with approximately 2700 m.w.e. overburden. Unlike the other detectors mentioned above, Super-K was designed to measure solar and supernova neutrinos via neutrino-electron scattering [23]. As in antineutrino-electron scattering, the neutrino-electron scattering angle peaks in the forward direction. The scattered electron will produce a Cherenkov cone in the direction of travel and will be detected in the PMTs surrounding the detector. Reconstructing the directions of the

scattered electrons using the triggered PMT times, locations, and charge intensities, Super-K was able to successfully demonstrate solar neutrino directionality [24]. Although the work was done with neutrinos, Super-K provides confidence in the extraction of antineutrino directionality in WATCHMAN because the cross-section for antineutrino-electron scattering is only ~ 2.4 times smaller than neutrino-electron scattering [17].

2.3 Reactor Antineutrino Energy Spectrum

Instead of measuring the energy spectrum of reactor antineutrinos with antineutrino detectors directly, methods have been developed to determine the energy spectrum by measuring the missing energy from the beta decays of nuclear reactor fission products [25]. Typically, six beta decays occur per fission fragment pair before reaching stability and each decay produces antineutrinos with different energies [25]. Therefore, simulations are used to study the production of fission products and the subsequent decays of the fission products to understand the reactor antineutrino energy spectrum. The work in this thesis will rely heavily on these studies in order to properly model the antineutrino flux and energy distribution incident on the WATCHMAN detector.

The antineutrino energy spectrum will approximately follow the parameterization of

$$\frac{dN_{\bar{\nu}_e}}{dE_{\bar{\nu}_e}} = e^{a_0 + a_1 E_{\bar{\nu}_e} + a_2 E_{\bar{\nu}_e}^2}, \quad (1)$$

with units of antineutrinos \cdot MeV $^{-1}$ \cdot fission $^{-1}$ and the parameters a_0 , a_1 , and a_2 given in Table 1 [26]. A plot of Eq. (1) with the four different isotopes provided in Table 1 is shown in Fig. 5. Typical fissioning percentages for a PWR half-way through its 18 month fuel cycle (49.6% ^{235}U , 35.1% ^{239}Pu , 8.7% ^{238}U , and 6.6% ^{241}Pu) were

used to produce the total curve shown in black [27]. Other fissionable isotopes were calculated to be less than 0.1% and thus neglected in the figure [27]. The plot has a lower bound of 2 MeV because most studies cut the spectrum off at the 1.8 MeV energy threshold for IBD [26].

Table 1

Parameter values for Eq. (1). The values reported for ^{235}U , ^{239}Pu , and ^{241}Pu are for thermal neutrons and the value for ^{238}U is for 0.5 MeV neutrons [26].

Isotope	a_0	a_1	a_2
^{235}U	0.870	-0.160	-0.0910
^{238}U	0.976	-0.162	-0.0790
^{239}Pu	0.896	-0.239	-0.0981
^{241}Pu	0.793	-0.080	-0.1085

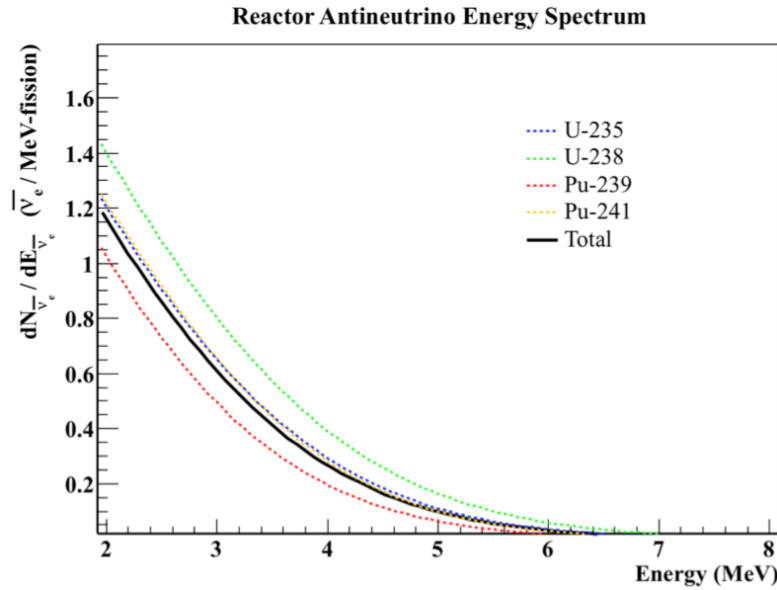


Fig. 5. Antineutrino energy spectrum from fissions occurring in ^{235}U , ^{239}Pu , ^{238}U , and ^{241}Pu . The black line represents a summation of the four isotopes with typical fission percentages of 49.6% ^{235}U , 35.1% ^{239}Pu , 8.7% ^{238}U , and 6.6% ^{241}Pu .

Unlike IBD however, antineutrino-electron scattering does not have an energy threshold, and thus the spectrum in Fig. 5 must be extended down to 0 MeV. The spectra at lower energies have yet to be calculated in a systematic way [26]. Instead, a study by Vogel and Engle used the summation of the allowed beta decay electron energy distributions for all fission fragments produced in the fissioning of the isotopes listed in Table 1 [26]. Their results are shown in Table 2 and the detailed ^{235}U values below 1 MeV are plotted in Fig. 6. It is clear from both Table 2 and Fig. 6 that the antineutrino spectra below 2 MeV for all four isotopes possess discontinuities. According to Vogel and Engle, this is due to the Coulombic attraction between the emitted electron and the parent nucleus during beta decay [26]. Due to the attraction, there is a non-zero probability that a zero-momentum electron will be produced, giving all the allowed energy to the antineutrino. When this type of decay occurs, a step in the spectrum is observed.

Table 2

Calculated antineutrino fluxes for energies below 2 MeV [26].

E (MeV)	^{235}U	^{239}Pu	^{238}U	^{241}Pu
2.0	1.26	1.08	1.50	1.32
1.5	1.69	1.48	1.97	1.75
1.0	2.41	2.32	2.75	2.63
0.75	2.66	2.58	2.96	2.90
0.50	2.66	2.63	2.91	2.82
0.25	2.16	2.08	2.18	2.14
0.125	1.98	1.99	2.02	1.85
6.25×10^{-2}	0.61	0.64	0.64	0.59
3.12×10^{-2}	0.35	2.13	1.32	3.00
1.563×10^{-2}	0.092	0.56	0.35	0.79
7.813×10^{-3}	0.024	0.14	0.089	0.20

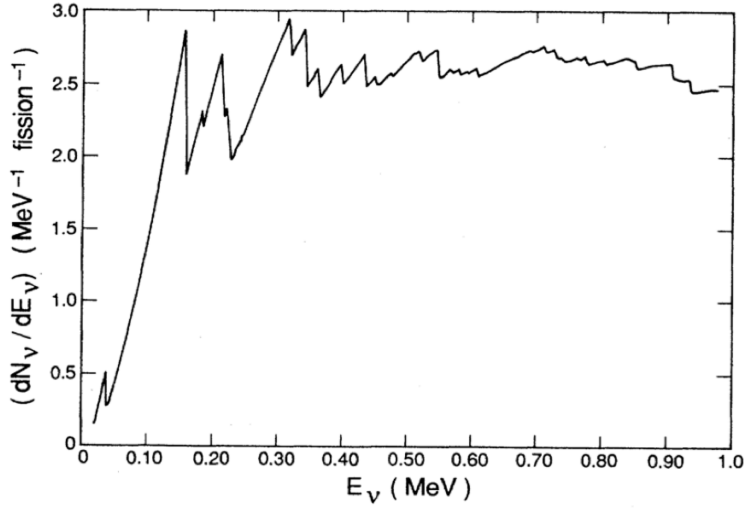


Fig. 6. Antineutrino energy spectrum below 1 MeV for the fission of ^{235}U [26].

For the ease of calculations and to avoid the discontinuities in the antineutrino spectrum below 2 MeV, this thesis will propose to simply extend Eq. (1) to 0 MeV. Fig. 7 shows a plot of Eq. (1) using the typical fissioning percentages extended down to 0 MeV superimposed on the values given in Table 2 (again assuming typical fissioning percentages). Although there is a discrepancy between the two, simply extending Eq. (1) to 0 MeV will not cause any significant effects, to at least within a few tens of percent. Therefore the antineutrino energy spectrum will be described by Eq. (1) from 0 to 8 MeV. Fig. 5 is thus reproduced in Fig. 8, extending Eq. (1) down to 0 MeV.

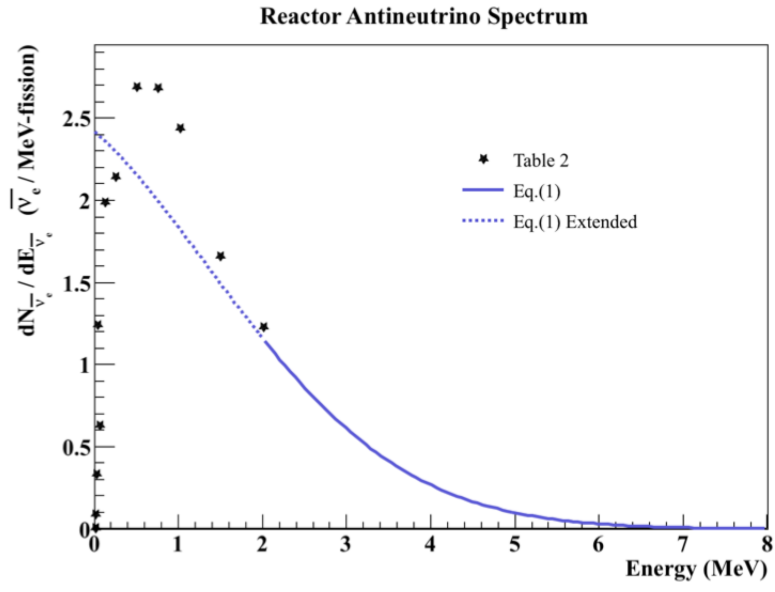


Fig. 7. Comparison of the extension of Eq. (1) to the values calculated in Table 2.

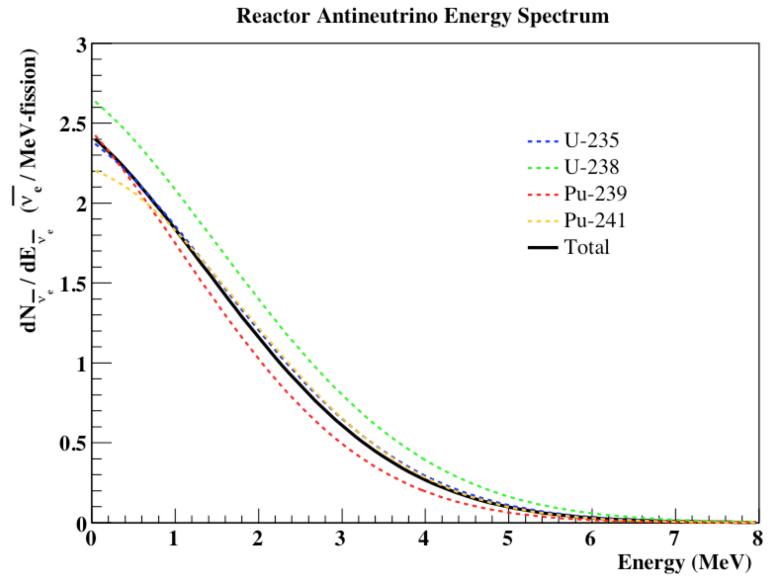


Fig. 8. Reactor antineutrino energy spectrum from fissions occurring in ^{235}U , ^{239}Pu , ^{238}U , and ^{241}Pu using Eq. (1) extended to 0 MeV.

From the figure, the antineutrino spectra for ^{235}U and ^{239}Pu differ slightly, with ^{239}Pu producing about 12% fewer antineutrinos per fission on average. Therefore, for a given power level, fresh fuel (with no ^{239}Pu built in yet) tends to produce more antineutrinos than burned fuel. Thus, as the fuel is burned in the core and plutonium builds in and becomes a significant contributor to the number of fissions in the core (recall about 35% of the fissions in typical mid-cycle PWR fuel are due to ^{239}Pu), it is expected that the antineutrino flux will slightly decrease. Thus, if continual measurements are made of the antineutrino flux and information such as the original isotopics and power level are known, then the process of burnup and plutonium production can be characterized. This effect was demonstrated in Fig. 4 using the SONGS detector.

All nuclear reactors produce plutonium, which can be subsequently used to make a nuclear weapon. Typical civilian nuclear reactors are operated in such a way that the produced plutonium will contain contaminants that make the fabrication of a nuclear weapon difficult. For instance, some isotopes of plutonium, such as ^{240}Pu , are high spontaneous fissioners, which increase the risk of pre-detonation if used in a weapon. Other isotopes, such as ^{238}Pu , are highly radioactive alpha-emitters and thus generate a large amount of heat in the material. This heat, as well as the high gamma activity associated with ^{241}Pu (due to its daughter product, ^{241}Am) makes the handling of the material difficult and hazardous. This type of plutonium is termed reactor grade, such that it contains the typical isotopics from that of a normally operated reactor that make it difficult to produce a weapon [28]. Nuclear reactors can easily adjust the way in which they operate in order to decrease the number of contaminants in the plutonium. This is typically done by only taking the fuel to a low burnup and removing it from the core, as to maximize the ^{239}Pu content while minimizing the ^{240}Pu , ^{238}Pu , and ^{241}Pu content. This plutonium ($> 93\%$ ^{239}Pu) is

termed weapons grade, such that it is ideal for producing plutonium-based nuclear weapons [28]. Thus, with the ability to monitor fuel burnup, antineutrino detectors may have the potential to determine whether the reactor is producing reactor grade or weapons grade plutonium. This potential is an interesting topic of current research, however this project will focus solely on directionality and will not discuss this topic any further.

2.4 Physics Experiments

Lastly, a physics experiment has been proposed for a water-based Cherenkov detector such as WATCHMAN using the antineutrinos produced from the Isotope Decay At Rest (IsoDAR) antineutrino generator [29,30]. IsoDAR is a cyclotron that accelerates protons into a ^9Be target to produce copious amounts of neutrons. The neutrons enter a ^7Li sleeve surrounding the accelerator where a neutron capture will result in the production of the unstable isotope, ^8Li . The subsequent beta decay of ^8Li results in an antineutrino with an energy spectrum shown in Fig. 9 and an average energy of about 6.5 MeV [29,30]. Fig. 10 shows a schematic of the IsoDAR target design. IsoDAR hopes to be used in conjunction with either a liquid scintillator or water Cherenkov detector in order to measure the antineutrino-electron scattering cross-section more precisely than any other experiment [29]. The uncertainty in the cross-section measurement currently leaves the possibility of particle interactions beyond the Standard Model of particle physics, or NonStandard Interactions (NSIs) [29]. Therefore, with a more precise measurement of the cross-section, the possibility of NSIs can be ruled out or confirmed. Analogous to the reactor research proposed here, IsoDAR aims to explore the antineutrino-electron scattering interaction, however at much higher energies (compare Fig. 8 and Fig. 9). Although IsoDAR has yet to be built, significant work has been done to model antineutrino-

electron scattering in water and scintillator detectors. This work can therefore be used as a reference in the proposed reactor antineutrino research. Much work has been done with antineutrino and neutrino detection in regards to nuclear reactor monitoring and directionality, however nothing has yet to be done specifically with water-based Cherenkov detectors using antineutrino-electron scattering for nuclear reactor antineutrinos.

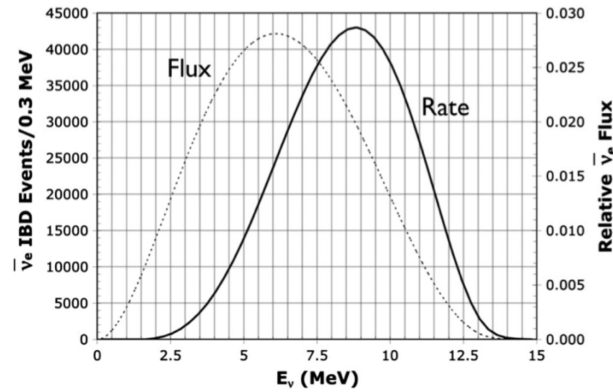


Fig. 9. Plot of the expected antineutrino spectrum from IsoDAR as well as the expected measured spectrum (incident flux folded with the total scattering cross section) [29].

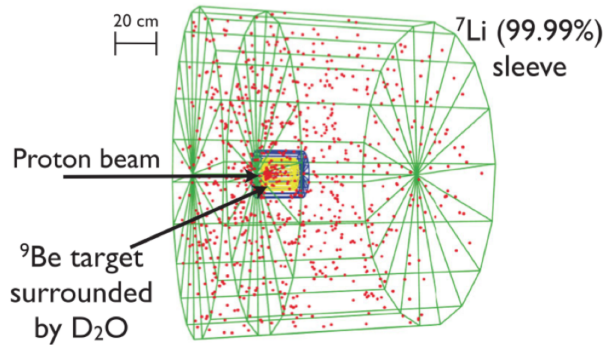


Fig. 10. Schematic of the IsoDAR antineutrino generator. The red dots represent antineutrino production points within the ${}^7\text{Li}$ sleeve [29].

3. THEORY

3.1 Antineutrinos

The antineutrino was first proposed by the Austrian physicist Wolfgang Pauli in 1930 while studying nuclear beta decay [31]. Prior to 1930, because the neutron was not yet discovered, nuclear beta decay was represented as the process in which a nucleus A decays into a slightly lighter nucleus B with the emission of an electron, such as

$$A \rightarrow B + e^{-}. \quad (2)$$

It is now understood that this process is actually the conversion of a neutron in nucleus A into a proton. The decay in Eq. (2) is a simple two-body problem and therefore, due to conservation of energy, if the parent nucleus is at rest, the daughter nucleus and electron will have discrete and calculable energies based off the rest masses of the three particles [31]. However, experiments in which the masses were known showed that the electron produced in nuclear beta decay was emitted with a continuous spectrum of energies. Pauli therefore proposed that a third neutral lightweight particle must be emitted along in the process. In 1933, the Italian physicist Enrico Fermi then developed a theory of beta decay including this unknown particle and proved that Pauli's hypothesis indeed solved the problem [31]. Fermi named the particle the neutrino, Italian for the "little neutral one". As a historical convention, the particle is called the antineutrino and nuclear beta decay was rewritten as

$$n \rightarrow p + e^{-} + \bar{\nu}. \quad (3)$$

In particle physics, the electron, muon, and tau particles are characterized as leptons. They are all assigned a lepton number of +1 and their corresponding antiparticles are given a lepton number of -1 [31]. Conservation of lepton number asserts that the neutrino in Eq. (3) must have a lepton number of -1. Therefore, to be consistent with the convention of antileptons possessing a -1 lepton number, it is called an antineutrino [31]. The neutrino comes in three flavors to match its leptonic particles, the electron-neutrino, muon-neutrino, and tau-neutrino. The antineutrino also comes in three flavors, the electron-antineutrino, muon-antineutrino, and tau-antineutrino. To be specific, nuclear beta decay should be written with an electron-antineutrino such as

$$n \rightarrow p + e^{-} + \bar{\nu}_e . \quad (4)$$

Neutrinos and antineutrinos are known as weakly interacting particles, meaning they can travel extreme distances in matter without attenuation. A gamma ray with very high energy can be stopped by a few centimeters of lead whereas an antineutrino with moderate energy can easily pass through a thousand light years ($\sim 10^{21}$ cm) of lead [31]. Therefore, antineutrinos produced in nuclear reactors are able to escape containment without any attenuation. Information about the reactor core can thus be obtained outside of containment by detecting and characterizing the antineutrinos. However, because the antineutrinos are weakly interacting particles, detecting them requires large detectors and sophisticated techniques.

3.2 Detection Methods

The antineutrino is an electrically neutral particle and, like other neutral particles, it cannot be detected directly. Typically in neutral particle detection, the particle must participate in an interaction that produces electrically charged daugh-

ter products, which can then be detected by conventional means. In the case of antineutrinos, interactions such as IBD and electron scattering are used in detection. Historically, liquid scintillator and water (pure or Gd-doped) have been used as the detection media.

3.2.1 *Inverse Beta Decay*

IBD is the process in which a free proton and electron-antineutrino collide and produce a neutron and positron as in

$$\bar{\nu}_e + p \rightarrow n + e^+, \quad (5)$$

and has an interaction energy threshold of 1.8 MeV [16]. Unlike neutron detection in ^3He tubes, which has a detection cross-section of 5330 barns (1 barn = 10^{-24} cm 2) for thermal neutrons, the cross-section for IBD is on the order of 10^{-19} barns, or 10^{-43} cm 2 [32,33]. Therefore, with an extremely large detector and intense antineutrino source, the best detection methods can only hope for a few interactions per day.

Once an interaction occurs, the positron will be emitted with kinetic energy proportional to the incident antineutrino (minus 1.8 MeV) and will deposit that energy (plus 1.022 MeV of annihilation energy) in the target medium. The energy will be deposited via scintillation or Cherenkov light (depending on the medium) and the light will be collected in PMTs surrounding the target material. The emitted neutron will eventually thermalize through multiple nuclear scattering. Depending on the target material, the thermalized neutron can be captured on a hydrogen, carbon, or gadolinium nucleus, raising the capturing nucleus into an excited state. The de-excitation of the nuclei result in gamma rays which will subsequently create scintillation or Cherenkov light that will be detected by the PMTs. The de-excitation energies as well as cross-sections associated with the typical neutron captures are

shown in Table 3.

Table 3

De-excitation energies associated with neutron captures in antineutrino detectors [33].

Capture Nucleus	Capture Cross-section (barns)	De-excitation Energy (MeV)
^1H	0.33	2.2
^{12}C	0.0035	4.9
^{157}Gd	2.54×10^5	8.0

The positron signal and neutron signal will be separated by approximately 20 - 50 μs , corresponding to the thermalization time of the neutron [16]. Thus state of the art detection electronics are used in conjunction with the PMTs to determine the time between each detected event to discriminate against non-coincident events. Reconstruction algorithms are also used in order to determine the position of the detected positron and neutron using the triggered PMT timings, locations, and charge intensities. The neutron will thermalize only a few centimeters away from the interaction vertex and thus the difference in position between the detected neutron and positron can be used to discriminate separate events that occur within 20 - 50 μs . The coincident detection in both time and space between the positron and neutron indicate a clear detection of an antineutrino and thus allows for good background rejection. However, background events do occur and must be kept to a minimum because only a few true reactor antineutrinos will be detected daily. The sources for IBD backgrounds will be discussed in Section 4.1. Detection electronics connected to the PMTs can also measure the deposited positron energy from the number of photoelectrons produced. The energy of the positron is strongly correlated to the

energy of the incident antineutrino, and thus antineutrino spectroscopy is possible with highly sensitive PMTs [16].

3.2.2 *Elastic Electron Scattering*

In addition to IBD, electron-antineutrinos can elastically scatter off electrons in the purely leptonic interaction via the exchange of a neutral Z^0 boson or a charged W^- boson [17]. The exchange of the Z^0 boson is termed the neutral current interaction and the exchange of the W^- boson is term the charged current interaction, for obvious reasons. The tree level Feynman diagrams for these processes are shown in Fig. 11. The scattered electrons will posses enough energy to produce either scintillation or Cherenkov light depending on the target material. This light will then be collected in the surrounding PMTs. The cross-section for antineutrino-electron scattering is on the order of 10^{-21} barns, or 10^{-45} cm^2 , roughly 100 times smaller than IBD [17]. See Fig. 12 for a comparison of the IBD and electron scattering cross-sections. For this reason, IBD is typically the favored interaction for antineutrino detection. Furthermore, because antineutrino-electron scattering only produces one daughter product (the electron), coincident detection techniques cannot be used. Therefore, more background events will exist in the antineutrino-electron scattering signal. These backgrounds will be discussed in Section 4.2. The appeal of antineutrino-electron scattering is that it provides the ability to determine the direction of the incident antineutrino flux. Technically, antineutrino directionality is also possible with IBD using the correlation between the antineutrino and neutron directions (as was shown with the CHOOZ detector). However, it requires specialized detectors, very sophisticated detection methods, and a large number of events to achieve a statistically significant signal. Antineutrino-electron scattering is peaked in the forward direction, providing a strong correlation between the scattered electron direction and the

incident antineutrino direction. This will be discussed in the next section.

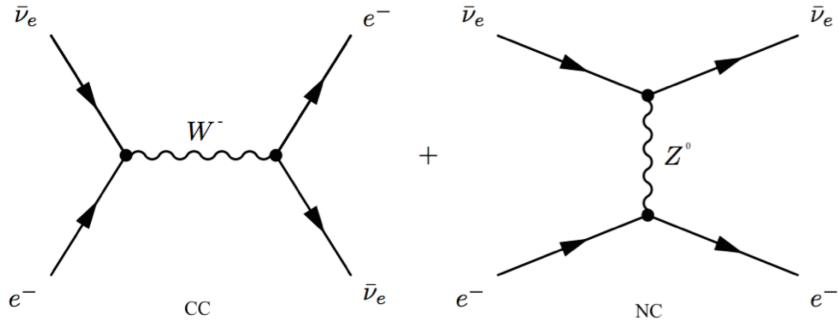


Fig. 11. Tree level Feynman diagrams of charged current (CC) and neutral current (NC) antineutrino-electron scattering [17].

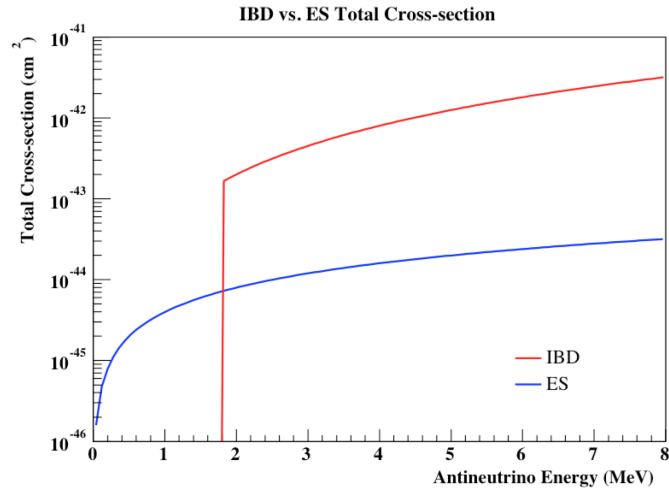


Fig. 12. Plot of the inverse beta decay (IBD) and electron scattering (ES) cross-sections as function of the incident antineutrino energy. IBD possesses an energy threshold of 1.8 MeV.

As was mentioned in an earlier section, when the reactor antineutrino energy spectrum and the available targets for each interaction are accounted for, the cross-sections for IBD and electron scattering become within the same order of magnitude.

Fig. 13 shows a plot of the total cross-sections for IBD and electron scattering folded with the reactor antineutrino energy spectrum from 0 to 8 MeV. Comparing the integrals of the curves in Fig. 13 from 0 to 8 MeV, IBD is about 26.9 times larger than electron scattering. The two hydrogen atoms in each water molecule in WATCHMAN function as quasi-free protons and will be the only available targets for IBD [16]. Electron scattering, however, can occur on any of the 10 electrons in each water molecule. Therefore, electron scattering has 5 times as many targets available than IBD. Combing the factors of 26.9 and 5 results in IBD being roughly 5.4 times larger than electron scattering over the energy range of 0 to 8 MeV. Thus, for reactor antineutrinos in water, electron scattering is not actually two orders of magnitude smaller than IBD, but instead within the same order of magnitude. This fact, along with the addition of directionality, gives electron scattering the potential to produce a significant signal in WATCHMAN.

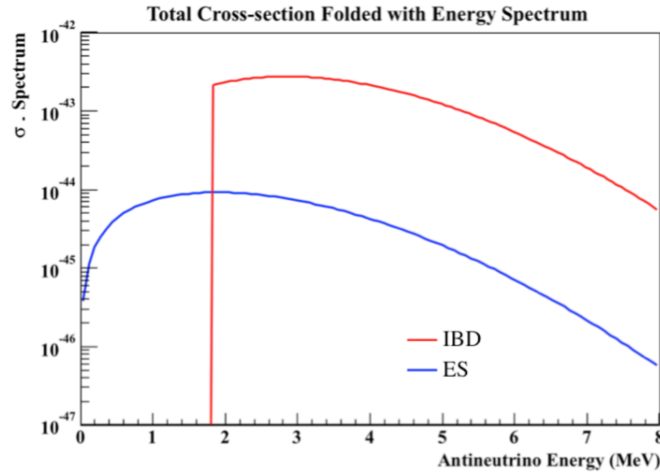


Fig. 13. Inverse beta decay (IBD) and electron scattering (ES) cross-sections as function of the incident antineutrino energy folded with the reactor antineutrino energy spectrum.

3.3 Directionality

In the laboratory frame, the electron is assumed to be at rest and the antineutrino mass is negligible (although once thought to be massless, it is now known that neutrinos do indeed possess mass, however a very small amount). Interestingly, experiments have determined what is known as the “mass hierarchy”, which is the ordering of the three neutrino masses, however it is not yet known which neutrino belongs to which mass or in which way the hierarchy is supposed to be ordered (forward or inverted). Though very interesting and a current topic in neutrino research, these details are not explored here. If the expression

$$\sqrt{2m_e E_{\bar{\nu}_e}} \gg m_e \quad (6)$$

is assumed, where m_e is the rest mass of the electron and $E_{\bar{\nu}_e}$ is the energy of the antineutrino, then the total interaction cross-section for antineutrino-electron elastic scattering can be written as

$$\begin{aligned} \sigma_{\bar{\nu}_e e}(E_{\bar{\nu}_e}) &= \left(\frac{G_F^2 m_e E_{\bar{\nu}_e}}{2\pi} \right) \left(\frac{1}{3} \left(1 + 2 \sin^2(\theta_\omega) + 4 \sin^4(\theta_\omega) \right) \right) \\ &\approx (7.8 \times 10^{-45}) m_e E_{\bar{\nu}_e} \frac{\text{cm}^2}{\text{MeV}^2}, \end{aligned} \quad (7)$$

where G_F is Fermi’s coupling constant ($= 1.166364 \times 10^{-5} \text{ GeV}^{-2} (\hbar c)^3$) and θ_ω is the Weinberg mixing angle ($\approx \sin^{-1}(\sqrt{0.23})$) [17]. It can be seen from Eq. (7) that the cross-section scales linearly with the incident antineutrino energy (see Fig. 12 above).

The differential cross-section as a function of the kinetic energy of the scattered electron (T_e) in the laboratory frame is given by

$$\frac{d\sigma_{\bar{\nu}_e e}}{dT_e}(E_{\bar{\nu}_e}, T_e) = \frac{2G_F^2 m_e}{\pi} \left[g_1^2 + g_2^2 \left(1 - \frac{T_e}{E_{\bar{\nu}_e}} \right)^2 - g_1 g_2 \frac{m_e T_e}{E_{\bar{\nu}_e}^2} \right], \quad (8)$$

where g_1 and g_2 are given by

$$g_1 = \frac{1}{2}(g_V - g_A) = \sin^2(\theta_w) \approx 0.23 \quad (9)$$

and

$$g_2 = \frac{1}{2}(g_V + g_A) = \frac{1}{2} + \sin^2(\theta_w) \approx 0.73, \quad (10)$$

where g_V and g_A are the weak vector and weak axial-vector coupling constants, respectively [17]. Eq. (8) is plotted for several antineutrino energies in Fig. 14. The differential cross-section as a function of scattered electron kinetic energy will be used in the event generator to sample scattered electron energies. This will be discussed further in Section 5.2.

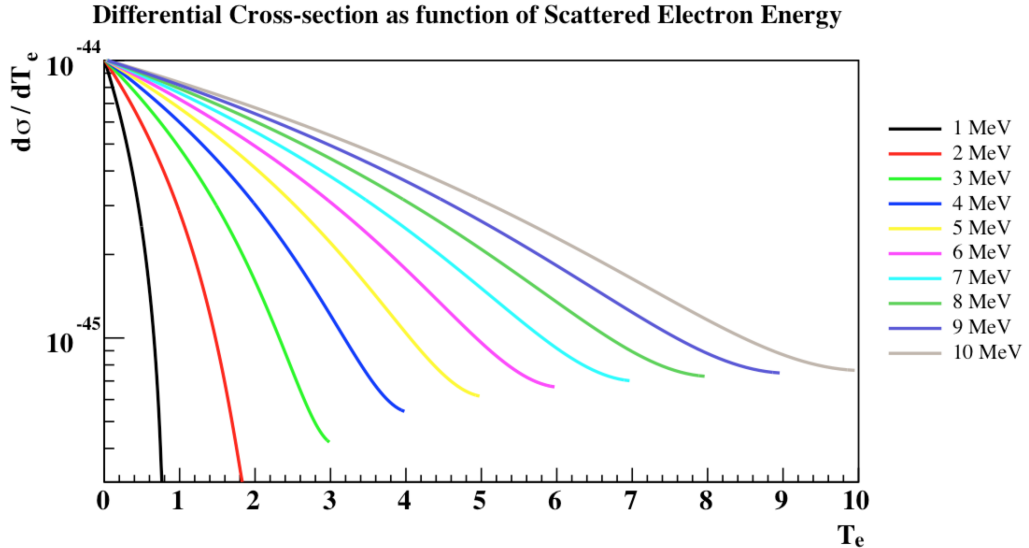


Fig. 14. Plot of the differential cross-section for antineutrino-electron scattering for several antineutrino energies.

The maximum kinetic energy given to the electron from the antineutrino is given by

$$T_e^{max} = \frac{2E_{\bar{\nu}_e}^2}{m_e + 2E_{\bar{\nu}_e}}, \quad (11)$$

and corresponds to a forward scatter of the electron (angle between the incident antineutrino and scattered electron equal to 0), or a complete backscatter of the antineutrino [17]. From energy and momentum conservation in the laboratory frame it can be shown that the kinetic energy of the scattered electron is given by

$$T_e = \frac{2m_e E_{\bar{\nu}_e}^2 \cos^2 \theta}{(m_e + E_{\bar{\nu}_e})^2 - E_{\bar{\nu}_e}^2 \cos^2 \theta}, \quad (12)$$

where θ is the angle between the incident antineutrino and the scattered electron [17]. Using this, the differential cross-section as a function of scattered electron energy can be rewritten as a function of the cosine of the scattering angle as

$$\begin{aligned} \frac{d\sigma_{\bar{\nu}_e e}}{d \cos \theta}(\cos \theta, E_{\bar{\nu}_e}) = & \frac{4\sigma_0 E_{\bar{\nu}_e}^2 (m_e + E_{\bar{\nu}_e})^2 \cos \theta}{\left[(m_e + E_{\bar{\nu}_e})^2 - E_{\bar{\nu}_e}^2 \cos^2 \theta \right]} \cdot \left[g_1^2 + g_2^2 \right. \\ & - \left(\frac{2g_2^2 m_e E_{\bar{\nu}_e} \cos^2 \theta}{(m_e + E_{\bar{\nu}_e})^2 - E_{\bar{\nu}_e}^2 \cos^2 \theta} \right)^2 \\ & \left. - g_1 g_2 \frac{2m_e^2 \cos^2 \theta}{(m_e + E_{\bar{\nu}_e})^2 - E_{\bar{\nu}_e}^2 \cos^2 \theta} \right], \quad (13) \end{aligned}$$

where σ_0 is a constant equal to $88.06 \times 10^{-46} \text{ cm}^2$ [18]. This function is plotted in Fig. 15 for various incident antineutrino energies.

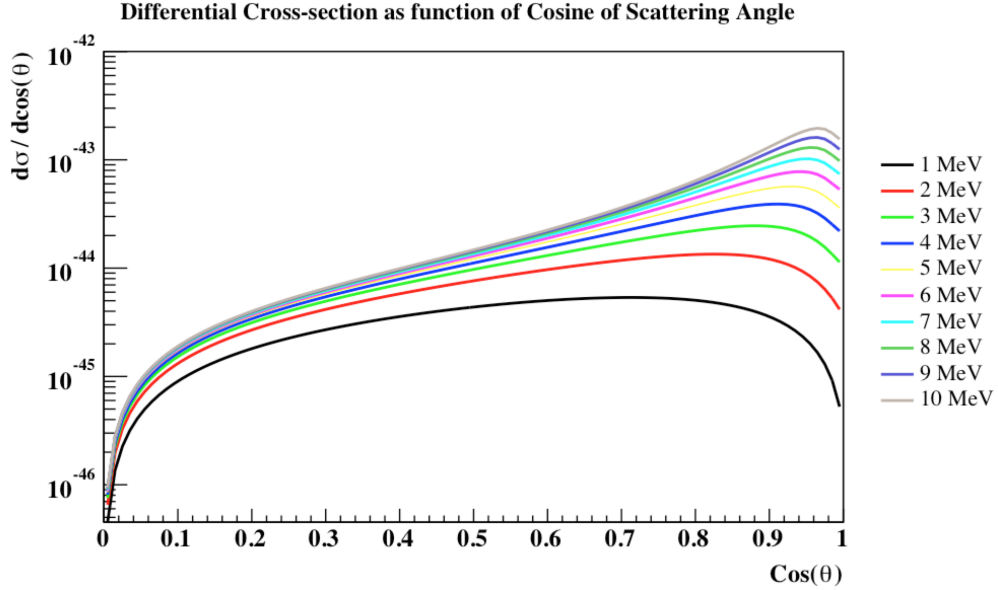


Fig. 15. Plot of the differential cross-section for antineutrino-electron scattering as a function of the cosine of the scattering angle for several incident antineutrino energies.

From the figure, the antineutrino-electron scattering interaction is indeed peaked towards the forward direction ($\cos(\theta) = 1$). Therefore, the scattered electron has the highest probability of scattering with a small scattering angle. This effect becomes more apparent as the incident antineutrino energy increases. In water-based Cherenkov detectors, the scattered electrons will possess enough energy to produce Cherenkov light cones in the direction of travel. The surrounding PMTs will then collect this light and the triggered PMT timings, locations, and charge intensities can be used to determine the direction of the Cherenkov cone. Because the scattered electrons will have small scattering angles, their directions will tend to align with the incident antineutrino directions. Background events will be isotropically distributed in direction and thus if the cosine of antineutrino-electron scattering angles are plotted with the cosine of the background scattering angles, an increase of counts should

be observed tending towards the direction of the incident antineutrinos atop the flat background.

In the Super-K experiment, this was done with solar neutrinos and the data collected over approximately 12 years is shown in Fig. 16. Because the Earth is orbiting the Sun, the location of the Sun constantly changes with respect to the detector. Therefore, the geometry of the scattering angles continually changes throughout the day. To account for this, a scattering angle of 0 ($\cos(\theta) = 1$) was taken to be the line from the Sun to the detector. The figure displays $\cos(\theta_{Sun})$, the cosine of the scattering angle with respect to the Sun, where a value of 1 indicates an event that points back towards the Sun, no matter the position of the Sun at that time. From the figure, the flat isotropic background is apparent at about 10,000 events per bin and the solar neutrino-electron scattering is seen as a peak above the background pointing back to the Sun. Also to note in the figure, the scattering signal appears to be an exponential peaking at 1 although the differential cross-section as a function of the cosine of the scattering angle in Eq. (13) is not purely exponential. This is due to the ability of the reconstruction software to reconstruct the direction of the Cherenkov light cones.

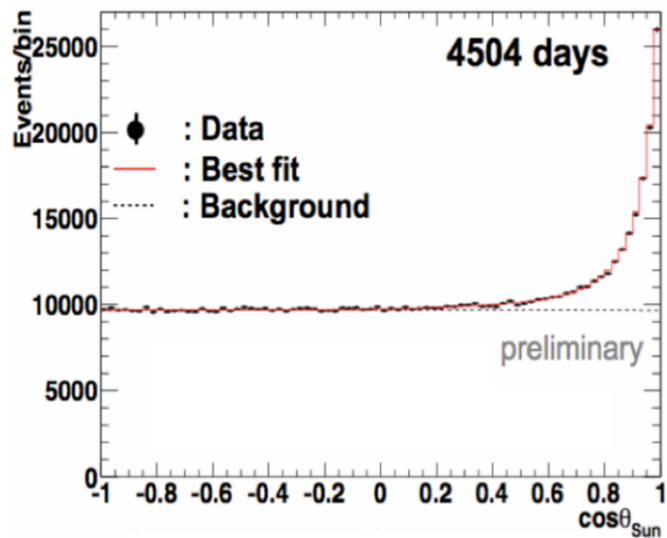


Fig. 16. Cosine of the scattering angle with respect to the Sun for the directionality experiment at the Super-K detector [24].

3.4 Event Reconstruction

In both IBD and electron scattering, it is crucial that each individual event can be reconstructed. Specifically, the event vertex, or the position in which the antineutrino interacts, needs to be known in order to apply spatial cuts and reduce background for IBD. In the case of directionality, the direction of the scattered electron needs to be known in order to determine the direction of the incident antineutrino flux. In water Cherenkov detectors, this is accomplished by using the timing, positions, and charge intensity of the triggered PMTs for each event. For electron scattering, the scattered electrons will produce a Cherenkov cone in the direction of travel. The cone will travel towards the PMTs lining the walls of the detector and will trigger the PMTs in a circular or ring shape (see Fig. 17).

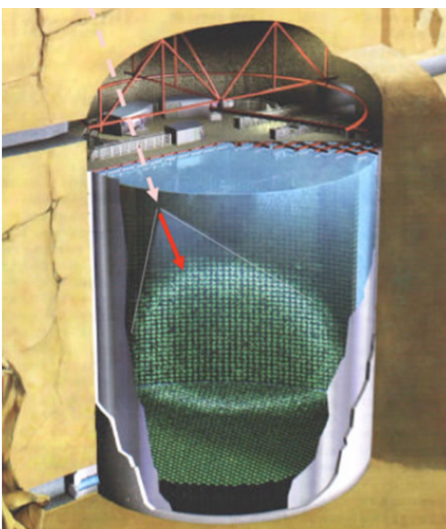


Fig. 17. Picture demonstrating the Cherenkov cone imparting a ring shape on an antineutrino detector [34].

After an event is triggered in the detector, the trigger times, locations, and charge intensities (number of photoelectrons produced) of the PMTs are fed into reconstruction software that will determine the track that best fits the data. A track is specified by seven kinematic variables: three for the vertex position (x, y, z) , two direction parameters (θ, ϕ) , one time (t) , and one energy (E) . The seven variables together make up a unique track. For each track, probability density functions for both charge and time can be produced for every PMT in the geometry. Typically, a likelihood function is created based off a given track and the generated PDFs, and the seven variables can be fit using the maximum likelihood method. This is repeated for multiple hypothesized tracks until the track with the largest likelihood is found [35].

4. BACKGROUNDS

Antineutrino detection is typically characterized as rare event detection. This is because only a few true interactions are detected per day. With such low count rates, the background levels in the detector must be kept to a minimum to maintain suitable statistics. In antineutrino detectors searching for IBD events, coincident detection techniques enable strong background rejection, however several sources of background still exist. In electron scattering, the level of background is much higher because coincident detection methods can no longer be used. Therefore, in order to confidently determine the antineutrino directionality capability in WATCHMAN, the expected background rates need to be well characterized.

4.1 Inverse Beta Decay Backgrounds

Typical background events in antineutrino detectors utilizing IBD include terrestrial decays, accidental coincidences, cosmogenic induced fast neutrons, cosmogenic radionuclide decays, and other nuclear reactors [16]. Terrestrial elements such as natural uranium, thorium, and potassium in the rock surrounding the detector can beta decay, mimicking the antineutrino signal. Accidental coincidences, or uncorrelated backgrounds, arise due to two individual physics processes producing events within the time and spatial coincidence requirements of the detector. These processes can include ambient radioactivity from the detector materials, such as the walls or the PMTs. Radioactivity from the surrounding rock can also contribute to the accidentals rate. This background is typically reduced by fiducialization, or rejecting events that do not occur within a virtual volume within the inner detector region [16]. The degree of fiducialization depends on the vertex reconstruction resolution of the detector, the size of the detector, and the needed detection efficiency.

Muons able to pass through the outer veto region of the detector without being vetoed can produce fast neutrons via spallation in the inner detector volume [16]. If a muon is detected in the outer region, the inner detector volume will veto all signals that occur for some specific period of time. Other techniques also employ spatial vetoes in the detector, such as only rejecting events that occur within a cylinder of some radius surrounding the muon track as it passes through the detector. The fast neutrons produced by unvetoes muons can produce signals that mimic the reactor antineutrino signal in both time and energy [16]. Muons are also able to produce long-lived (> 1 s) radionuclides, which, through decay, can mimic the antineutrino signal [16]. The long lifetimes of such cosmogenic induced radionuclides make vetoing such events difficult without significantly reducing the detection efficiency. The production of cosmogenic radionuclides in water has not been directly measured and thus simulations are done to estimate and bound the production yields [16].

4.2 Electron Scattering Backgrounds

Electron scattering relies on the detection of a single Cherenkov light cone and thus it is unable to employ coincident detection methods. Therefore, additional background in the signal is inevitable. In addition to the background processes discussed above, the electron scattering signal can be mimicked by solar neutrinos as well as by single gamma rays from terrestrial radionuclides (such as ^{208}Tl (from the thorium decay chain) and other radionuclides in the water and surrounding rock) and the detector materials (such as the steel supports and PMTs) [16]. The PMT glass is known to contain traces of uranium, thorium, and potassium, which (through their respective decay chains) can all produce backgrounds in WATCHMAN. Specifically, ^{40}K and ^{208}Tl emit high-energy gamma rays and the decay of uranium leads to the production of ^{222}Rn . The radon can migrate out of the PMT glass and into the

inner target region water where the eventual decay of ^{214}Bi will mimic the electron scattering signal. Radon from the air surrounding the detector can also contaminate the water. Lastly, misidentified IBD events will also contribute to the backgrounds. If the neutron is not detected within the time or spatial coincidence requirements, or if it is simply not captured, then the high-energy positron signal will mimic a scattered electron [16].

Due to the forward peaked nature of the electron scattering interaction, directional cuts can be applied to significantly reduce the backgrounds. The background events will be isotropically distributed in direction and thus will produce a constant offset to the directional reconstruction for all events. Thus if all the true electron scatters are expected to forward scatter, then a peak will exist in the cosine plot corresponding to the direction of the incident antineutrinos (as was seen in Fig. 16). A directional cut can then be applied to isolate the peak, discarding a significant amount of the nondirectional background.

4.2.1 WATCHMAN Estimation

As was discussed in Section 4.1, the radionuclide production in water due to cosmic muons has yet to be measured directly. Therefore, generated values such as from FLUKA simulations of the Super-K detector are typically used. FLUKA (FLUktuierende KAskade, German for Fluctuating Cascade) is a fully integrated Monte Carlo simulation package used to model the interactions and transport of particles in matter [36]. The Super-K FLUKA study presented the high yield and long lifetime cosmogenic radionuclides produced in water and are shown in Table 4 [37].

Table 4

Cosmogenic radionuclide yields generated from a Super-K FLUKA simulation [37].

Isotope	Half-life (s)	Decay Mode	Yield ($10^{-7}\mu^{-1}\text{g}^{-1}\text{cm}^2$)	Production Process (on ^{16}O)
^{16}N	7.13	$\beta^{-}\gamma$ (66%) β^{-} (28%)	18	(n, p)
^{15}C	2.45	$\beta^{-}\gamma$ (63%) β^{-} (37%)	0.8	$(n, 2p)$
^{11}Be	13.8	β^{-} (55%) $\beta^{-}\gamma$ (31%)	0.8	$(n, \alpha + 2p)$
^8B	0.77	β^{+}	5.8	$(\pi^{-}, \alpha + 2p + 2n)$
^8Li	0.84	β^{-}	13	$(\pi^{-}, \alpha + ^2\text{H} + p + n)$

The given yields are converted into rates for each nuclide using

$$R_i = \rho Y_i L_\mu R_\mu, \quad (14)$$

where ρ is the density of the target ($\text{g}\cdot\text{cm}^{-3}$), Y_i is the yield of isotope i ($10^{-7}\cdot\mu^{-1}\cdot\text{g}^{-1}\cdot\text{cm}^2$), L_μ is the average muon path length in the detector (cm), and R_μ is the muon rate ($\mu\cdot\text{s}^{-1}$ or Hz) [16]. To calculate the rates for WATCHMAN, the reported values for the average muon path length and muon rate from the KamLAND experiment were used. A target density of $1\text{ g}\cdot\text{cm}^{-3}$ was assumed. The results were appropriately scaled to the WATCHMAN size and depth by scaling the differences in muon rate and detector volume. KamLAND values were used because they are readily available, and the detector is of similar size to WATCHMAN and similar depth to Super-K (recall Table 4 is for cosmogenic radionuclide production at the 2700 m.w.e. Super-K depth). To determine the scaling factor between the muon rates at

KamLAND and WATCHMAN, an existing GEANT4 simulation of the muon flux as a function of depth was used [39]. The simulation predicted the showering muon rate in WATCHMAN to be about 2.6 times larger than KamLAND due to its shallower depth (1500 m.w.e.) [16]. The reported total muon rate of 0.198 Hz at KamLAND was thus scaled to 0.515 Hz for WATCHMAN [38]. The average muon path length in KamLAND was reported as 874 cm for the 1150 m³ detector balloon [38]. Therefore in order to adjust to the 1000 m³ WATCHMAN fiducial volume, a scaling factor of $\frac{1000}{1150}$ was applied.

The production rates for each radionuclide were then used to determine the amount of each radionuclide present in the WATCHMAN detector after one year. WATCHMAN is currently assumed to employ an entire detector veto for 2 s following a muon event [16]. Therefore, after a cosmogenic radionuclide production event occurs in WATCHMAN, only the decays that occur after 2 s will contribute to background. To account for this, the half-lives of each radionuclide in Table 4 were used to construct their respective decay curves. Each curve was normalized such that the area under each curve was equal to the number of radionuclides produced in the one-year timeframe. The number of decays occurring after 2 s was then calculated by integrating the decay curves with a lower bound of 2 s.

A study done by KamLAND on muon activation concluded that > 80% of the radionuclides are produced by muons that generate more than 70,000 photoelectrons [38]. These muons are termed bright muons and were reported to have a rate of 0.037 Hz in the KamLAND detector. This muon rate was scaled to WATCHMAN and used to define the deadtime associated with the veto [16]. The scaled bright muon rate of 0.0962 Hz and veto time of 2 s results in detector deadtime of 18% or a livetime of 82%. This livetime was therefore applied to all background events.

The background rates for ²⁰⁸Tl decay in the water, single gamma rays from the

surrounding rock and the steel supports, and solar neutrinos were directly scaled from a study performed by the IsoDAR experiment [29]. The numbers reported by the IsoDAR study were for the KamLAND detector and thus were scaled to WATCHMAN using the differences in the KamLAND and WATCHMAN fiducial volumes (524 m³ and 1000 m³). The background rates due to solar neutrinos, however, were scaled using the differences in KamLAND and WATCHMAN fiducial masses (0.408 kilotons and 1 kiloton). The fiducial masses were used in this instance because the solar neutrino flux is assumed to be similar at the two depths and thus the interaction rate depends solely on the number of available targets, which is proportional to the fiducial mass. Radioactivity due to the PMTs was not included in the IsoDAR study, assuming it to be insignificant with low activity PMTs and a sufficiently large buffer region between the PMTs and the fiducial volume. Radon contamination was also not included in the IsoDAR study. The KamLAND detector is reported to have a livetime of 90%, and thus the scaled KamLAND values were adjusted to represent an 82% livetime.

Finally, the misidentified IBD events were calculated using the expectation of 20 IBD events per day in WATCHMAN [16]. An estimated 50% detection efficiency and a 20% missed neutron rate were then applied to estimate the background [16]. A breakdown of the all the background estimates is given in Table 5.

Table 5

Estimated background contributions to the WATCHMAN detector for one year.

Background Source	Number of Events (yr ⁻¹)
¹⁶ N	14995
¹⁵ C	460
¹¹ Be	732
⁸ B	970
⁸ Li	2526
Solar Neutrinos	398
²⁰⁸ Tl gammas	208
Rock gammas	187
Steel gammas	80
Misidentified IBD	730
Total	21286

The estimated backgrounds in Table 5 were simulated in a GEANT4 simulation modeling the WATCHMAN detector using their respective energy spectra. The spectra for solar neutrinos, ²⁰⁸Tl gammas, rock gammas, steel gammas, ¹¹Be, ⁸B, and ⁸Li were provided by the IsoDAR collaboration. The spectra for ¹⁶N and ¹⁵C were determined using their respective Fermi distributions and the misidentified IBD spectrum was taken from a previous study done by the WATCHMAN collaboration [16]. The detector response was then analyzed using the number of photoelectrons produced in the surrounding PMTs for each event. The results are displayed in Fig. 18 for a data acquisition time of one year [16].

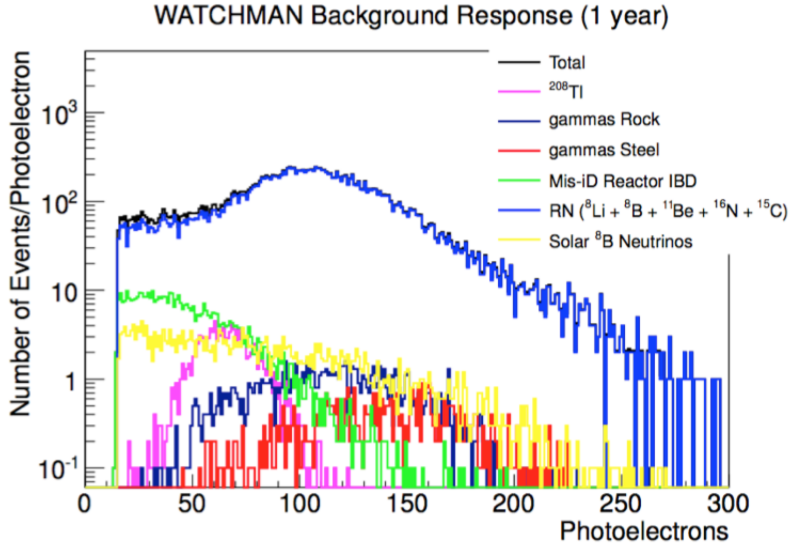


Fig. 18. Plot of the number of photoelectrons produced for each simulated source of background in WATCHMAN over one year [16].

As seen from the plot, the dominant background is due to the cosmogenic radionuclides. The radionuclides predominately produce events with high energy (> 6 MeV) and high photoelectron production (> 100 photoelectrons). The reactor antineutrino-electron scattering signal is of much lower energy (< 6 MeV) and thus an upper level photoelectron production cut can be applied to further reduce the backgrounds. If a cut is made at 65 photoelectrons to these results, approximately 84% of the background is discarded and a total of about 3530 total background events per year will remain.

It is very important to note that these background estimates assume the same background due to ^{208}Tl and detector wall activity as in KamLAND, with an appropriate scaling. In its current state, these backgrounds are significantly smaller than the cosmogenic radionuclide background. Depending on the detector cleanliness at WATCHMAN, this could be a reasonable or a large underestimate. Also,

PMT activity and radon contamination were not included in the background estimates assuming low activity PMTs, sufficient fiducialization, and adequate water recirculation to render them negligible.

The current background estimates in Table 5 will first be used to determine the directional sensitivity of WATCHMAN. After the results are obtained, a preliminary investigation into the PMT and radon backgrounds will be carried out in Section 6.4 and the directional capability of WATCHMAN will be reexamined.

5. CALCULATIONS AND SIMULATIONS

5.1 Expected Number of Events

In order to simulate one year of reactor antineutrino-electron scattering in the WATCHMAN detector, the expected number of events over the course of one year must be determined. The interaction rate in WATCHMAN can be calculated using

$$\int_0^{8\text{MeV}} N_e \Phi(E_{\bar{\nu}_e}) \sigma(E_{\bar{\nu}_e}) dE_{\bar{\nu}_e}, \quad (15)$$

where N_e is the number of available electrons in WATCHMAN, $\sigma(E_{\bar{\nu}_e})$ is the scattering cross-section (cm^2) given in Eq. (7), and $\Phi(E_{\bar{\nu}_e})$ is antineutrino flux incident on the detector given by

$$\Phi(E_{\bar{\nu}_e}) = \frac{dN_{\bar{\nu}_e}}{dE_{\bar{\nu}_e}} \cdot \frac{f}{4\pi d^2}, \quad (16)$$

where $\frac{dN_{\bar{\nu}_e}}{dE_{\bar{\nu}_e}}$ is the antineutrino energy distribution ($\text{antineutrinos} \cdot \text{MeV}^{-1} \cdot \text{fission}^{-1}$) as in Eq. (1), f is the fission rate in the core ($\text{fissions} \cdot \text{s}^{-1}$), and d is the distance from the Perry reactor to WATCHMAN (cm). The reactor is assumed to be an isotropic source of antineutrinos and because the reactor-detector distance is so large (13 km), the simple $\frac{1}{4\pi d^2}$ factor should suffice to account for the solid angle from the reactor to the detector. The fission rate for the Perry reactor is easily calculable using the power output of 3.758 GW(th) and an assumption of 200 MeV of available energy released per fission in the core. ^{235}U and ^{239}Pu release different amounts of energy per fission, and thus the average energy released per fission will change with time due to fuel burnup. However, this is less than a 10% difference and thus assumed to be negligible [40]. Carrying out the calculation results in a fission rate of about 1.17×10^{20} fissions $\cdot\text{s}^{-1}$ in the Perry reactor core. The number of electrons in WATCHMAN

was calculated assuming that the fiducial volume will contain exactly 1 kiloton of pure water. This amounts to about 3.3×10^{32} total electrons available for scattering.

Using the fission rate, a reactor-detector distance of 13 km, the antineutrino energy distribution in Eq. (1), the total scattering cross-section in Eq. (7), and the total number of electrons in WATCHMAN, the integral in Eq. (15) results in an interaction rate of about 5.9×10^{-5} scatters per second. Assuming a constant reactor power and constant isotopics over the course of one year, a total of 1853 electron scattering interactions are expected in WATCHMAN. Varying the fuel isotopics would change the energy distribution of the antineutrinos, however due to the small difference in the uranium and plutonium antineutrino spectra, it was neglected. As was discussed in Section 4.2.1, an 82% livetime is expected in WATCHMAN. Thus about 1520 total scatters are expected in one year (not including detection efficiency).

In order to quickly verify the calculations, the expected number of scatters was compared to the expected number of IBD events in WATCHMAN. Roughly 20 IBD events are expected in WATCHMAN per day [16]. In Section 3.3.2, it was shown that the IBD interaction rate will be about 5.4 times higher than electron scattering, and therefore about 3 or 4 scattering events are expected per day. This agrees with the results of scaling the calculated 1520 scattering events per year to a daily rate.

To generalize the calculation, a simple ROOT script was written to calculate the expected number of scatters in any sized water detector from any reactor power level with any fission fractions. The code is attached in Appendix A. ROOT is a mathematical and data analysis C++ interpreter software developed by CERN and used by many particle physics experiments for data handling and graphics. It provides a set of object-oriented frameworks with an extensive amount of functionality needed to analyze data [41]. The code shown in Appendix A can be run through the terminal (if ROOT is installed on the machine) and prompts the user to input parameters

used in the calculations.

5.2 Event Generator

To simulate the transport of a given particle, the initial position and momentum of that particle must be known. In common Monte Carlo particle transport software, such as GEANT4, this is done with the use of what is called an event generator. The purpose of the generator is to produce an initial position (x, y, z) and momentum (p_x, p_y, p_z) for each simulated particle. The particle is then born with the specified parameters and the Monte Carlo method is used to determine the particles interactions until absorption or termination. In the case of antineutrino-electron scattering, only the scattered electrons are simulated as if a scattering event has already occurred. This is to reduce the almost endless time it would take to simulate enough antineutrinos to acquire the desired number of interactions.

To simulate the scattered electrons, their initial positions need to be specified. Because the reactor is 13 km away from the detector, a scattering event is assumed to take place anywhere within the fiducial volume with equal probability. Therefore, a random position within the cylindrical fiducial volume is sampled for each scattered electron. In similar fashion, a kinetic energy and direction of travel are sampled to specify the initial momentum of the scattered electron. To sample the kinetic energy, the differential scattering cross-section as a function of the kinetic energy of the scattered electron given in Eq. (8) is treated as a probability density function (PDF). A kinetic energy is then randomly sampled from this distribution. However, the differential cross-section in Eq. (8) is dependent on the incident antineutrino energy. Therefore, an antineutrino energy first needs to be sampled and then used to calculate the scattered electron kinetic energy PDF. To sample an antineutrino energy, the reactor antineutrino spectrum in Eq. (1) is folded with the total scat-

tering cross-section in Eq. (7) and treated as a PDF. An energy is then randomly sampled from the distribution. This sampled energy is then be used to calculate the differential scattering cross-section PDF. Once the antineutrino and scattered electron energies are known, the scattering angle can be calculated via energy and momentum conservation as in Eq. (12). Written in another form, this amounts to

$$\theta = \cos^{-1} \left(\sqrt{\frac{T_e(m_e + E_{\bar{\nu}_e})^2}{2m_e E_{\bar{\nu}_e} + T_e E_{\bar{\nu}_e}^2}} \right), \quad (17)$$

where θ represents the angle between the incident antineutrino and the scattered electron as shown in Fig. 19.

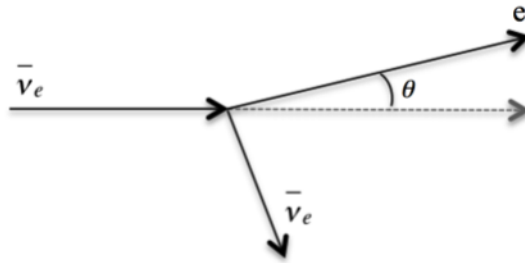


Fig. 19. Diagram of antineutrino-electron elastic scattering.

In spherical coordinates, the direction of a particle can be completely specified by the polar angle (θ) and the azimuthal angle (ϕ). Therefore, for the ease of calculating a direction of travel from the scattering angle, the incident antineutrinos are assumed to all be traveling in the $+Z$ direction (from the bottom to the top of the detector), such that the scattering angle corresponds to the polar angle, shown in Fig. 20.

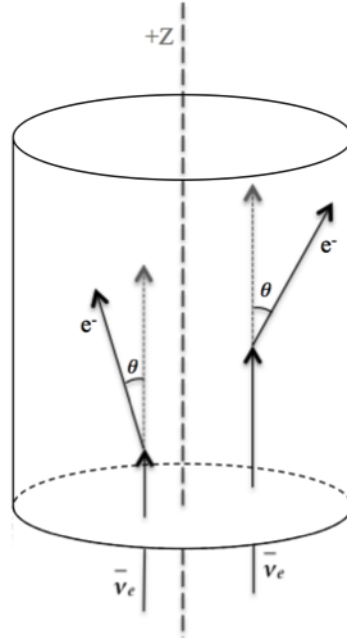


Fig. 20. Diagram of antineutrinos travelling in the $+Z$ direction, such that electron scattering angle corresponds to the polar angle.

The azimuthal angle is then determined by randomly sampling a value from 0 to 2π . With the polar and azimuthal angle, a unit vector can be calculated to represent the direction of the particles using the standard spherical to Cartesian transformation. Antineutrinos constrained to entering the bottom of the detector and traveling in the $+Z$ direction is of course nonphysical, the detector will be placed upright and thus antineutrinos from the Perry reactor will enter the sides of the detector. Although nonphysical, it demonstrates the basic principles of directionality being investigated here. In the future, the direction of the incident antineutrinos could be changed to a more realistic direction.

The steps outlined above were written in the form of a ROOT script and the code can be found in Appendix B. To demonstrate the generator, 10,000 events with

the reactor spectrum given in Eq. (1) and with the typical mid-cycle PWR fissioning percentages were produced and the results are shown in Fig. 21 and 22. Fig. 21 represents the reactor antineutrino spectrum folded with the total scattering cross-section. Notice its similarity to Fig. 13. Fig. 22 shows both the sampled electron kinetic energy as well as the scattering angles for the 10,000 events. Both plots resemble their expected distributions in Fig. 14 and 15.

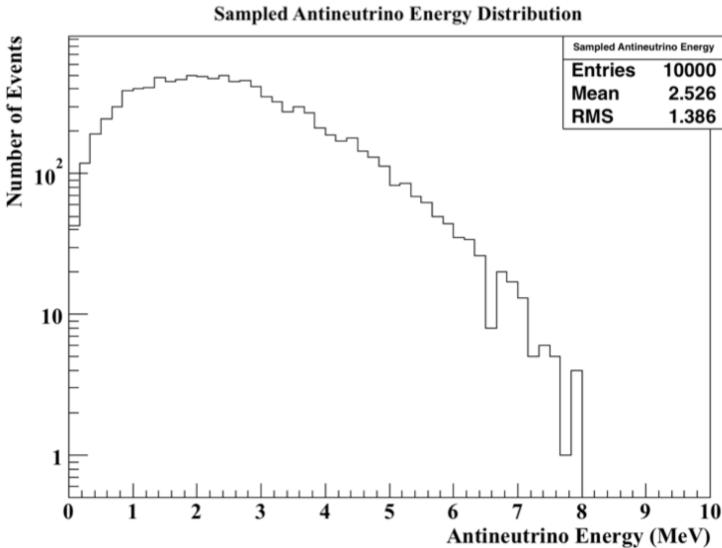


Fig. 21. Plot of the sampled antineutrino energies from the event generator.

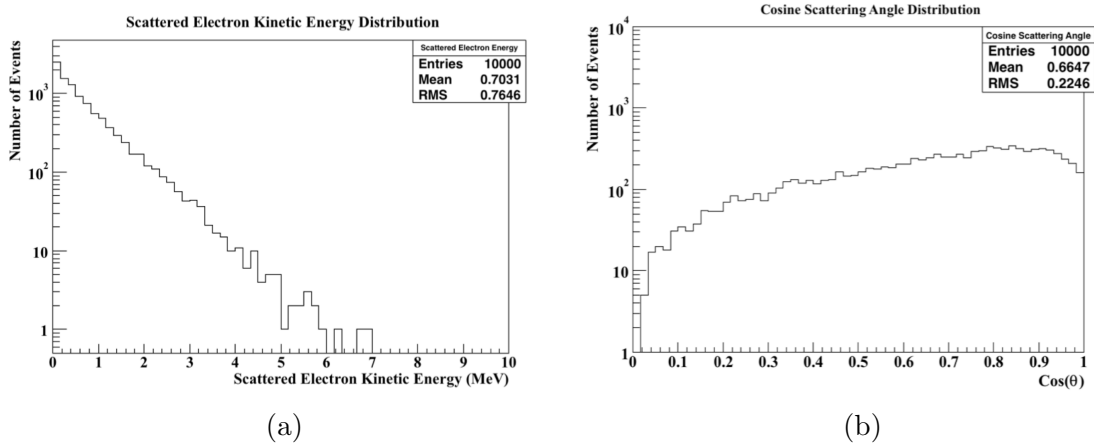


Fig. 22. (a) Plot of the sampled scattered electron kinetic energies. (b) Plot of the cosine of the scattering angles.

It is worth noting that the generator shown in Appendix B first samples an electron energy and then calculates the scattering angle. This process could very well be reversed, in which the scattering angle is sampled from the differential cross-section as a function of the cosine of the scattering angle given in Eq. (13) and then used to calculate the scattered electron energy with Eq. (12). To ensure no difference between the methods, a second generator employing this method was written and the results compared to the original generator. No differences were observed. The original generator was used because it was significantly faster in its computation, mainly due to the complexity of the differential cross-section as a function of scattering angle in Eq. (13). In addition to the four isotope energy spectrum given by Eq. (1), the generator also includes the option to use a three isotope spectrum from a study done at Virginia Tech, a monoenergetic spectrum, a user defined spectrum, and the IsoDAR spectrum.

5.2.1 Comparison to IsoDAR

To ensure the event generator was working properly, it was compared to results from the IsoDAR experiment [29]. A collaborator on the IsoDAR experiment provided the IsoDAR data [42]. The IsoDAR antineutrino energy spectrum, shown in Fig. 9 in Section 2.4, was incorporated into the generator and folded with the total scattering cross-section. The IsoDAR experiment imposes a 3 MeV threshold to the scattered electron kinetic energy, and thus this was included in the generator for comparison. Fig. 23 and 24 show the comparison of the IsoDAR generator to the newly constructed generator.

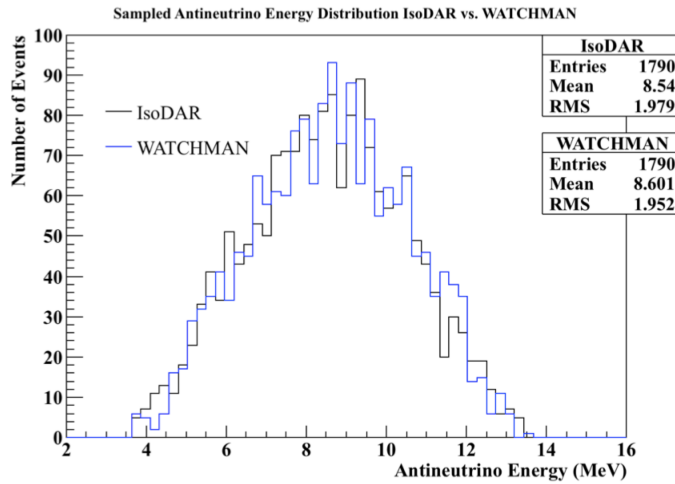


Fig. 23. Plot of the sampled antineutrino energy distribution from the IsoDAR spectrum using the IsoDAR generator (black) and the generator created for the WATCHMAN detector (blue). The distribution represents the antineutrinos that interacted (the energy spectrum folded with the scattering cross-section).

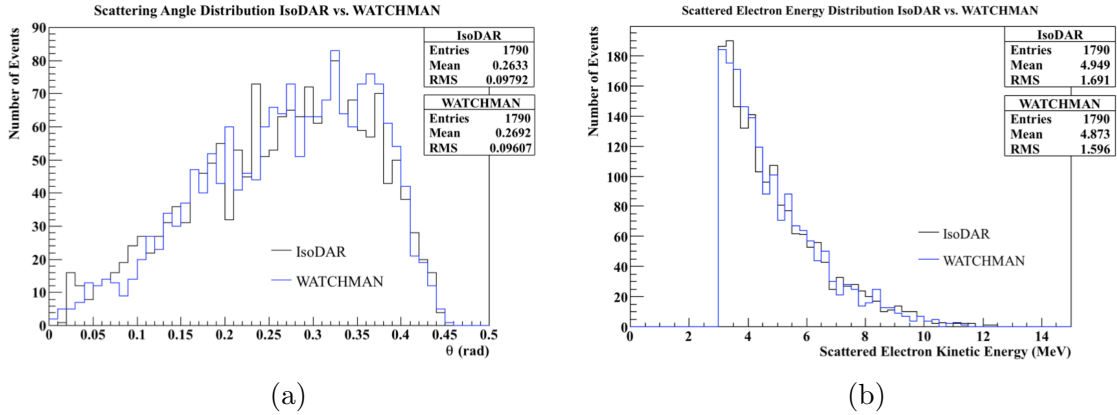


Fig. 24. Plot of (a) the scattering angle distribution and (b) the electron energy distribution from the IsoDAR spectrum using the IsoDAR generator (black) and the generator created for the WATCHMAN detector (blue). Notice the 3 MeV threshold in the electron energy distribution.

The data produced by the generator created for this research was within 3σ of the provided IsoDAR data for each bin in Fig. 23, 24a, and 24b. The uncertainty in the counts for each bin were assumed to follow Poisson statistics and thus follow the square root of the counts. This assumption is valid due to the random sampling done in the generators. Therefore, the newly constructed generator was deemed acceptable and was ready to be implemented into a WATCHMAN simulation package.

5.3 Monte Carlo Simulations

In this work, simulations were performed with GEANT4 to model antineutrino-electron scattering interactions in the WATCHMAN detector. GEANT4 (GEometry ANd Tracking) is a Monte Carlo particle transport toolkit, maintained by the GEANT4 international collaboration, used to simulate the passage of particles through matter [43]. It has been utilized in numerous applications in the fields of high energy, nuclear, and accelerator physics as well as medical and space science [43]. GEANT4 provides an object-oriented set of tools for detector simulations in-

cluding geometry, materials, fundamental particles, tracking, electromagnetic fields, detector response, run, event and track management/storage, visualization, and user interface [43]. The toolkit also includes an extensive set of physics processes to handle various particle interactions over broad energy ranges [43]. GEANT4 is the successor of the FORTRAN-based GEANT series developed by CERN, and is now completely written in the C++ programming language [43].

This work utilized a preexisting GEANT4 simulation package developed for the WATCHMAN project. The simulation contains all relevant physics processes such as particle generation and transport, Cherenkov physics, optical photon production and transport, PMT sensitivity, digitization, and timing [16]. Detailed detector geometry, materials, and optical properties are also included. The package is named Reactor Monitoring Simulation (RMSim) and is currently maintained by the University of California, Davis.

As was discussed in Section 5.2, particles are generated in GEANT4 through the use of event generators. Because WATCHMAN will be primarily searching for IBD events, RMSim did not include antineutrino-electron scattering generators. Therefore, the newly created event generator was incorporated into RMSim in order to model scattering events in WATCHMAN. For each simulated event, the code is directed to the generator where it will define the specified particle (mass, charge, etc.), assign a starting position within the geometry, and then assign a kinetic energy and momentum direction. The simulation will store all relevant data accumulated during each run such as energy deposition, triggered PMT times, locations, and photoelectron production, as well as the initial energy, position, and direction of the starting particles.

Before the antineutrino-electron scattering generator was used within RMSim, a benchmark study was done to ensure a simple generator could function within the

simulation. To begin, 20,000 5 MeV electrons were generated evenly throughout the detector volume and given isotropic directions. Fig. 25 displays the results for the initial positions and directions of the simulated electrons.

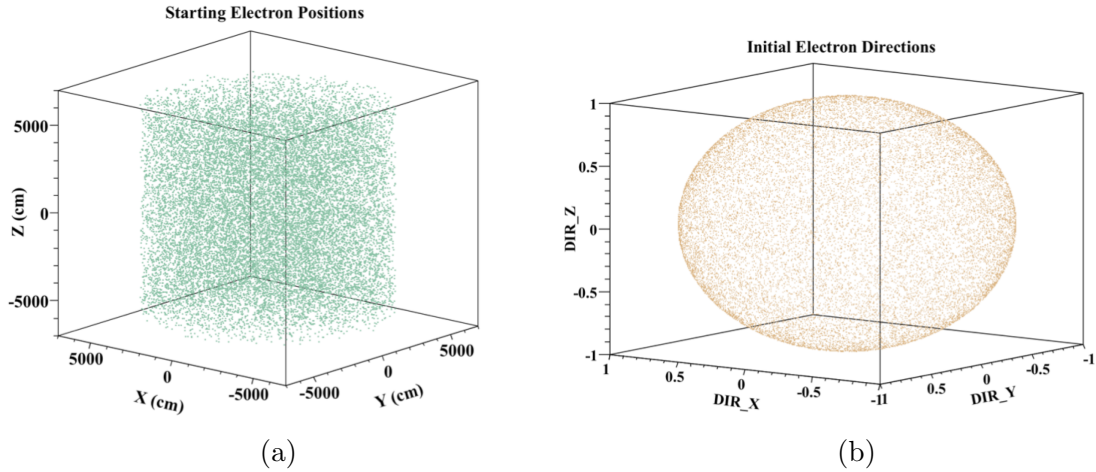


Fig. 25. (a) Plot of the starting positions for electrons evenly distributed throughout the detector volume. (b) Plot of the initial electron directions where the points represent unit vectors from the origin.

From the plots, the simple generator in RMSim was able to successfully initiate the electrons evenly throughout the volume and in isotropic directions. As an example of collected data, Fig. 26 shows the photoelectron production in the surrounding PMTs as well as the number of PMTs hit for each of the 20,000 simulated events. As an example of visualization, Fig. 27 shows a picture of an event in RMSim. In the picture, the blue lines represent the Cherenkov light produced as a result of the scattered electron and the yellow, orange, and red dots represent the timings of the hit PMTs. Notice the ring shape observed in the hit PMTs.

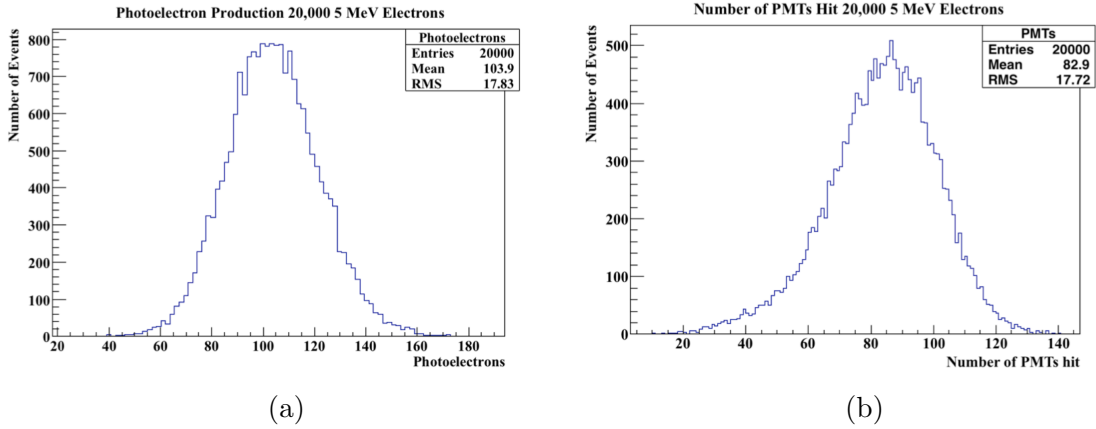


Fig. 26. (a) Histogram of the total photoelectrons produced per event. (b) Histogram of total number of PMTs hit per event.

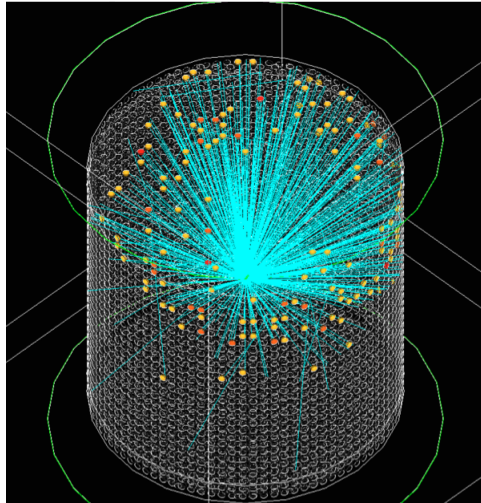


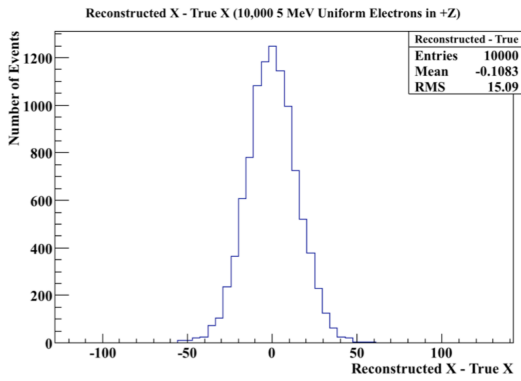
Fig. 27. Visualization of an electron scattering event in WATCHMAN using RM-Sim. The blue lines represent Cherenkov light and the yellow, orange, and red dots correspond to the hit PMT times.

5.3.1 Event Reconstruction with BONSAI

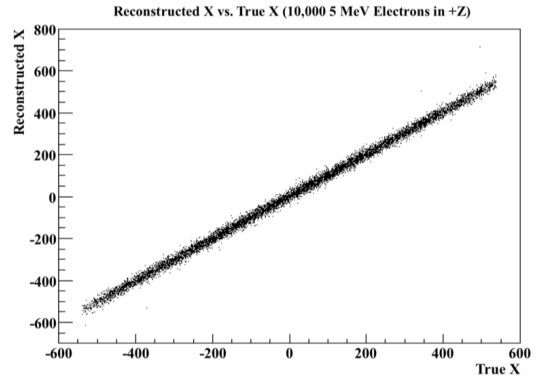
As was discussed in Section 3.4, once an event is triggered in WATCHMAN, the event needs to be reconstructed in order to determine the vertex (interaction loca-

tion), direction, event time, and energy. In the case of antineutrino-electron scattering, the direction of the Cherenkov cones need to be reconstructed to determine the direction of the incident antineutrino flux. The reconstruction software used for this project is known as BONSAI (Branching Optimization Navigating Successive Annealing Iterations) and is currently maintained by the University of California, Irvine [44]. The software was developed for use with Super-K and has since been updated for use with WATCHMAN. BONSAI performs a maximum likelihood fit to the timing residuals as well as the dark noise background for each iterated track (vertex, direction, time, and energy) [44]. The track with the largest likelihood is then chosen as the reconstructed track [44]. Dark noise refers to the noise associated with the small electric current that flows in the PMTs even when no light is impinging the photocathode. RMSim was designed to include dark noise, however at the time of this work, it was not functioning. Therefore, dark noise was not included in any simulations and its effect on event reconstruction was not investigated. In addition to the reconstructed track, the BONSAI software provides the likelihood and goodness of fit parameters used in the fits. These parameters can be used to reject poorly reconstructed events.

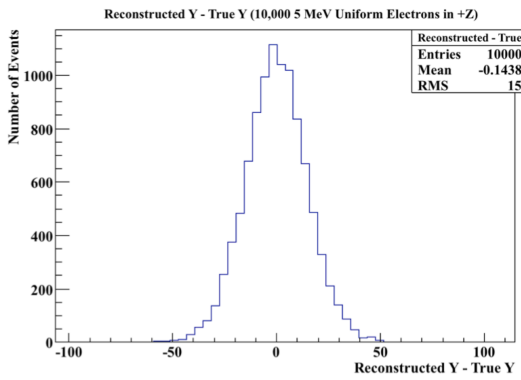
To benchmark BONSAI, a simulation was run in RMSim with 10,000 5 MeV electrons evenly distributed throughout the detector all travelling in the $+Z$ direction. Fig. 28 shows the results of the vertex reconstructions compared to the true vertices. Fig. 29 shows the results of the directional reconstruction compared to the true directions.



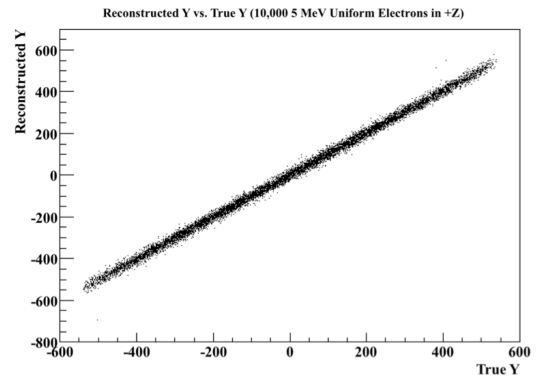
(a)



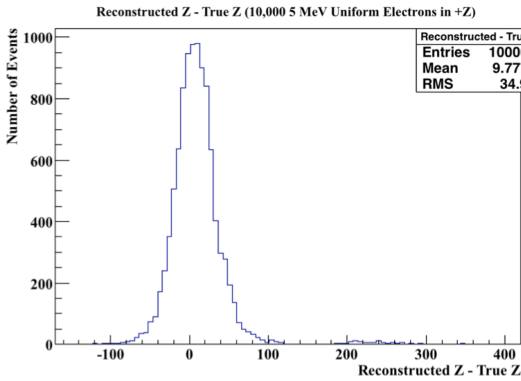
(b)



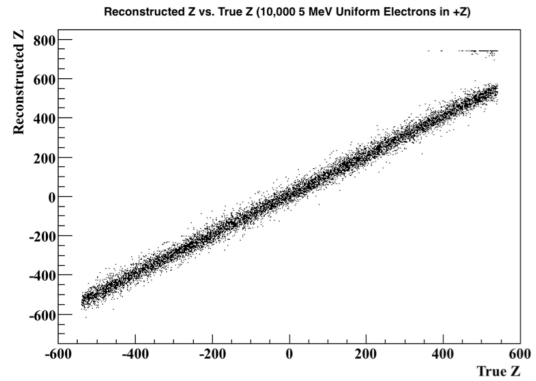
(c)



(d)



(e)



(f)

Fig. 28. Plots of the differences between the reconstructed and true x , y , and z vertex coordinates in cm (shown in (a), (c), and (e)). Plots of the reconstructed vs. true x , y , and z vertex coordinates in cm (shown in (b), (d), and (f)).

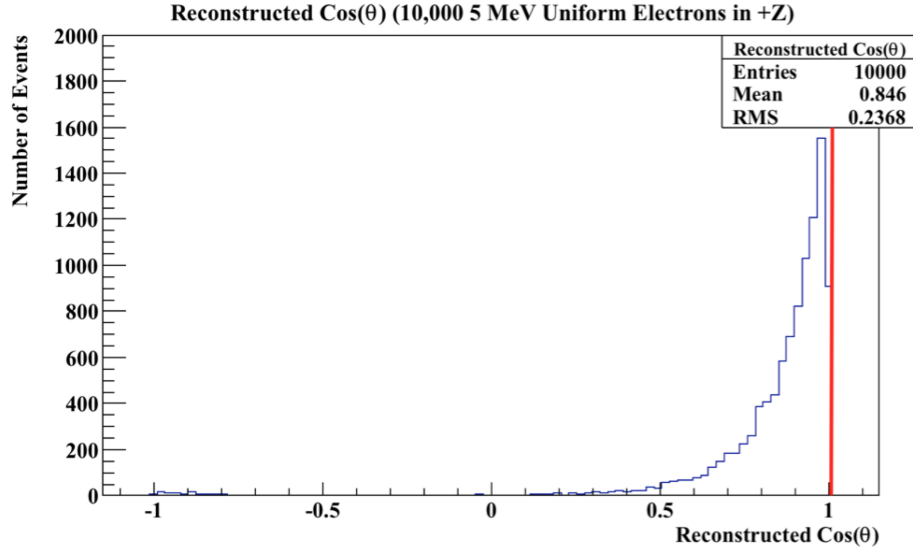


Fig. 29. Plot of the directional reconstructions (cosine of the polar angle) from BONSAI (shown in blue) compared to the true directions (shown in red).

The root mean square (RMS) values in Fig. 28a and 28c indicate that BONSAI was able to accurately reconstruct the X and Y vertex coordinates with an uncertainty of about 15 cm. Fig. 28b and 28d demonstrate that no matter where in the detector, the X and Y reconstructions are close to the true values. The Z reconstruction has a much larger uncertainty (~ 35 cm) and a few events completely fail near the top of the detector (notice the small grouping of events between 200 and 300 cm in Fig. 28e). This grouping of events correspond to events that reconstructed above the detector, as shown by the small grouping of events with a reconstructed Z of 800 cm in Fig. 28f.

In Fig. 29, the directional reconstruction is smeared away from the truth value ($= 1$) in an exponential fashion (recall the exponential shape of the Super-K reconstruction) and has a mean value of about 0.85. A few events are actually observed near $\cos(\theta) = -1$, which correspond to the failed Z reconstructions discussed above. Instead of an event near the top of the detector traveling in $+Z$, BONSAI reconstructed

an event above the detector traveling in $-Z$.

To observe the energy dependence of the reconstruction, 5,000 uniform electrons traveling in $+Z$ were simulated with varying energies. The results for the directional reconstruction are shown in Fig. 30. The reconstructions for electrons with energy of 2 MeV or greater exhibit similar behavior and thus there is no apparent dependence on energy above 2 MeV. For each of these energy values, the truth value of $\cos(\theta) = 1$ is exponentially smeared to about $\cos(\theta) = -0.2$, below which a number of completely failed ($\cos(\theta) \approx -1$) reconstructions are found. At 1 MeV, the exponential behavior is evident only to about $\cos(\theta) = 0.2$ and has a much shallower slope. Below $\cos(\theta) = 0.2$, there exists a fairly constant number of reconstructions down to $\cos(\theta) = -1$. As the energy is decreased, the number of Cherenkov photons produced decreases, and thus the number of total PMTs hit and the photoelectrons produced decreases. As a result, the ability to successfully reconstruct the event decreases.

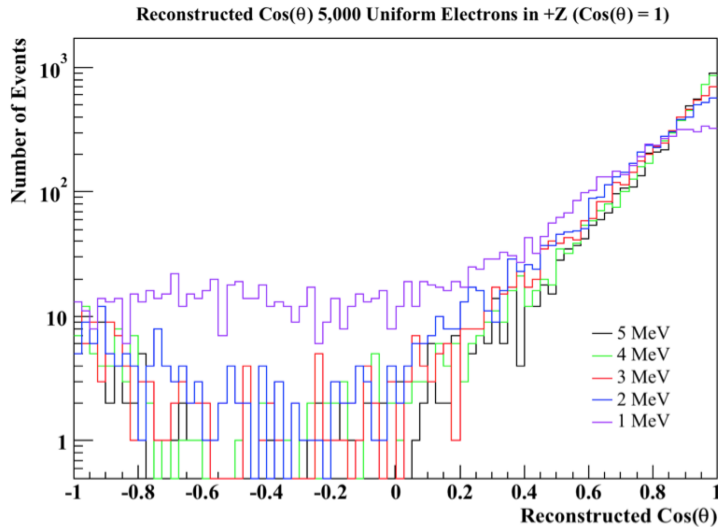


Fig. 30. Plot of the reconstructed cosine of the scattering angle for electrons generated uniformly within the detector volume all travelling in the $+Z$ direction.

In the physical WATCHMAN detector, a lower level threshold will be applied to reduce low energy background noise in the signal. In RMSim, this is represented as a trigger mechanism using the total number of photoelectrons produced per event. If an event does not produce at least 16 total photoelectrons, the event is discarded and the detector is said to not trigger. Fig. 31 shows the number of total photoelectrons produced per event for the 5,000 electron events at various energies.

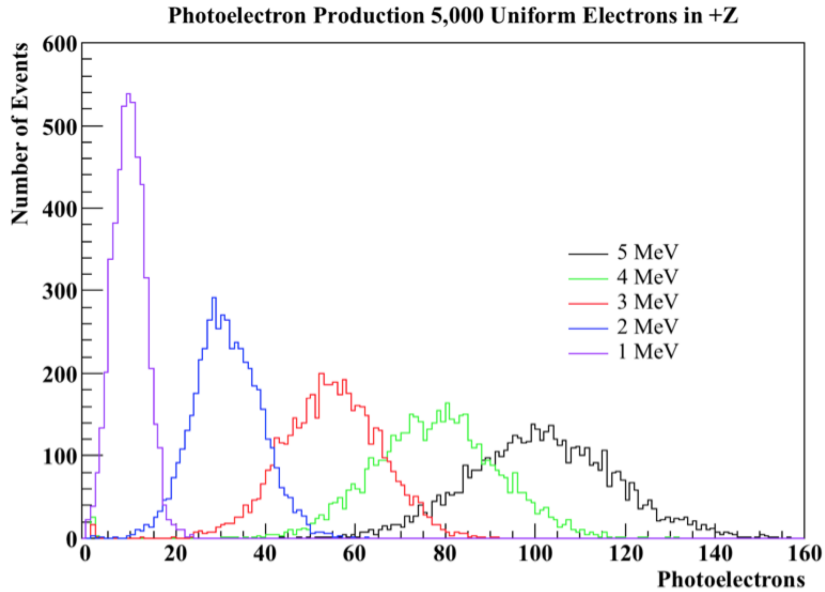


Fig. 31. Plot of the photoelectron production for electrons at various energies.

Most of the 1 MeV electrons produce less than 16 total photoelectrons and thus will not be able to trigger the detector (only a 4% detection efficiency). As the energy is increased to 2 MeV, the detection efficiency becomes about 98%, and above 3 MeV the detection efficiency becomes 100%. If the directional reconstruction is compared before and after the trigger mechanism is applied, no significant differences are expected at 2 MeV and above, because of the $\sim 100\%$ detection efficiency. However,

at 1 MeV, only 4% of the events will trigger. Because the reconstruction improves with the number of photoelectrons produced in the hit PMTs, it is expected that the 1 MeV events that survive the trigger (> 16 photoelectrons) will exhibit better directional reconstructions than the 1 MeV events that do not survive the trigger (< 16 photoelectrons). Fig. 32 demonstrates this effect. The proportion of events above $\cos(\theta) = 0.4$ before and after the 16 photoelectron trigger mechanism is applied are 82% and 95%, respectively. Although 96% of the total events are discarded, the directional reconstruction significantly improved with the trigger.

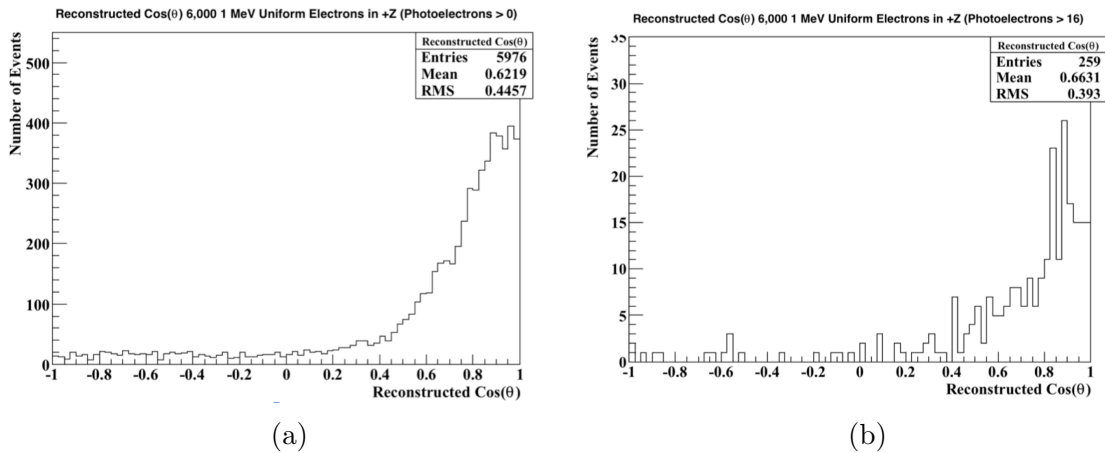


Fig. 32. Plot of the 1 MeV electron directional reconstructions before (a) and after (b) the trigger mechanism is applied. Although the trigger discards 96% of the events, the directional reconstruction improves.

5.3.2 Reactor Antineutrino-Electron Scattering

Once RMSim and BONSAI were shown to produce acceptable results, the reactor antineutrino-electron scattering generator was implemented and used to simulate one year of data (~ 1520 events). Again, the antineutrinos were assumed to enter the

bottom face of the detector and travel in the $+Z$ direction. Therefore, the incident antineutrino flux has a true direction of $\cos(\theta) = 1$, where θ represents both the polar angle and scattering angle. It is expected that the scattering angles of the electrons would follow the differential cross-section curve shown in Fig. 15. However, as was seen in the previous section, the BONSAI reconstruction will smear this distribution into an exponential.

As was discussed in Section 4.2.1, the dominant backgrounds in WATCHMAN will arise from cosmogenic radionuclide decays (again assuming no PMT radioactivity and radon contamination). It was also shown that the radionuclide background tended to create high-energy events, thus producing large numbers of photoelectrons (> 100) per event. The reactor antineutrino signal is in the low energy range (see Fig. 8), and thus will not produce large amounts of photoelectrons per event (see Fig. 31). Therefore to reduce the high-energy backgrounds, an upper level cut of 65 photoelectrons was imposed on the number of the photoelectrons detected, resulting in about 3530 total events per year (16% of the total before the cut). The same cut was then placed on the scattering signal.

The scattering angle distribution was organized into a histogram comprising of 80 bins from -1 to 1. The backgrounds were incorporated into the histogram following a flat $\cos(\theta)$ distribution. The 3530 background events were placed in randomly sampled bins, assuming a uniform PDF across all 80 bins. Due to the random sampling, statistical variations will exist from bin to bin. The statistical significance of the signal therefore depends on it being observable above the statistical variations in the background. Two methods were used to determine the statistical significance of the scattering signal and will be discussed in the next section.

To determine the effects of varied data acquisition times, the total signal was analyzed for six month, two year, and three year run times. Because the background

is assumed to follow Poisson statistics, the variation in the background is expected to follow the square root of the detected events. If the number of backgrounds is directly proportional to the acquisition time and the signal significance is directly proportional to the uncertainty in the backgrounds, it is expected that the signal significance will increase according to the square root of the acquisition time.

Also, due to statistical fluctuations in the signal, background, and detection processes, it is expected that the statistical significance will be normally distributed about some mean value. 64 one-year simulations were performed to determine the distribution of the statistical significances for a one-year run. The same data was then used to analyze 128 six-month simulations, 32 two-year simulations and 21 three-year simulations.

6. RESULTS AND DISCUSSION

6.1 One-Year Directional Reconstruction

A total of 1520 antineutrino-electron scattering events were simulated in the WATCHMAN detector, assuming an equal probability of interactions throughout the volume and that the incident antineutrino flux was traveling in the $+Z$ direction. The directional reconstructions (with a trigger of 16 photoelectrons) with and without an upper level cut at 65 photoelectrons are shown in Fig. 33. The 65 photoelectron cut discarded roughly 6.6% of the signal (as compared to 84% of the background). A total of 241 signal counts results in an approximate 16% intrinsic detection efficiency. The estimated 3530 background events were then incorporated into the signal, assuming a flat $\cos(\theta)$ distribution. The result is shown in Fig. 34 with a histogram comprising of 80 bins.

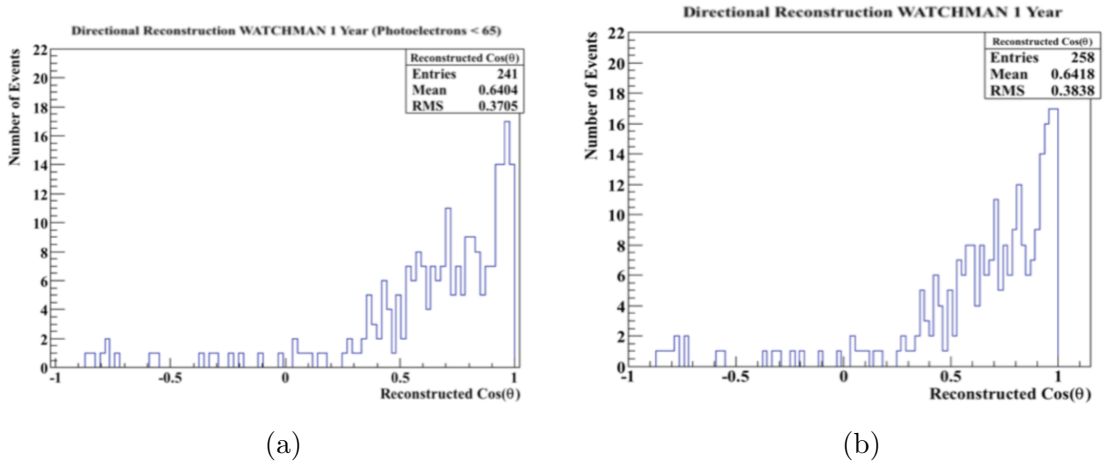


Fig. 33. Plot of the directional reconstruction for reactor antineutrino-electron scattering in WATCHMAN for one year with (a) and without (b) a 65 photoelectron cut.

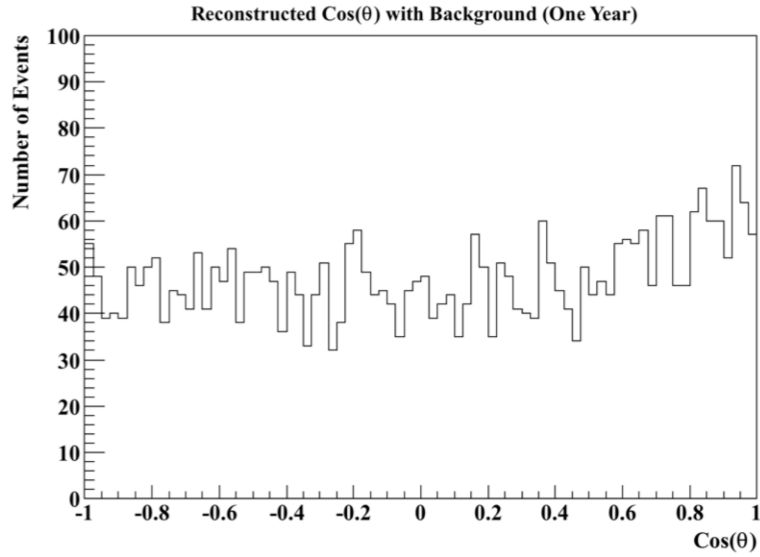


Fig. 34. Total signal (background plus scattering) in the WATCHMAN detector over one year.

From Fig. 34, the flat background is apparent and fluctuates around a value of about 44 events for each of the 80 bins. Above $\cos(\theta) = 0.5$, the counts slightly increase, according to the scattering signal peaking at a value of $\cos(\theta) = 1$. However, due to the somewhat large fluctuations in the background (ranging from 30 to 60 counts per bin), this result could be due entirely to the background fluctuations. One could imagine a case in which the background in all the bins above $\cos(\theta) = 0.5$ were to fall on the larger side, thus making it seem like there was a peak tending toward $\cos(\theta) = 1$. Therefore, a statistical analysis must be performed to determine how likely it is to observe the data given the uncertainty in the background.

6.1.1 Analysis and Statistical Significance Calculations

In order to compare the scattering signal with the uncertainty in the background, the background and signal must be fit. The background is assumed to be a flat distribution and thus a straight line can be used to fit the background. Because the

scattering signal is only expected to be significantly present in the right half of the distribution (0 to 1), the counts in the left half of the distribution can be assumed to be purely from background. Therefore, using the MINUIT fitter in ROOT, a straight line was fit to the background from -1 to 0, and was then extended to +1 (the background from -1 to 0 should not differ from 0 to +1). The scattering signal is expected to follow an exponential curve, as was shown in Fig. 29, and thus a constant plus an exponential of the form

$$y = A + Be^{Cx}, \quad (18)$$

was used to fit the signal plus background data. A , B , and C represent the free floating parameters that are fit to the data. When data is fit in ROOT, error estimates for the floating parameters are automatically provided and are carried through calculations. The background fit was then subtracted from the signal plus background fit to determine the curve describing the scattering signal. Fig. 35 below shows the total signal with all fits included. The figure also includes the background without the addition of the scattering signal for comparison.

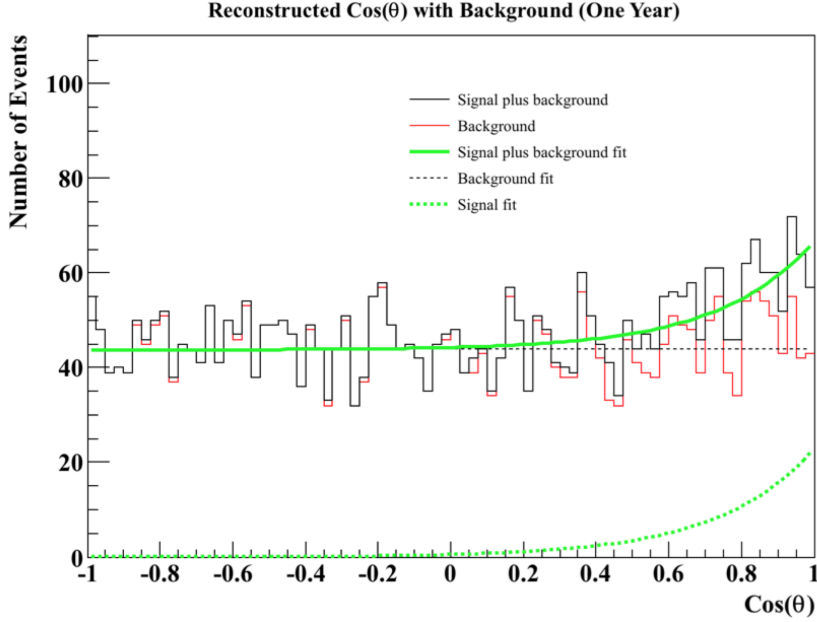


Fig. 35. Plot of the total one-year scattering signal with background and fits included.

To determine the statistical significance of the scattering signal, the total number of signal counts over a specified domain is divided by the uncertainty in the total number of background counts over the same domain. This can be written as

$$\text{Significance } (\sigma) = \frac{\int_a^b \text{SF } d \cos \theta}{\delta \left(\int_a^b \text{BF } d \cos \theta \right)}, \quad (19)$$

where SF is the signal fit function, BF is the background fit function, and $\delta(x)$ represents the uncertainty in x . The calculation will determine how many standard deviations the signal is above the background. The 3σ and 5σ significance levels represent 99.7% and 99.9999% probabilities that the signal was not a result of statistical fluctuations in the background, respectively.

The significance is highly dependent on the bounds used in Eq. (19). For example, if the bounds were taken from -1 to 0, the significance would be 0, because there is

no signal in this domain. The signal would be present if the bounds were taken as 0 to +1, however a significant amount of background (and thus a significant amount of uncertainty) exists within this domain. The calculation of the signal significance then becomes an optimization of keeping as much signal while cutting out as much background. This was done by iterating through different $\cos(\theta)$ bounds in the integrals and determining where the maximum significance is achieved. The bounds began at 0 to 1 in order to enclose most of the scattering signal, and the left bound was then incremented by 0.01 until it reached 0.99. The significance was determined for each iteration. The uncertainty in the background integral was determined using built in functions in ROOT. The significances were plotted as a function of the left integral bound (see Fig. 36) and the maximum of the curve was found.

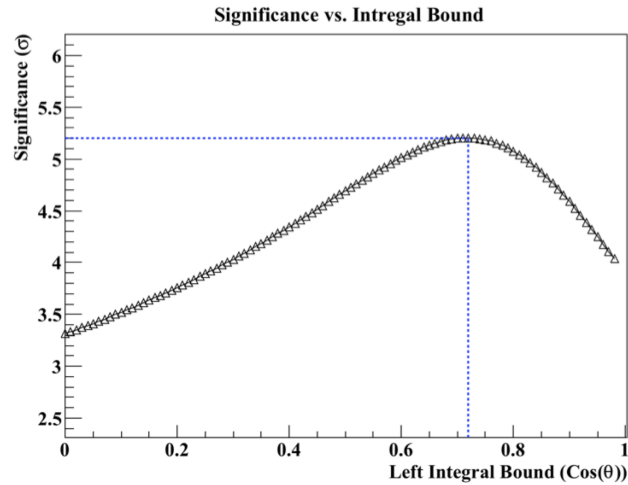


Fig. 36. Plot of the signal significance as a function of the left integral bound used in Eq. (19).

For the data shown in Fig. 35, a maximum signal significance of about 5.2σ was observed when the $\cos(\theta)$ cut was placed at 0.72. In the real WATCHMAN detector

however, only a single predefined $\cos(\theta)$ cut will be used. Due to statistical variations in each data set, the best $\cos(\theta)$ cut will fluctuate. To determine the best overall cut, several one-year simulations were performed and the best $\cos(\theta)$ cuts for each simulation were stored. The results were averaged to determine the optimal $\cos(\theta)$ cut for any given data set. The optimal $\cos(\theta)$ cut was determined to be 0.74. This value was used in all calculations.

Instead of fitting all three parameters in Eq. (18), it is suggested that a calibration source, such as an electron accelerator, could be used with WATCHMAN in order to determine the exponential slope parameter, C . In this research so far, the incident antineutrinos have been assumed to be traveling in the $+Z$ direction and thus it is expected that the scattered electrons will travel close to $+Z$ as well. Therefore, electrons accelerated to typical antineutrino-electron scattering energies through the detector in the $+Z$ direction will replicate antineutrino-electron scattering events. Thus the reconstruction curve for the accelerated electrons should exhibit the same exponential slope as that of the expected antineutrino-electron scatter reconstruction curve. The electron accelerator allows the detector to be calibrated in the sense that the exponential slope of the reconstructed directions can be determined beforehand. To simulate the scenario of an electron accelerator calibration source, a large amount of electrons traveling in $+Z$ with typical antineutrino-electron energies were simulated in the WATCHMAN detector. The directional reconstruction distribution was then fit to determine the exponential slope. See Fig. 37 for a plot of the reconstructed scattering angles and the exponential fit. The exponential slope was determined to be 3.4 and was used to fix the C parameter in Eq. (18).

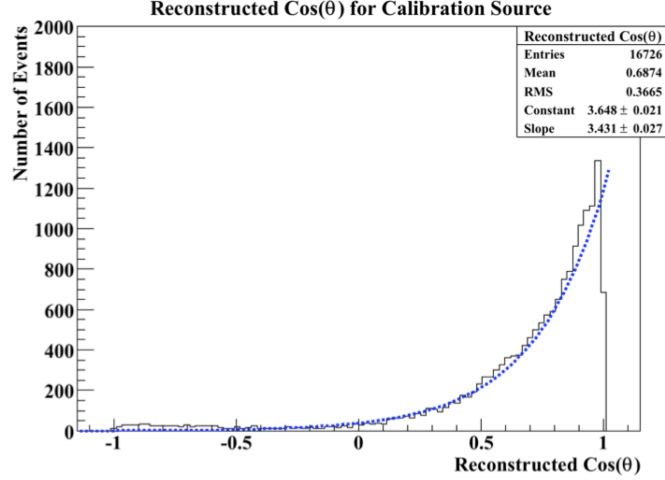


Fig. 37. Plot of directional reconstructions assuming a calibration source at WATCHMAN.

If the entire distribution in Fig. 35 is shifted to -2 to 0, then the factor B in

$$y = A + Be^{3.4x}, \quad (20)$$

will represent the y -intercept of the exponential fit. In this case, the y -intercept is directly proportional to area beneath the curve, hence the number of detected scatters. The fractional uncertainty in the number of detected scattering events is therefore given by the fractional uncertainty in the y -intercept. When ROOT fits Eq. (20) to the data, it will propagate the uncertainty in A (the background offset) into the uncertainty in B , and thus the significance can be easily calculated by

$$\text{Significance } (\sigma) = \frac{B}{\delta B}, \quad (21)$$

where δB represents the uncertainty in B .

The fitting and statistical significance calculations for the one-year data sets were done in the form of a ROOT program, which can be found in Appendix C. The code

assumes the RMSim simulation output has already been sent through the BONSAI reconstruction software. It will incorporate the background into the reconstructed $\cos(\theta)$ distribution, perform all the fitting (fitting as well as fixing the exponential slope parameter), and produce similar plots to Fig. 33 and Fig. 35.

6.2 Multiple One-Year Directional Reconstruction

Due to random fluctuations in the antineutrino-electron scattering signal, background events, and detection processes, the statistical significance for an individual one-year run will also be random. Due to the Central Limit Theorem however, it is expected that the significances will be normally distributed about a mean value when enough one-year data sets are accumulated. To demonstrate this effect and to determine the average significance, 64 one-year reactor antineutrino-electron scattering data sets were simulated in the WATCHMAN detector. Backgrounds were incorporated into each of the one-year data sets and both fitting methods were used to calculate the signal significance. Fig. 38 displays the distributions of significances for the two different methods for the 64 one-year simulations. Fig. 39 displays quantile-quantile (QQ) plots of the data to demonstrate the normality of the distributions. The code used to analyze the data and produce these plots (in ROOT) is shown in Appendix D.

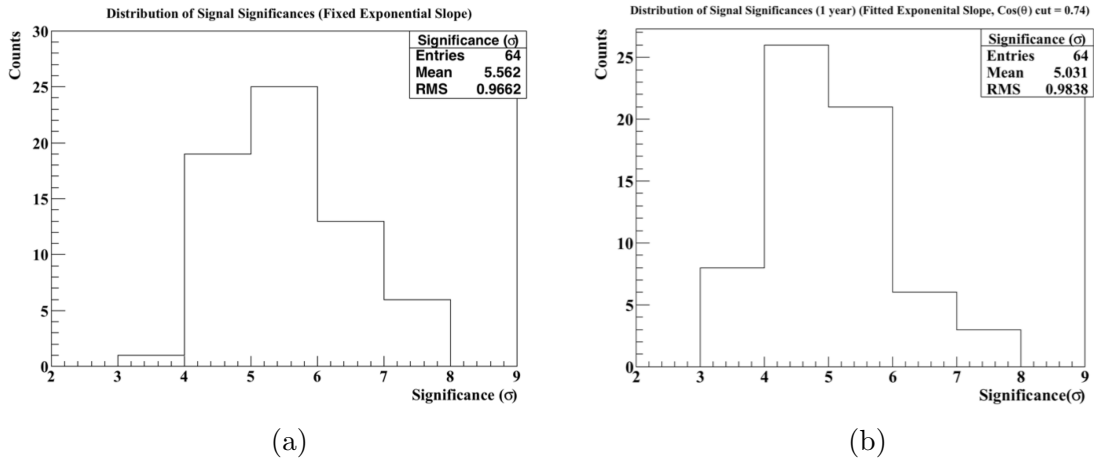


Fig. 38. Distributions of the signal significances for 64 one-year simulations calculated by with (a) and without (b) calibration.

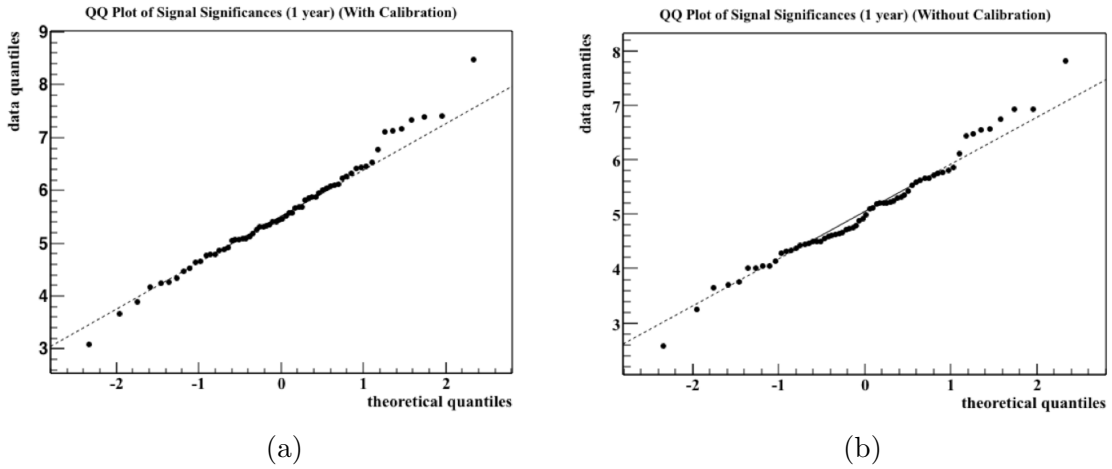


Fig. 39. QQ plots for the 64 signal significances with (a) and without (b) calibration.

To report a discovery in new particle physics experiments and rare event particle detection (such as antineutrino detection), it has become convention that a signal significance of at least 5σ is required [45]. A 3σ significance is typically regarded as evidence, but more data is needed to be certain. There have been instances in

which experiments have reported a 3σ significance, but were later disproved with the accumulation of more data [45]. In the safeguards regime however, the IAEA aims to only verify declared activities (or verify the absence of undeclared activities). Typically these verifications do not rely on a single measurement from one piece of equipment but from a collection of measurements. Directionality, for example, could be complemented with satellite imagery and field measurements. Therefore, in regards to safeguards, a 3σ significance may be acceptable. From Fig. 38, an average signal significance of 5σ is expected over the one-year of data acquisition without the use of a calibration source. The calibration source increases the one-year significance to about 5.6σ . In Fig. 39, both distributions are observed to follow normal distributions, with only slight deviations towards the larger significances. With the 5σ confidence, these preliminary results conclude that reactor antineutrino directionality can be feasible in a kiloton scale water Cherenkov detector 13 km away from a 3.758 GW(th) reactor with one year of data, an assumed known direction, and the current background estimates.

6.3 Directional Reconstruction for Various Acquisition Times

For the sake of completeness, the 64 one-year data set was also used to determine the signal significance after six months, two years, and three years. The distributions for each acquisition period are shown in Fig. 40. In each instance, the significances were calculated with and without the use of a calibration source. For each acquisition time in Fig. 40, the use of a calibration source slightly increases the average significance, as expected. The Gaussian shape of the distributions seems to degrade as the acquisition time is increased, however this is just due to the fact that a smaller number of data points are present. If more data points were collected, it is expected that the Gaussian shape would be recovered.

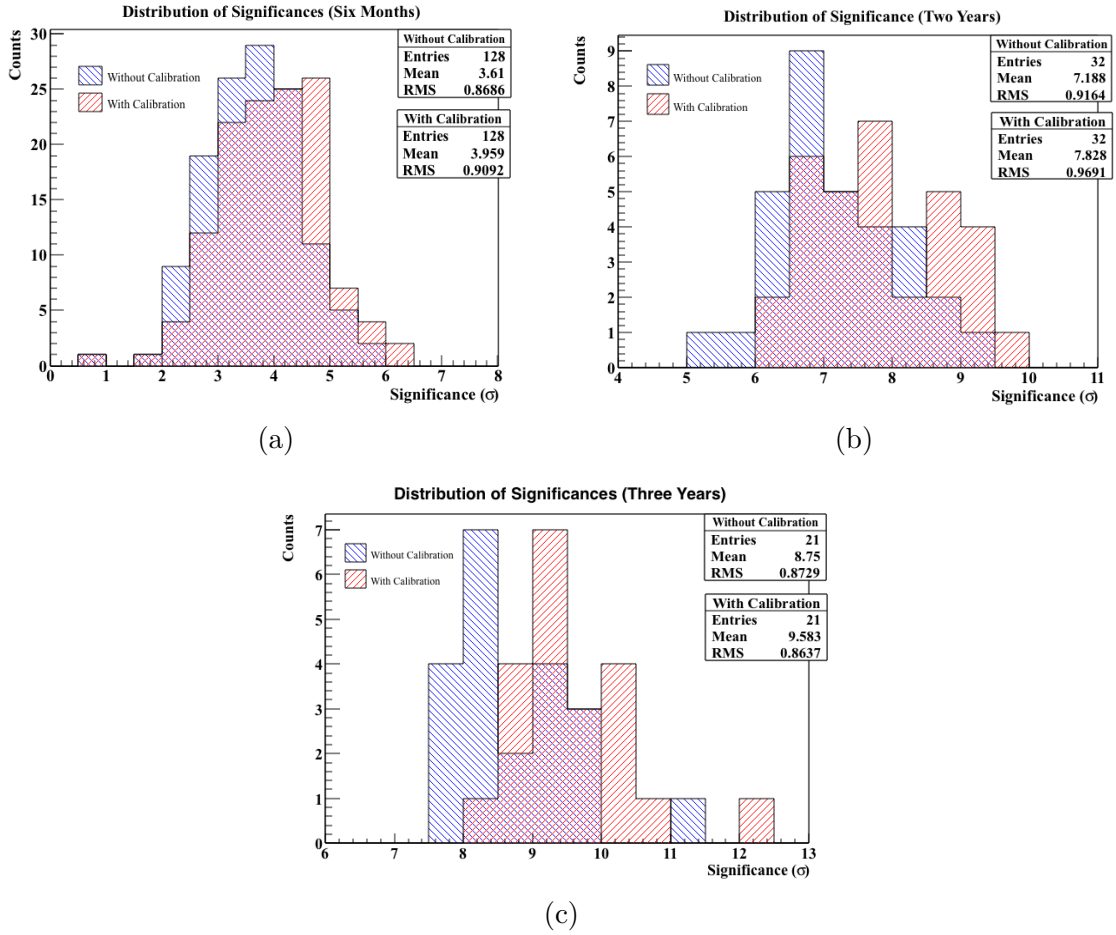


Fig. 40. Distributions of the signal significances for (a) six-month acquisitions, (b) two-year acquisitions, and (c) three-year acquisitions.

The signal significances are also plotted as functions of their acquisition periods in Fig. 41 and listed in Table 6. Because the significance distributions follow a normal distribution, the uncertainties associated with each value is about 1σ . The blue and green horizontal lines correspond to the typical 3σ and 5σ detection thresholds. As discussed earlier, the uncertainty in the background is expected to follow the square root of the number of counts. Background collection in the detector is assumed to be linear (3530 counts in one year means 7060 counts in two years, etc.) and thus

the significances should be proportional to the square root of the acquisition time. To demonstrate this effect, the data was fit with a function of the form

$$y = A \cdot \sqrt{x}, \quad (22)$$

where A is a free parameter that will be fit to the data.

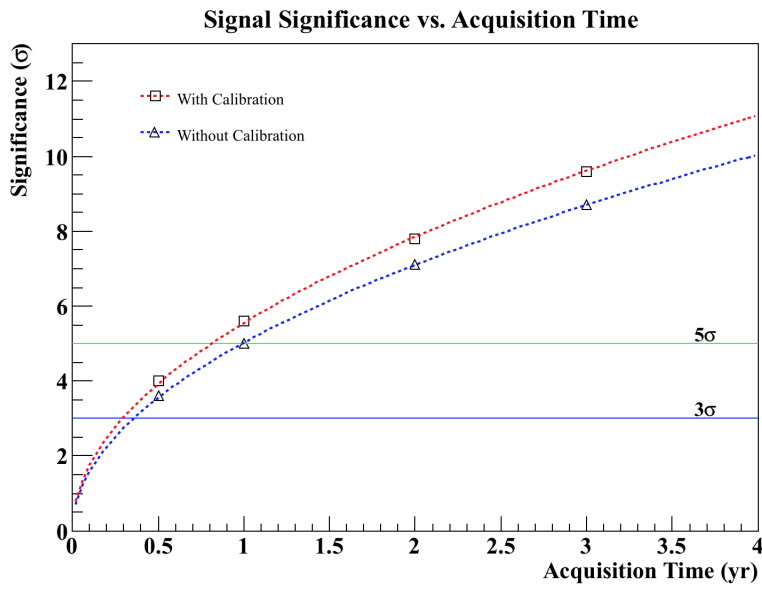


Fig. 41. Plot of the signal significances as a function of the acquisition time. The blue and green lines represent the typical 3σ and 5σ detection thresholds.

Table 6

Signal significances for various acquisition times with and without the use of calibration.

Acquisition Time (yr)	Signal Significance (σ)	
	Without Calibration	With Calibration
0.5	3.6	4.0
1	5.0	5.6
2	7.2	7.8
3	8.8	9.6

From Fig. 41, the significances follow the \sqrt{x} behavior both with and without the calibration source. Without the calibration source, the 3σ and 5σ thresholds can be reached with about 4.5 and 12 months of data, respectively. The calibration source reduces the time needed to achieve the 3σ and 5σ thresholds to about 4 and 10 months, respectively.

6.4 PMT and Radon Backgrounds

So far in this research, the backgrounds due to the PMT gammas and radon contamination have been assumed to be insignificant compared to the cosmogenic radionuclides, and thus neglected from the background estimates. With this assumption, antineutrino directionality may be feasible in the WATCHMAN detector in one year. However, preliminary PMT studies done by the WATCHMAN collaboration and radon studies done by the Sudbury Neutrino Observatory (SNO) collaboration indicate that both the PMT gammas and radon will be significant contributors to background [16,46].

As discussed in Section 4, the decays of ^{40}K and ^{208}Tl in the PMT glass result in high-energy gamma rays that can mimic the antineutrino-electron scattering signal. Typically, these gammas will interact in the buffer region between the PMT support

structure and fiducial volume. However, due to uncertainty in event reconstruction, some events will be reconstructed within the fiducial volume and contribute to background. To investigate this effect, 840,000 PMT gamma rays were simulated in RMSim and a plot of the distance from the reconstructed vertex to the nearest PMT is shown by the black curve in Fig. 42. The simulation assumed that the buffer region was extended to 1.5 m thick instead of 1 m as stated in Section 1.4. From the figure, a significant amount of events are reconstructed inside the fiducial volume (> 1.5 m away from the PMTs).

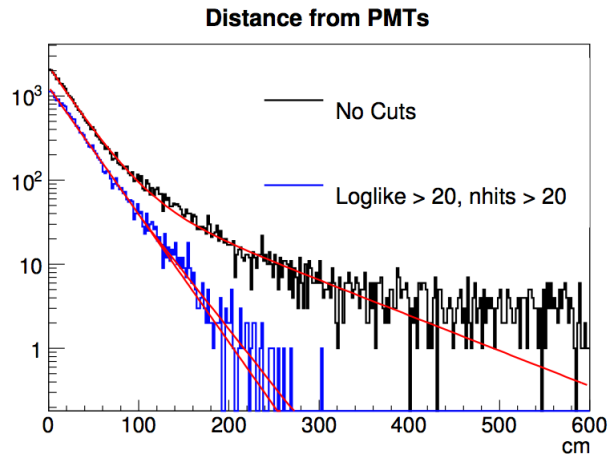


Fig. 42. Plot of the distance from the reconstructed event vertex to the nearest PMT.

In hopes to reduce the low-energy and poorly fit events, cuts were placed on the number of PMTs triggered and the log likelihood function. Recall from Section 5.3.1 that the likelihood variable represents the goodness of fit and can be used to reject poorly reconstructed events. Only events with > 20 triggered PMTs (nhits) and > 20 log likelihood (loglike) are shown by the blue curve in Fig. 42. The cuts remove a

significant amount of events that reconstructed within the fiducial volume. All that is left is an exponential distribution decreasing away from the PMTs. Although several events still exist within the fiducial volume (> 1.5 m), this is a promising result for antineutrino-electron scattering because it indicates that the PMT gamma rays can be almost entirely removed using a large enough buffer region. The blue curve was fit with a single exponential function with and without an additional shallower exponential component. If the true distribution has a shallower exponential component, then more background events will reconstruct within the fiducial volume. However, not enough events were simulated to determine if the second component is significant and not enough time was available to simulate more particles.

One way to decrease the number of background events due to PMT gamma rays is to simply use smaller PMTs or PMTs with a higher glass purity. Another option is to increase the size of the buffer region by reducing the size of the fiducial volume. A smaller fiducial volume, however, will significantly reduce the number of detected antineutrino-electron scattering events. Therefore, the acquisition time must be increased. A study was done to investigate the effects of using different types of PMTs and reducing the fiducial volume from 1000 m^3 to 225 m^3 and 187 m^3 . The total number of background events (all the backgrounds listed in Table 5 as well as PMT gammas) over a 5 year period for the 225 m^3 and 187 m^3 fiducial volumes were determined. Two different PMTs were investigated, the 27.94 cm (11 inch) low background PMT from Electron Tubes Limited (ETL) and the 25.4 cm (10 inch) low background PMT from Hamamatsu. The backgrounds from both PMTs were estimated using both the single exponential distribution (Low) as well as the shallower double exponential distribution (High). The results are shown in Table 7.

Table 7

Total estimated background levels for two different fiducial volumes and two different PMTs for a 5 year run time including the 82% livetime. For each PMT, the backgrounds are estimated assuming both the single exponential function (denoted by Low) as well as the double exponential distribution (denoted by High).

Fiducial Volume (m ³)	Total Background (27.94 cm ETL)		Total Background (25.4 cm Hama.)	
	Low	High	Low	High
225	3200	11130	2600	8130
187	1555	6640	1295	5140

Five years of electron scattering events were simulated in the entire 1000 m³ WATCHMAN fiducial volume. Spatial cuts were then used to remove events that reconstructed outside the 225 m³ and 187 m³ fiducial volumes. The < 65 photoelectrons, > 20 triggered PMTs, and > 20 log likelihood cuts were also applied. The various background estimates in Table 7 were then incorporated into the signal and the signal significances were determined. A calibration source was assumed to be present and thus the y -intercept method described in Section 6.1.1 was used. The process was repeated four times and the average significances for each of the 8 estimates were determined. The results are shown in Table 8 and each are assumed to have an uncertainty of about 1σ .

Table 8

Average antineutrino-electron scattering signal significances for various fiducial volume sizes and PMT types for a 5 year acquisition time. As in Table 7, each PMT was given a low and high background estimate.

Fiducial Volume (m ³)	Significance (σ) (27.94 cm ETL)		Significance (σ) (25.4 cm Hama.)	
	Low	High	Low	High
225	3.8	2.6	4.6	3.1
187	4.5	2.8	5.0	2.9

From the table, 5σ directionality may be possible using a 225 m^3 fiducial volume and the 25.4 cm low background Hamamatsu PMTs (assuming the low estimate). It also may be possible using a 187 m^3 fiducial volume with either the 27.94 cm low background ETL PMTs or the 25.4 cm low background Hamamatsu PMTs (both assuming the low estimates). If the high estimates are assumed, directionality may still be possible with a 3σ significance. In every case, the acquisition time must be at least 5 years. It is evident that the backgrounds due to the PMT gamma rays are not negligible as was assumed earlier. They in fact make a significant contribution to the background rate, so much so that directionality will only be possible if the fiducial volume is greatly decreased, smaller PMTs with high glass purity are used, and the acquisition time is increased.

Although directionality may still be feasible in WATCHMAN with the PMT gamma rays included, the effects of water-borne radon still need to be considered. As discussed in Section 4, the decay of ^{238}U in the PMT glass will ultimately result in the production of ^{222}Rn . The radon can migrate out of the glass and into the fiducial volume where the eventual decay of ^{214}Bi will mimic the antineutrino-electron scattering signal. Radon from the air surrounding the detector can also contaminate the water. Finally, the water itself can possess trace amounts of ^{238}U .

The SNO detector is a 1 kiloton water Cherenkov neutrino detector filled with heavy water (D_2O), located in Ontario, Canada [46]. The collaboration has reported a uranium concentration of $3 \times 10^{-14} \text{ gU/gD}_2\text{O}$ in the inner detector volume [46]. The half-life of ^{222}Rn is much shorter than the half-life of ^{238}U , therefore the ^{222}Rn can be assumed to be in secular equilibrium with ^{238}U . In secular equilibrium, the number of ^{222}Rn atoms will be related to the number of ^{238}U atoms by

$$N_{\text{Rn}} = \frac{\lambda_{\text{U}}}{\lambda_{\text{Rn}}} \cdot N_{\text{U}}, \quad (23)$$

where N_{Rn} is the number of radon atoms, N_{U} is the number of uranium atoms, λ_{U} is the decay constant of uranium (s^{-1}), and λ_{Rn} is the decay constant of radon (s^{-1}). Carrying out the calculation for the 1000 m^3 WATCHMAN fiducial volume, a total of about 188,000 ^{222}Rn atoms will exist in the water. This amounts to an activity of about 0.4 Bq. If a detection efficiency of 15 - 20% is assumed, a total of about 6000 events will occur within the fiducial volume per day. This rate as it stands significantly exceeds the acceptable limit for directional sensitivity in WATCHMAN (both 3σ and 5σ). However, it is unclear whether the water purity at SNO is a legitimate representation of the water purity at WATCHMAN. This will depend on water recirculation methods, the level of detector cleanliness upheld during construction, and the radon levels in the mine air. It should also be noted that the SNO detector employs an acrylic barrier between the fiducial volume and the buffer region [47]. While this barrier will prevent some of the radon from the PMTs to migrate into the water, the acrylic barrier itself will possess trace amounts of ^{238}U and thus contribute to the radon background. As discussed in Section 1.4, the current WATCHMAN design does not include a barrier between the fiducial volume and buffer region. It is not yet clear how much of an effect this will make. Ultimately, the water-borne radon levels need to be investigated further before claims of antineutrino directionality in WATCHMAN can be made confidently.

7. SUMMARY AND CONCLUSIONS

Remote monitoring systems have significantly strengthened the safeguards regime, providing the IAEA with the ability to maintain continuity of knowledge between inspection periods with physical measurements. These systems also eliminate the need for a physical inspector to be present at the facility and can be used to perform measurements that inspectors would otherwise not be allowed to perform. Finally, these systems can continuously store data, thus allowing for constant online monitoring of nuclear facilities. Among these systems, antineutrino detectors have demonstrated their potential as a safeguards tool with the ability to remotely measure the operational status of a reactor, the power output, and the isotopic evolution of the fissile fuel in the core. The WATCHMAN detector aims to be the first to demonstrate the potential of kiloton scale Gd-doped water Cherenkov antineutrino detectors in mid-to far-field (> 10 km) remote nuclear reactor monitoring.

This research specifically investigated the use of antineutrino-electron elastic scattering to determine the direction of the incident reactor antineutrino flux. The expected antineutrino-electron scattering rate as well as background rates were estimated in the WATCHMAN detector and were simulated in the GEANT4 simulation package, RMSim. The directions of the Cherenkov cones for each event were reconstructed with the BONSAI fitter software. The initial results concluded that reactor antineutrino directionality is feasible over the timescale of one year with a confidence of about 5σ without the use of a directional calibration source. If a directional calibration source is available, such as an electron accelerator, the one-year confidence can be increased to about 5.6σ . In the safeguards regime, a 5σ confidence may be unnecessarily high and a 3σ confidence may be deemed appropriate. The

3σ confidence level can be reached with and without a calibration source in about 4 and 4.5 months, respectively. These results are firmly based off the following assumptions: a continuously operated reactor at full power (3.758 GW(th)) with no shutdown periods, constant fission fractions that of a typical mid-cycle PWR, and background rates due to the PMT gammas and radon contamination are much lower than the cosmogenic radionuclide backgrounds. Lastly, the results assumed a known reactor location and did not investigate the situation in which the reactor location is unknown and must be searched for.

Preliminary studies suggest that both the radon contamination and PMT gammas may in fact be significant contributors to background in the WATCHMAN detector. Antineutrino directionality may still be feasible in WATCHMAN if the PMT gammas are included, though it will require a much smaller fiducial volume (225 m³ instead of 1000 m³), smaller PMTs with high glass purity, and at least 5 years of data. While it may be possible, antineutrino directionality will serve no practical purpose in nuclear reactor safeguards at this timescale because timeliness detection goals for nuclear material range from 1 to 12 months. Even still, the backgrounds due to the radon contamination in the water are likely to exceed the acceptable limit for directional sensitivity in WATCHMAN. To recover directionality (in 5 years), the current radon levels would need to be reduced by roughly two or three orders of magnitude. The SNO detector was constructed over 15 years ago and thus some progress may have been made in radon reduction since then. If so, the required reduction in radon may be achievable and directionality may be possible. But if not, WATCHMAN will prove to be a great testbed for new methods to reduce radon contamination. Ultimately, the results of this research demonstrate the potential of remote reactor antineutrino directionality in water Cherenkov detectors and thus further research in this subject is warranted.

In future work, the simulations should be generalized such that different sized detectors, standoff distances, detector depths, and reactor power levels could be analyzed. The reactor location should also be changed in order to develop a model to test directionality in different directions. This would include developing techniques to iterate through various directions and applying a penalty for each tested direction. Once this is completed, the detector would then be able to truly search for clandestine reactors surrounding the detector. Physical processes that affect the antineutrino signal such as refueling times and fuel burnup should also be incorporated into the results. Moreover, the event reconstruction software is believed to utilize the dark noise in the PMTs and should therefore be incorporated into the simulations. Finally, a more systematic approach should be taken into the placement of energy thresholds. Radon backgrounds typically produce lower energy events while cosmogenic radionuclides produce high energy events, and thus there might be some advantages to alter the $16 \rightarrow 65$ photoelectron window used in this thesis.

Ultimately, a more thorough investigation into the expected backgrounds needs to be carried out, with an emphasis placed on radon contamination and PMT activity as a function of PMT choice, fiducialization, and water purity. This investigation could also include possible methods to further reduce backgrounds, such as employing a more sophisticated vetoing system or more overburden to reduce the cosmogenic radionuclide backgrounds, using a barrier in the buffer region to contain the PMT-based backgrounds, or developing a more advanced water recirculation system to reduce radon contamination.

REFERENCES

- [1] The International Atomic Energy Agency, “INFCIRC/26: The Agency’s Safeguards”, International Atomic Energy Agency Publications, 1961.
<http://www.iaea.org/Publications/Documents/Infcircs/Others/infcirc26.pdf>.
Accessed November 2014.
- [2] The International Atomic Energy Agency, “INFCIRC/66: The Agency’s Safeguards (1965)”, International Atomic Energy Agency Publications, 1965.
<http://www.iaea.org/Publications/Documents/Infcircs/Others/infcirc66.pdf>.
Accessed November 2014.
- [3] The International Atomic Energy Agency, “INFCIRC/140: Treaty on the Non-Proliferation of Nuclear Weapons”, International Atomic Energy Agency Publications, 1970.
<http://www.iaea.org/Publications/Documents/Infcircs/Others/infcirc140.pdf>.
Accessed November 2014.
- [4] The International Atomic Energy Agency, “INFCIRC/153: The Structure and Content of Agreements between the Agency and States Required in Connection with the Treaty on the Non-Proliferation of Nuclear Weapons”, International Atomic Energy Agency Publications, 1970.
<http://www.iaea.org/Publications/Documents/Infcircs/Others/infcirc153.pdf>.
Accessed November 2014.
- [5] The International Atomic Energy Agency, “INFCIRC/540: Model Protocol Additional to the Agreement(s) between State(s) and the International Atomic Energy Agency for the Application of Safeguards”, International Atomic

- Energy Agency Publications, 1997.
<http://www.iaea.org/Publications/Documents/Infcircs/1997/infcirc540c.pdf>.
Accessed November 2014.
- [6] The International Atomic Energy Agency, “The Evolution of IAEA Safeguards”, International Nuclear Verification Series No. 2, International Atomic Energy Agency Publications, 1998.
http://www-pub.iaea.org/MTCD/Publications/PDF/NVS2_web.pdf. Accessed December 2014.
- [7] The International Atomic Energy Agency, “Implementation of the NPT Safeguards Agreement and Relevant Provisions of Security Council Resolutions in the Islamic Republic of Iran”, The International Atomic Energy Agency Board Report, IAEA and Iran Reports, International Atomic Energy Agency Publications, 2014. <https://www.iaea.org/newscenter/focus/iran>. Accessed December 2014.
- [8] Nuclear Threat Initiative, “Iran Turn Away IAEA Inspectors”, 2007.
<http://www.nti.org/gsn/article/iran-turns-away-iaea-inspectors/>. Accessed December 2014.
- [9] S. Chirayath, “Safeguards for an Enrichment Plant”, Texas A&M University Presentation, College Station, Texas, 2014.
- [10] United Nations Office for Disarmament Affairs, “Treaty on the Non-Proliferation of Nuclear Weapons: Status of the Treaty”.
<http://disarmament.un.org/treaties/t/npt>. Accessed November 2014.
- [11] The International Atomic Energy Agency, “The IAEA Annual Report”, International Atomic Energy Agency Publications, 2013.

- https://www.iaea.org/sites/default/files/anrep2013_full_0.pdf. Accessed December 2014.
- [12] S. Chirayath, “Nuclear Material Accountancy”, Texas A&M University Presentation, College Station, Texas, 2014.
- [13] The International Atomic Energy Agency, “New Safeguards Equipment Systems: Teaming IAEA Inspectors with Technology”, International Atomic Energy Agency Publications, 2002.
www.iaea.org/Publications/Booklets/TeamingInspectors/teaming_inspectors.pdf. Accessed December 2014.
- [14] A. Bernstein, N.S. Bowden, A. Misner, T. Palmer, “Monitoring the Thermal Power of Nuclear Reactors with a Prototype Cubic Meter Antineutrino Detector”, arXiv:0804.4723 (2008).
- [15] O.M. Boyarkin, “Advanced Particle Physics Volume II: The Standard Model and Beyond”, CRC Press, Boca Raton, 2011.
- [16] A. Bernstein, et. al., “The Physics and Nuclear Nonproliferation Goals of WATCHMAN: A WATER CHerenkov Monitor for ANTineutrinos”, arXiv:1502.01132 (2015).
- [17] C. Giunti, C.W. Kim, “Fundamentals of Neutrino Physics and Astrophysics”, Oxford University, New York, 2007.
- [18] N.S. Bowden, et. al., “Observation of the Isotopic Evolution of Pressurized Water Reactor Fuel Using an Antineutrino Detector”, arXiv:0808.0698v2 (2008).
- [19] N.S. Bowden, et. al., “Experimental Results from an Antineutrino Detector for Cooperative Monitoring of Nuclear Reactors”, Nuclear Instruments and

- Methods in Physics Research A 572 (2006) 985-998.
- [20] A. Bernstein, et. al., “Nuclear Security Applications of Antineutrino Detectors: Current Capabilities and Future Prospects”, arXiv:0908.4338 (2009).
- [21] K. Eguchi, et. al., “First Results from KamLAND: Evidence for Reactor Antineutrino Disappearance”, Phys. Rev. Lett. 90 (2003) 021802.
- [22] M. Apollonio, et. al., “Determination of Neutrino Incoming Direction in the CHOOZ Experiment and its Application to Supernova Explosion Location by Scintillator Detectors”, Physical Review D 61 (1999) 012001.
- [23] J. Hosaka, et. al., “Solar Neutrino Measurements in Super-Kamiokande-I”, arXiv:0508053v2 (2005).
- [24] Y. Koshio, “Solar Results from Super-Kamiokande”, Talk given at the XXVI International Conference on Neutrino and Astrophysics, Boston, Massachusetts, 2014.
- [25] P. Huber, “On the Determination of Antineutrino Spectra from Nuclear Reactors”, arXiv:1106.0687v4 (2012).
- [26] P. Vogel, J. Engel, “Neutrino Electromagnetic Form Factors”, Physical Review D 39 (1988) 3378.
- [27] G. Zacek, et al., “Neutrino-oscillation Experiments at the Gosgen Nuclear Power Reactor”, Physical Review D 34 (1986) 2621.
- [28] R.F. Mozely, “The Politics and Technology of Nuclear Proliferation”, University of Washington, Seattle, 1998.
- [29] M. Toups, et. al., “Precision $\bar{\nu}_e$ -electron Scattering Measurements with IsoDAR to Search for New Physics”, arXiv:1307.5081v2 (2013).

- [30] A. Bungau, et. al., “Proposal for an Electron Antineutrino Disappearance Search Using High-Rate ^8Li Production and Decay”, *Phys. Rev. Lett.* 109 (2012) 141802.
- [31] D. Griffiths, “Introduction to Elementary Particles”, 2nd edition, KGaA, Weinheim, 2008.
- [32] G.F. Knoll, “Radiation Detection and Measurement”, 4th edition, John Wiley & Sons, New Jersey, 2010.
- [33] Korean Atomic Energy Research Institute, “Table of Nuclides”, 2000.
<http://atom.kaeri.re.kr/>. Accessed January 2015.
- [34] Super Kamiokande Home Page, Kamioka Observatory, ICRR, University of Tokyo, Japan, 2013. <http://www-sk.icrr.u-tokyo.ac.jp/sk/index-e.html>. Accessed January 2015.
- [35] M. Wilking, “A New Method for Event Reconstruction in Large Cherenkov Detectors”, Talk given at the New Directions in Neutrino Physics Workshop, Aspen Center for Physics, Colorado, 2013.
<https://indico.cern.ch/event/224351/contribution/8/material/slides/0.pdf>. Accessed January 2015.
- [36] FLUKA Home Page. <http://www.fluka.org/fluka.php>. Accessed January 2015.
- [37] S.W. Li, J.F. Beacom, “First Calculation of Cosmic-Ray Muon Spallation Backgrounds for MeV Astrophysical Neutrino Signals in Super-Kamiokande”, *arXiv:1402.4687v3* (2014).
- [38] S. Abe, et al., “Measurement of the ^8B Solar Neutrino Flux with the KamLAND Liquid Scintillator Detector”, *Physical Review C* 84 (2011) 035804.

- [39] D. Reyna, “A Simple Parameterization of the Cosmic-Ray Muon Momentum Spectra at the Surface as a Function of Zenith Angle”, arXiv:0604145v2 (2006).
- [40] W.M. Stacey, “Nuclear Reactor Physics”, 2nd edition, KGaA, Weinheim, 2007.
- [41] ROOT Home Page. <https://root.cern.ch/drupal/>. Accessed January 2015.
- [42] M. Toups., M. Shaevitz. Personal Communication. 2014.
- [43] GEANT4 Home Page. <http://GEANT4.cern.ch/>. Accessed January 2015.
- [44] M. Smy, “Low Energy Event Reconstruction and Selection in Super-Kamiokande-III”, Proceedings of the 30th International Cosmic Ray Conference, Vol. 5 (HE part 2), Mexico City, Mexico, pp. 1279-1282, 2008.
- [45] L. Lyons, “Discovering the Significance of 5σ ”, arXiv:1310.1284v1 (2013).
- [46] I. Blevis, et. al., “Measurement of ^{222}Rn Dissolved in Water at the Sudbury Neutrino Observatory”, arXiv:0305022v2 (2003).
- [47] N.A. Jelley, et. al., “The Sudbury Neutrino Observatory”, Nuclear Instruments and Methods in Physics Research A 449 (2000) 172-207.

APPENDIX A

EXPECTED EVENTS CALCULATION IN ROOT

This code is used to calculate the expected number of electron scattering events in a water Cherenkov detector and was written in the form of a ROOT script, which, if ROOT is installed and sourced on the current machine, can be executed by entering:

```
$ root filename.C
```

in the terminal (in the same directory as the script).

```
{
////////////////////////////////////////////////////////////////////////////////////////////////////////////////////////////////
//                                     //
//           Expected Events Generator           //
//   D. Hellfeld (created 28 September 2014)   //
//                                     //
////////////////////////////////////////////////////////////////////////////////////////////////////////////////////////////////

// oOoOooOOOoOoOooOOOoOoOooOOOOoOooOOOOoOooOOO //

// _____
// Set up the welcome screen
// _____

cout << "\n~-----";
cout << "\nWelcome to the expected scattering event generator!";
cout << "\n~-----";

cout << "\n~-----";
cout << "\nThis code will calculate the number of antineutrino scattering expected
events in the WATCHMAN detector";
cout << "\n~-----\n";

// _____
// Calculate the fissions per second based off reactor power output
// _____

double thermalpower;
cout << "\n\nPlease enter the thermal power output of the reactor of interest (
in GW): ";
```

```

cin >> thermalpower;

string yesorno;
cout << "\n\nI will assume a fission energy of 200 MeV per fission. Do you want
to change this?\nEnter 'Yes' or 'No': ";
cin >> yesorno;

double energyperffission;

if (yesorno == "Yes" || yesorno == "yes" || yesorno == "Y" || yesorno == "y"){

    cout << "\n\nOK... Enter what you would like to use for the energy released
per fission (in MeV): ";
    cin >> energyperffission;
}

else if (yesorno == "No" || yesorno == "no" || yesorno == "N" || yesorno == "n"
){

    energyperffission = 200.0;

}

else {

    cout << "\n-----\n\n";
    cout << "That input is not recognized. Please try again.\n";
    cout << "\n-----\n\n";

    string name = ".q";
    gROOT->ProcessLine(name.c_str());

}

double fissionspersecond = (thermalpower * pow(10,9)) * (6.2415 * pow(10,12)) /
energyperffission;
//
// GW    -> J/S      (1 GW = 1e9 J/s)
// J/S   -> MeV/s    (1 J = 6.2415e12 MeV)
// MeV/s -> fissions/s (1 fission = energyperffission MeV)
//

// -----
// Calculate the number of electrons in the detector
// -----

double detectorsize;
cout << "\n\nPlease enter the size of the water detector (in kilotons): ";
cin >> detectorsize;

double numelectrons = (detectorsize * pow(10,9)) * (6.02 * pow(10,23)) * (10) /
(18);
//
// kton    -> g      (1 kton = 1e9 g)
// g       -> mol     (18 g = 1 mol)
// mol     -> molecules (1 mol = 6.02e23 molecules)
// molecules -> electrons (1 molecule = 10 electrons)
//

// -----
// Set isotopics
// -----

```

```

double U235;
double U238;
double Pu239;
double Pu241;

cout << "\n\nWould you like to use the default isotopics (49.6% U-235, 8.7% U
-238, 35.1% Pu-239, and 6.6% Pu-241)?\nEnter 'Yes' or 'No': ";
string yesorno2;
cin >> yesorno2;

if (yesorno2 == "Yes" || yesorno2 == "yes" || yesorno2 == "y" || yesorno2 == "Y
"){
    U235 = 0.496;
    U238 = 0.087;
    Pu239 = 0.351;
    Pu241 = 0.066;
}

else if (yesorno2 == "No" || yesorno2 == "no" || yesorno2 == "n" || yesorno2 ==
"N"){

    int condition;

    do {
        cout << "\nPlease enter the fractional isotopic concentrations for the
fissioning in the reactor (U-235, Pu-239, Pu-241, U-238):\n";
        cout << "\nU-235: ";
        cin >> U235;
        cout << "\nPu-239: ";
        cin >> Pu239;
        cout << "\nU-238: ";
        cin >> U238;
        cout << "\nPu-241: ";
        cin >> Pu241;

        if (U235+Pu239+Pu241+U238 > 1){
            cout << "\nOops, those concentrations do not add up to 1... Try
again.\n\n";
            condition = 1;
        }

        else {
            condition = 0;
        }

    } while (condition);

}

else {

    cout << "\n-----\n\n";
    cout << "That input is not recognized. Please try again.\n";
    cout << "\n-----\n\n";

    string name = ".q";
    gROOT->ProcessLine(name.c_str());

}

// -----
// Calculate antineutrino energy spectrum, total cross section, and interaction
cross section density

```

```

// -----
TF1 *energyspectrum = new TF1("energyspectrum", "((((([0]*exp(0.870+(-0.160*x)
+(-0.0910*x*x)))+([1]*exp(0.896+(-0.239*x)+(-0.0981*x*x)))+([2]*exp
(0.793+(-0.080*x)+(-0.1085*x*x)))+([3]*exp(0.976+(-0.162*x)+(-0.0790*x*x))))
)))",0,8);

energyspectrum->SetParameter(0,U235);
energyspectrum->SetParameter(1,Pu239);
energyspectrum->SetParameter(2,Pu241);
energyspectrum->SetParameter(3,U238);

TF1 *totalcrosssection = new TF1("totalcrosssection", "39*pow(10,-46)*2*0.511*x
",0,8);

double detectordist;
cout << "\n\nPlease enter the distance from the reactor to the detector (in km):
";
cin >> detectordist;

TF1 * interactionratedensity = new TF1("interactionratedensity", "(
energyspectrum*[0]*[1]*totalcrosssection)/(4*[2]*([3]*[3]))",0,8);

interactionratedensity->SetParameter(0, fissionspersecond);
interactionratedensity->SetParameter(1, numelectrons);
interactionratedensity->SetParameter(2, 3.14159);
interactionratedensity->SetParameter(3, detectordist*100000);

// -----
// Integrate interaction rate density to get interaction rate
// -----

double interactionrate = interactionratedensity->Integral(0,8);

//cout << "\nInteraction Rate = " << interactionrate << " scatters per second\n
";

// -----
// Calculate the number of interactions for some period of time
// -----

double time;
cout << "\n\nPlease enter the acquisition time (in days): ";
cin >> time;

double expectedevents = interactionrate * time * 3600 * 24;

// -----
// Include muon livetime?
// -----

string yesorno3;
cout << "\n\nWould you like to include muon veto livetime in this calculation?\n
nEnter 'Yes' or 'No': ";
cin >> yesorno3;

if (yesorno3 == "Yes" || yesorno3 == "yes" || yesorno3 == "y" || yesorno3 == "Y
") {

double livetime;

```

```

    cout << "\n\nPlease enter the livetime as a fraction (for example 0.89): ";
    cin >> livetime;

    cout << "\n-----\n";
    cout << "\nOK! The total number of scatters expected over " << time << "
        days = " << expectedevents * livetime << "\n";
    cout << "\n-----\n";
}

else if (yesorno3 == "No" || yesorno3 == "no" || yesorno3 == "n" || yesorno3 ==
"N"){

    cout << "\n-----\n";
    cout << "\nOK! The total number of scatters expected over " << time << "
        days = " << expectedevents << "\n";
    cout << "\n-----\n";
}

else {

    cout << "\n-----\n\n";
    cout << "That input is not recognized. Please try again.\n";
    cout << "\n-----\n\n";

    string name = ".q";
    gROOT->ProcessLine(name.c_str());

}

// -----
// Exit screen
// -----

    cout << "\n\n-----\n\n";
    cout << "Enter .q to exit\n";
    cout << "\n-----\n\n";

// -----
}

```

APPENDIX B

EVENT GENERATOR IN ROOT

This code demonstrates how the event generator essentially works using the ROOT libraries. It can generate events based of two different antineutrino reactor spectra, the IsoDAR spectrum, a histogram in a provided text file, or a monoenergetic spectrum. This code uses the expected events root script above and assumes it will be called ExpectedEvents.C. Both files must be placed in the same directory.

The code will produce relevant plots and output information to a file that the user specifies. The output will include the antineutrino energies in MeV, the scattered electron energies in MeV, and the scattering angles in radians.

```
{
////////////////////////////////////////////////////////////////////////////////////////////////////////////////////////////////
//
//  ElectronAntineutrino-Electron Scattering Generator
//          D. Hellfeld (created 31 July 2014)
//
////////////////////////////////////////////////////////////////////////////////////////////////////////////////////////////////

// oOoOooOOOOoOOooOOOooOOOOOOOoOOooOOoOOooOO //

// _____
// Set up the welcome screen
// _____

int calculator;
double events;
double threshold;
string filename2;

cout << "\n-----\n";
cout << "Welcome to the Antineutrino Electron Scattering Generator!\n";
cout << "-----\n";

// Ask to run expected event calculator
cout << "\nEnter (1) to if you already know how many events you want to run\n
or (2) if you would like to run the expected event calculator: ";
cin >> calculator;

if (calculator == 1){
```



```

        cout << "\nPlease enter the number of events you want to run: ";
        cin >> events;
    }

    else if (calculator == 2){
        string name = ".x ExpectedEvents.C";
        gROOT->ProcessLine(name.c_str());

        cout << "Ok, we will run " << int(expectedevents) << " events\n";
        events = int(expectedevents);
    }

    else {
        cout << "\n-----\n\n";
        cout << "That input is not recognized. Please try again.\n";
        cout << "\n-----\n\n";

        string name = ".q";
        gROOT->ProcessLine(name.c_str());
    }

    // Input scattered electron energy threshold
    cout << "\nPlease enter the scattered electron energy threshold in MeV: ";
    cin >> threshold;

    // Ask for the filename in which to write data to
    cout << "\nPlease enter the name of the output file (including the extension)
        you would like to write the generated data to: ";
    cin >> filename2;

// -----

// -----
// Sample an energy from either a histogram, three isotope nuclear reactor spectrum
// with user defined
// isotopics, four isotope nuclear reactor spectrum, or from ISODAR spectrum
// -----

    gRandom->SetSeed(0);

    // Which spectrum do you want to use?
    cout << "\n-----\n";
    cout << "\nFrom where are your incident antineutrino energies being sampled
        from?\n\nEnter:\n(1) for a text file (histogram)\n(2) for a three
        isotope nuclear reactor spectrum (from 2 to 8 MeV)\n(3) for a four
        isotope nuclear reactor spectrum (from 0 to 8 MeV)\n(4) for ISODAR
        spectrum\n(5) for monoenergetic\n\nEnter: ";
    int input;
    cin >> input;

    if (input == 1){

        // From histogram (read in a text file, ** List needs to have the total
        // interaction cross section folded into it already **)

        cout << "\nPlease enter the text file name including the extension: ";
        string filename;
        cin >> filename;
        cout << "\nPlease enter the lower limit of the distribution: ";
        double lowerlimit;
        cin >> lowerlimit;
    }

```

```

cout << "\nPlease enter the upper limit of the distribution: ";
double upperlimit;
cin >> upperlimit;
cout << "\nPlease enter the number of bins you would like to use for the
    histogram: ";
int bins;
cin >> bins;

cout << "\n-----\n\n";
cout << events << " events coming up!" << "\n\n";

// Read in data and create histogram
TH1F * energydist1 = new TH1F("Nuebar Energy Dist", "Nuebar Energy
    Distribution",bins, lowerlimit, upperlimit);
FILE * file1 = fopen(filename.c_str(),"r");
float energies;
    while (!feof(file1)){
        fscanf(file1,"%f",&energies);
        energydist1->Fill(energies);
    }
fclose(file1);

// Sample from histogram and store in vector
vector<double> EnuSample;
for (int w = 0; w < events; w++){EnuSample.push_back(energydist1->GetRandom
    ());}
}

else if (input == 2){

// From an analytic function (summing nuebar energy distributions from U235,
    Pu239, and Pu241 wih respective concentrations).
// Taken from "On the Determination of Anti-Neutrino Spectra From Nuclear
    Reactors" (Huber).
// arXiv:1106.0687v4
//
// This spectrum only has 3 isotopes

// Set isotopics

double U235concentration;
double Pu239concentration;
double Pu241concentration;

    cout << "\nWould you like to use the default isotopics (90% U235, 5% Pu239
        , and 5% Pu241)?\n\nEnter Yes or No: ";
string yesorno;
cin >> yesorno;

if (yesorno == "Yes" || yesorno == "yes" || yesorno == "y" || yesorno == "Y
    ") {
    U235concentration = 0.90;
    Pu239concentration = 0.05;
    Pu241concentration = 0.05;
}

else if (yesorno == "No" || yesorno == "no" || yesorno == "n" || yesorno ==
    "N"){

    int condition;

```

```

do {
    cout << "\nPlease enter the isotopic concentrations for the
            fissioning in the reactor (U-235, Pu-239, Pu-241):\n\
            nU-235: ";
    cin >> U235concentration;
    cout << "\nPu-239: ";
    cin >> Pu239concentration;
    cout << "\nPu-241: ";
    cin >> Pu241concentration;

    if (U235concentration+Pu239concentration+
        Pu241concentration > 1){
        cout << "\nOops, those concentrations do not
                add up... Try again.\n\n";
        condition = 1;
    }

    else {
        condition = 0;
    }

    } while (condition);
}

cout << "\n~~~~~\n\n";
cout << events << " events coming up!" << "\n\n";

// Generate distribution curve (with total interaction cross section folded in)
TF1 * energydist2 = new TF1("energydist2", "((([0]*(exp(((4.367*(pow(x,0))) +
(-4.577*(pow(x,1))) + (2.100*(pow(x,2))) + ((-5.294*pow(10,-1))*(pow(x,3)))
+ ((6.186*pow(10,-2))*(pow(x,4))) + ((-2.777*pow(10,-3))*(pow(x,5)))))))
+([1]*(exp(((4.757*(pow(x,0))) + (-5.392*(pow(x,1))) + (2.563*(pow(x,2))) +
((-6.596*pow(10,-1))*(pow(x,3))) + ((7.820*pow(10,-2))*(pow(x,4))) +
((-3.536*pow(10,-3))*(pow(x,5))))))) + ([2]*(exp(((2.990*(pow(x,0))) +
(-2.882*(pow(x,1))) + (1.278*(pow(x,2))) + ((-3.343*pow(10,-1))*(pow(x,3)))
+ ((3.905*pow(10,-2))*(pow(x,4))) + ((-1.754*pow(10,-3))*(pow(x,5)))))))
*((39*pow(10,-46))*2*0.511*x)",2,8);

energydist2->SetParameter(0,U235concentration);
energydist2->SetParameter(1,Pu239concentration);
energydist2->SetParameter(2,Pu241concentration);

// Sample from function and store in vector
vector<double> EnuSample;
for (int q = 0; q < events; q++){EnuSample.push_back(energydist2->GetRandom())
;};
}

else if (input == 3){

// From an analytic function (summing nuebar energy distributions from U235,
U238, Pu239, and Pu241 wih respective concentrations).
// Taken from "Energy Spectra of Reactor Neutrinos at KamLAND" (Murayama and
Pierce).
// arXiv:hep-ph/0012075v3
//
// The spectrum has 4 isotopes

// Set isotopics

```

```

double U235concentration;
double Pu239concentration;
    double Pu241concentration;
    double U238concentration;

cout << "\nWould you like to use the default isotopics (49.6% U235, 8.7%
    U238, 35.1% Pu239, and 6.6% Pu241)?\n\nEnter Yes or No: ";
string yesorno;
cin >> yesorno;

if (yesorno == "Yes" || yesorno == "yes" || yesorno == "y" || yesorno == "Y
    ") {
    U235concentration = 0.496;
    U238concentration = 0.087;
    Pu239concentration = 0.351;
    Pu241concentration = 0.066;
}

else if (yesorno == "No" || yesorno == "no" || yesorno == "n" || yesorno ==
    "N") {

    int condition;

    do {
        cout << "\nPlease enter the isotopic concentrations for the
            fissioning in the reactor (U-235, Pu-239, Pu-241, U-238)
            :\n\nU-235: ";
        cin >> U235concentration;
        cout << "\nPu-239: ";
        cin >> Pu239concentration;
        cout << "\nU-238: ";
        cin >> U238concentration;
        cout << "\nPu-241: ";
        cin >> Pu241concentration;

        if (U235concentration+Pu239concentration+Pu241concentration+
            U238concentration > 1) {
            cout << "\nOops, those concentrations do not add up
                ... Try again.\n\n";
            condition = 1;
        }

        else {
            condition = 0;
        }

    } while (condition);

}

cout << "\n-----\n\n";
cout << events << " events coming up!" << "\n\n";

// Generate distribution curve (does this really go to 0 MeV? I am not sure)
TF1 * energydist3 = new TF1("energydist3", "((((([0]*exp(0.870+(-0.160*x)
    +(-0.0910*x*x)))+([1]*exp(0.896+(-0.239*x)+(-0.0981*x*x)))+([2]*exp
    (0.793+(-0.080*x)+(-0.1085*x*x)))+([3]*exp(0.976+(-0.162*x)+(-0.0790*x*x
    ))))))*(39*pow(10,-46))*2*0.511*x)", 0,8);

energydist3->SetParameter(0,U235concentration);
energydist3->SetParameter(1,Pu239concentration);

```



```

else if (input == 5){
    // Monoenergetic spectrum

    cout << "\nPlease enter the antineutrino energy in MeV: ";
    double nuenergy;
    cin >> nuenergy;

    cout << "\n-----\n\n";
    cout << events << " events coming up!" << "\n\n";

    // Make a vector filled with the specified energy
    vector<double> EnuSample;
    for (int xx = 0; xx < events; xx++){EnuSample.push_back(nuenergy);}
}
// -----

// -----
// Take sampled energy, calculate total cross section vs. Te curve, and then sample
// a Te
// -----

// Equation comes from Eq.(5.25) in "Neutrino Physics and Astrophysics" (Giunti
// and Kim).

double Me = 0.511;
double sigma0 = 88.06*(pow(10,-46));
double g1 = 0.23;
double g2 = 0.73;

vector<double> EelectronSample;

double counter = 0;
int i = 0;
vector<double> triggerednuenergies;

while (i < events){
    // Maximum scattered energy
    double TeMax = ((2*(pow(EnuSample[i],2)))/(Me+(2*EnuSample[i])));

    // total cross section
    //TF1 *sigma_Te = new TF1("sigma_Te", "([2]/[1])*(((pow([3],2))+
    pow([4],2))*x) - (((pow([3],2)/[0]) + (([3]*[4]*[1])/(2*[0])))*
    pow(x,2) + ((pow([3],2)*pow(x,3))/(3*pow([0],2))))", 0, TeMax);

    // Differential cross section
    TF1 *sigma_Te = new TF1("sigma_Te", "([2]/[1])*(pow([3],2)+(pow([4],2)*pow
    (1-(x/[0]),2)) - (([3]*[4]*[1]*x)/pow([0],2)))", 0, TeMax);

    sigma_Te->SetParameter(0, EnuSample[i]);
    sigma_Te->SetParameter(1, Me);
    sigma_Te->SetParameter(2, sigma0);
    sigma_Te->SetParameter(3, g1);
    sigma_Te->SetParameter(4, g2);

    double sample_energy = sigma_Te->GetRandom();

    if (sample_energy > threshold){
        EelectronSample.push_back(sample_energy);
        triggerednuenergies.push_back(EnuSample[i]);
    }
}

```

```

    }

    i++;
    counter++;

    // For purposes of the output display (percentage of job done)
    int p = events/10;
    if (int(counter)%p == 0){cout << "[" << (counter/events)*100 << "%]"
        << endl;}

    }

    // How many events passed the threshold?
    int triggeredevents = triggerednuenergies.size();
    cout << "\nOnly " << triggeredevents << " events triggered!\n";

// -----

// -----
// Take sampled Te's and calculate theta's
// -----

// Equation taken Eq.(5.27) in "Neutrino Physics and Astrophysics" (Giunti and
Kim).

vector<double> calculated_angle;

for (int i = 0; i < triggeredevents; i++){
    calculated_angle.push_back(acos(((sqrt(((EelectronSample[i]*(pow((Me+
    triggerednuenergies[i],2)))/(2*Me*(pow(triggerednuenergies[i]
    ],2)))+(pow(triggerednuenergies[i],2)*EelectronSample[i])))))));
}

// -----

// -----
// Print out histograms
// -----

if (input == 1){

    // Draw the original nuebar energy distribution
    TCanvas * c1 = new TCanvas("c1", "Nuebar Energy Distribution", 800,
        600);
    energydist1->Draw();
    energydist1->SetTitle("Nuebar Energy Distribution (that interact)");
    energydist1->GetXaxis()->SetTitle("Nuebar energy (MeV)");

    // Draw the sampled nuebar energy distribution
    TCanvas * c2 = new TCanvas("c2", "Sampled Nuebar Energy Distribution
        ", 800, 600);
    TH1F *samplednuenergies = new TH1F("Sampled Nuebar Energy", "Sampled
        Nuebar Energy Distribution",60, lowerbound-2, upperbound+2);
    for (i = 0; i < triggeredevents; i++){samplednuenergies->Fill(
        triggerednuenergies[i]);}

    samplednuenergies->Draw();
    samplednuenergies->SetTitle("Sampled Nuebar Energy Distribution");
    samplednuenergies->GetXaxis()->SetTitle("Nuebar energy (MeV)");
}

```

```

else if (input == 2) {
    // Draw the original nuebar energy distribution
    TCanvas * c1 = new TCanvas("c1", "Nuebar Energy Distribution", 800,
        600);
    energydist2->Draw();
    energydist2->SetTitle("Nuebar Energy Distribution (that interact)");
    energydist2->GetXaxis()->SetTitle("Nuebar energy (MeV)");

    // Draw the sampled nuebar energy distribution
    TCanvas * c2 = new TCanvas("c2", "Sampled Nuebar Energy Distribution
        ", 800, 600);
    TH1F *samplednuenergies = new TH1F("Sampled Nuebar Energy", "Sampled
        Nuebar Energy Distribution",60, 0, 10);
    for (i = 0; i < triggeredevents; i++){samplednuenergies->Fill(
        triggerednuenergies[i]);}

    samplednuenergies->Draw();
    samplednuenergies->SetTitle("Sampled Nuebar Energy Distribution");
    samplednuenergies->GetXaxis()->SetTitle("Nuebar energy (MeV)");
}

else if (input == 3) {
    // Draw the original nuebar energy distribution
    TCanvas * c1 = new TCanvas("c1", "Nuebar Energy Distribution", 800,
        600);
    energydist3->Draw();
    energydist3->SetTitle("Nuebar Energy Distribution (that interact)");
    energydist3->GetXaxis()->SetTitle("Nuebar energy (MeV)");

    // Draw the sampled nuebar energy distribution
    TCanvas * c2 = new TCanvas("c2", "Sampled Nuebar Energy Distribution
        ", 800, 600);
    TH1F *samplednuenergies = new TH1F("Sampled Nuebar Energy", "Sampled
        Nuebar Energy Distribution",60, 0, 10);
    for (i = 0; i < triggeredevents; i++){samplednuenergies->Fill(
        triggerednuenergies[i]);}

    samplednuenergies->Draw();
    samplednuenergies->SetTitle("Sampled Nuebar Energy Distribution");
    samplednuenergies->GetXaxis()->SetTitle("Nuebar energy (MeV)");
}

else if (input == 4) {
    // Draw the original nuebar energy distribution
    TCanvas * c1 = new TCanvas("c1", "Nuebar Energy Distribution", 800,
        600);
    energydist4->Draw();
    energydist4->SetTitle("Nuebar Energy Distribution (that interact)");
    energydist4->GetXaxis()->SetTitle("Nuebar energy (MeV)");

    // Draw the sampled nuebar energy distribution
    TCanvas * c2 = new TCanvas("c2", "Sampled Nuebar Energy Distribution
        ", 800, 600);
    TH1F *samplednuenergies = new TH1F("Sampled Nuebar Energy", "Sampled
        Nuebar Energy Distribution",60, lowerbound-2, upperbound+2);
    for (i = 0; i < triggeredevents; i++){samplednuenergies->Fill(
        triggerednuenergies[i]);}

    samplednuenergies->Draw();
    samplednuenergies->SetTitle("Sampled Nuebar Energy Distribution");
    samplednuenergies->GetXaxis()->SetTitle("Nuebar energy (MeV)");
}

```



```

}

else if (input == 5) {

    // Draw the original nuebar energy distribution
    TCanvas * c1 = new TCanvas("c1", "Nuebar Energy Distribution", 800,
        600);
    TH1F *monoenergy = new TH1F("Sampled Nuebar Energy", "Sampled Nuebar
        Energy Distribution",60, 0, nuenergy+(nuenergy/2));
    for (i = 0; i < triggeredevents; i++){monoenergy->Fill(nuenergy);}
    monoenergy->Draw();
    monoenergy->SetTitle("Nuebar Energy Distribution");
    monoenergy->GetXaxis()->SetTitle("Nuebar energy (MeV)");

}

// Draw scattered electron energy distribution

TCanvas * c3 = new TCanvas("c3", "Scattered Electron Energy", 800, 600);

double upperbound2 = 10;
if (input == 5){upperbound2 = nuenergy;}

TH1F *scatteredenergies = new TH1F("Scattered Electron Energy", "Scattered
    Electron Energy Distribution",60, 0, upperbound2);

for (i = 0; i < triggeredevents; i++){scatteredenergies->Fill(
    ElectronSample[i]);}

scatteredenergies->Draw();
scatteredenergies->GetXaxis()->SetTitle("Scattered electron energy (MeV)");

// Draw cosine of the scattering angle distribution

TCanvas * c4 = new TCanvas("c4", "Cosine Scattering Angle", 800, 600);
TH1F *scatteringangles = new TH1F("Cosine Scattering Angle", "Cosine
    Scattering Angle Distribution",60, 0, 1);

for (i = 0; i < triggeredevents; i++){scatteringangles->Fill(cos(
    calculated_angle[i]));}

scatteringangles->Draw();
scatteringangles->GetXaxis()->SetTitle("cos(#theta)");

// -----

// -----
// Print out plots in png format
// -----

cout << "\n-----\n\n";
cout << "Saving plots to /path/to/currentdirectory/Plots...\n\n";

c1->Print("Plots/NuebarEnergyDistribution(ThatScatter).png");
if (input != 5){c2->Print("Plots/SampledNuebarEnergyDistribution.png");}
c3->Print("Plots/ScatteredElectronEnergyDistribution.png");
c4->Print("Plots/CosineScatteringAngleDistribution.png");

// -----

```

```

// -----
// Print data to a file set by the user
// -----

    cout << "\n-----\n";
    cout << "\nWriting generated output to " << filename2 << "... " << endl;

// Set up output file
ofstream myfile(filename2.c_str());
myfile << "-----\n\n";
myfile << "Antineutrino energy spectrum sampled from ";
if (input == 1){myfile << filename << ".\n\n";}
else if (input == 2){myfile << "a nuclear reactor spectrum with
    concentrations\nof U-235 = " << U235concentration << ", Pu-239 = " <<
    Pu239concentration << ", and Pu-241 = " << Pu241concentration << ".\n\n
    ";}
else if (input == 3){myfile << "a nuclear reactor spectrum with
    concentrations\nof U-235 = " << U235concentration << ", U-238 = " <<
    U238concentration << ", Pu-239 = " << Pu239concentration << " and Pu-241
    = " << Pu241concentration << ".\n\n";}
else if (input == 4) {myfile << "ISODAR spectrum.\n\n";}
else if (input == 5) {myfile << "monoenergetic antineutrinos with energy = "
    << nuenergy << "\n\n";}
myfile << "Scattered electron energy threshold set to " << threshold << "
    MeV.\n\n";
myfile << events << " total events.\n";
myfile << triggeredevents << " triggered events.\n";
myfile << (triggeredevents/events)*100 << "% scattered electron energy threshold
    trigger efficiency.\n\n";
myfile << "-----\n\n";
myfile << "Antineutrino Energies (MeV)" << "\t" << "Scattered electron
    energies (MeV)" << "\t" << "Scattering Angle (rad)\n\n";
myfile.setf(ios::fixed);
myfile.precision(10);

// Dump data
for (int i = 0; i < triggeredevents; i++){
    myfile << triggerednuenergies[i] << "\t\t" << EelectronSample[i]
        << "\t\t\t" << calculated_angle[i] << endl;
}

    myfile.close();

cout << "... Done!\n";
cout << "\n-----\n\n";
}

```

APPENDIX C

SIGNAL/BACKGROUND FITTING IN ROOT

This code demonstrates how the signal and background fitting were accomplished with and without a calibration source. It also demonstrates how the plots were constructed. To run, the script needs to be in the same directory as the ROOT file outputted by BONSAI.

```
{  
  
////////////////////////////////////  
////  
////      Signal Analysis for Directionality in WATCHMAN      ////  
////              D. Hellfeld (December 2014)              ////  
////      //////////////////////////////////////  
  
gRandom->SetSeed(0);  
  
// =====  
// Read in data from file  
// =====  
  
TFile f("filename.root");  
  
TTree * dst = (TTree*) f.Get("dst");  
  
Int_t n = dst->Draw("theta", "photoelectrons <65");  
Double_t * costheta_ = dst->GetV1();  
  
// =====  
  
// =====  
// Create histogram of data then add in background events  
// =====  
  
TH1F * cosplot = new TH1F("cosplot", "Reconstructed Cos(#theta) with Background  
  (One Year)", 80, -1.0, 1.0);  
  
for(int q = 0; q < n; q++){  
  cosplot->Fill(costheta_[q]);  
}  
  
TCanvas * c10 = new TCanvas("c10", "Reconstruction", 800, 600);  
cosplot->Draw();  
  
double time = 365;
```

```

double bins = 80;
double totalbackground = 3530*(time/365);
double backgroundperbin = totalbackground/bins;
double bkgrnderrorperbin = sqrt(backgroundperbin);

TH1F * blah20 = new TH1F("blah20","blah20",80,-1.0,1.0);
TF1 * blah3 = new TF1("blah3", "50",-1.0,1.0);

TRandom3 rr;
rr->SetSeed(0);

double __bkgrndsample = rr.Gaus(totalbackground,sqrt(totalbackground));
double __bkgrndsampleperbin=__bkgrndsample/bins;

for (int i = 0; i < __bkgrndsample; i++){
    double w = blah3->GetRandom();
    blah20->Fill(w);
}

blah20->SetLineColor(kRed);
blah20->Draw("same");
cosplot->Add(blah20);

gStyle->SetOptStat(0);
cosplot->Draw("same");
cosplot->GetYaxis()->SetRangeUser(0,backgroundperbin*2.5);
cosplot->GetXaxis()->SetTitle("Cos(#theta)");
cosplot->GetXaxis()->SetTitleOffset(1.2);
cosplot->GetYaxis()->SetTitle("Counts");
cosplot->GetYaxis()->SetTitleOffset(1.2);

// =====
// =====
// Fit the signal and background, add them to plot
// =====

TF1 * signalfit = new TF1("signalfit", "[0]+[1]*exp([2]*x)", -1.0,1.0);
TF1 * backgroundfit = new TF1("backgroundfit", "[0]", -1.0,0.0);

cout << "-----\n";
cout << "Signal + background fitting parameter table\n";
cout << "-----\n\n";

TFitResultPtr q_ = cosplot->Fit("signalfit","SR0");

cout << "\n-----\n\n";

cout << "-----\n";
cout << "Background fitting parameter table\n";
cout << "-----\n\n";

TFitResultPtr p_ = blah20->Fit("backgroundfit","SR+0"); // "0" means dont bkgrd
plot fit right now

cout << "\n-----\n\n";

```

```

TF1 * bkggroundline = new TF1(" bkggroundline", "[0]", -1.0,1.0);
TF1 * sigandbakline = new TF1(" sigandbakline", "[0]+[1]*exp([2]*x)", -1.0,1.0);
TF1 * sigOnly = new TF1(" sigandbakline", "[0]*exp([1]*x)", -1.0,1.0);

bkggroundline->SetParameter(0, backgroundfit->GetParameter(0));
bkggroundline->SetParError (0, backgroundfit->GetParError (0));

sigandbakline->SetParameter(0, signalfit->GetParameter(0));
sigandbakline->SetParameter(1, signalfit->GetParameter(1));
sigandbakline->SetParameter(2, signalfit->GetParameter(2));
sigandbakline->SetParError (0, signalfit->GetParError (0));
sigandbakline->SetParError (1, signalfit->GetParError (1));
sigandbakline->SetParError (2, signalfit->GetParError (2));

sigOnly->SetParameter(0, signalfit->GetParameter(1));
sigOnly->SetParError (0, signalfit->GetParError (1));
sigOnly->SetParameter(1, signalfit->GetParameter(2));
sigOnly->SetParError (1, signalfit->GetParError (2));

bkggroundline->SetLineColor(kBlack);
bkggroundline->SetLineWidth(1);
bkggroundline->SetLineStyle(2);
bkggroundline->Draw(" same");
sigandbakline->SetLineColor(kGreen);
sigandbakline->Draw(" same");
sigOnly->SetLineColor(kGreen);
sigOnly->SetLineStyle(2);
sigOnly->Draw(" same");

TLegend* leg = new TLegend(0.5, 0.3, 0.75, 0.5);
leg->AddEntry(cosplot," Signal plus background", "l");
leg->AddEntry(blah20," Background", "l");
leg->AddEntry(sigandbakline, "Signal plus background fit", "l");
leg->AddEntry(bkggroundline, "Background fit", "l");
leg->AddEntry(sigOnly, "Signal fit", "l");
leg->Draw(" same");

// =====

// =====
// Calculate statistical significance
// =====

// -----
// Loop and find integral bound that results in largest sigma
// -----

TGraph * conf = new TGraph();
int qq = 0;

for (double vv = 0.0; vv < 0.99; vv += 0.01){

double lowerbound = 0.0 + vv;
double upperbound = 1.0;

double SigIntegral = sigandbakline->Integral(lowerbound, upperbound);
double SigIntegralError = sigandbakline->IntegralError(lowerbound, upperbound
, sigandbakline->GetParameters(), q->GetCovarianceMatrix()->
GetMatrixArray());

double BkgrdIntegral = bkggroundline->Integral(lowerbound, upperbound);

```

```

double BkgrdIntegralError = bkgroundline->IntegralError(lowerbound,
    upperbound, bkgroundline->GetParameters(), p->GetCovarianceMatrix()->
    GetMatrixArray());

double SigMinusBkgrdIntegral = SigIntegral - BkgrdIntegral;
double SigMinusBkgrdIntegralError = sqrt(pow(SigIntegralError,2) + pow(
    BkgrdIntegralError,2));

// Add signal error and background error in quadrature, divide siganl by
    this
double confidence = SigMinusBkgrdIntegral/(sqrt(pow(BkgrdIntegralError,2)+
    pow(SigMinusBkgrdIntegralError,2)));

conf->SetPoint(qq, lowerbound, confidence);
qq++;
}

TCanvas * c11 = new TCanvas("c11", "blah1", 800, 0, 800, 600);
conf->Draw("AL*");
conf->SetTitle("Sigma vs. Intregal Bound");
conf->GetXaxis()->SetTitle("Left integral bound (cos(#theta))");

int n_ = conf->GetN();
double * y_ = conf->GetY();
double * x_ = conf->GetX();
int locmax = TMath::LocMax(n_, y_);
int locmin = TMath::LocMin(n_, y_);
double max = x_[locmax];
double min = x_[locmin];

conf->GetXaxis()->SetRangeUser(0,1);
conf->GetYaxis()->SetRangeUser(conf->Eval(min)-1, conf->Eval(max)+1);

TLine * maxline_x = new TLine(max, conf->Eval(min)-1, max, conf->Eval(max));
maxline_x->SetLineColor(kBlue);
maxline_x->SetLineStyle(2);
maxline_x->Draw("same");
TLine * maxline_y = new TLine(0, conf->Eval(max), max, conf->Eval(max));
maxline_y->SetLineColor(kBlue);
maxline_y->SetLineStyle(2);
maxline_y->Draw("same");

// - - - - -

cout << "_____ \n";
cout << "Confidence analysis \n";
cout << "_____ \n \n";

double SigIntegral = signalfit->Integral(max, upperbound);
double SigIntegralError = signalfit->IntegralError(max, upperbound, q->
    GetParams(), q->GetCovarianceMatrix()->GetMatrixArray());

double BkgrdIntegral = bkgroundline->Integral(max, upperbound);
double BkgrdIntegralError = bkgroundline->IntegralError(max, upperbound, p->
    GetParams(), p->GetCovarianceMatrix()->GetMatrixArray());

double SigMinusBkgrdIntegral = SigIntegral - BkgrdIntegral;
double SigMinusBkgrdIntegralError = sqrt(pow(SigIntegralError,2) + pow(
    BkgrdIntegralError,2));

double confidence = SigMinusBkgrdIntegral/(sqrt(pow(BkgrdIntegralError,2)+pow(
    SigMinusBkgrdIntegralError,2)));

```

```

cout << "Maximum confidence in signal (from " << max << " to " << upperbound <<
" ) = " << confidence << " sigma\n\n";

cout << "Area under signal (from " << max << " to " << upperbound << ") =
" << SigMinusBkgrdIntegral << "\n\n";
cout << "Error in signal area (from " << max << " to " << upperbound << ") =
" << SigMinusBkgrdIntegralError << "\n\n";
cout << "Area under background (from " << max << " to " << upperbound << ") =
" << BkgrdIntegral << "\n\n";
cout << "Error in background area (from " << max << " to " << upperbound << ") =
" << BkgrdIntegralError << "\n\n";

cout << "-----\n\n";
// -----

cout << "-----\n";
cout << "Exponential slope fixed fit\n";
cout << "-----\n\n";

TH1F * cosplot_ = new TH1F("cosplot_", "Reconstructed Cos(#theta) with
Background (One Year)", 80, -2.0, 0.0);

for(int q = 0; q < n; q++){
    cosplot_>Fill(costheta_[q] - 1);
}

cosplot_>Add(blah20);

TCanvas * c111 = new TCanvas("c111", "blah11", 800, 0, 800, 600);
cosplot_>Draw();
cosplot_>GetYaxis()->SetRangeUser(0, backgroundperbin*2.5);

TF1 * expofit = new TF1("expofit", "[0]+[1]*exp(3.4*x)", -2.0,0.0);
TFitResultPtr k_ = cosplot_>Fit("expofit","SR");

backgroundline->Draw("same");

double confidence_2 = expofit->GetParameter(1)/expofit->GetParError(1);

cout << "\n\nY intercept = " << expofit->GetParameter(1) << " +/- " << expofit->
GetParError(1) << "\n";
cout << "This results in a confidence of " << confidence_2 << " sigma\n\n";

cout << "-----\n";

// -----

cout << "\n\n% difference between method 1 and method 2 = " << fabs(((confidence
-confidence_2)/confidence_2)*100) << "%\n\n";

// =====
}

```

APPENDIX D

MULTIPLE YEAR FITTING IN ROOT

This code demonstrates how the signal and background fitting were accomplished with and without a calibration source for the 64 one-year data sets. To run, the script needs to be in the same directory as the ROOT file outputted by BONSAI.

```
{  
// =====  
// Read in file , pull out data (one year at a time), calculate significances  
// =====  
  
TFile f("filename.root");  
  
TTree * dst = (TTree*) f.Get("dst");  
  
Int_t n = dst->Draw("theta:evtN", "photoelectrons <65");  
  
Double_t * costheta_ = dst->GetV1();  
Double_t * evtN_ = dst->GetV2();  
  
vector<double> confidences;  
vector<double> confidences_2;  
vector<double> pcentDiffs;  
vector<double> bestcosthetacuts;  
  
int lower = 0;  
int upper = 1517;  
  
for (int r = 0; r < 64; r++){  
  
    TH1F * cosplot = new TH1F("cosplot", "cosplot", 80, -1, 1);  
    TH1F * cosplot_ = new TH1F("cosplot_", "Reconstructed Cos(#theta) with  
        Background (One Year)", 80, -2.0, 0.0);  
  
    for(int q = 0; q < n; q++){  
  
        if (evtN_[q] > lower && evtN_[q] < upper){  
            cosplot->Fill(costheta_[q]);  
            cosplot_->Fill(costheta_[q] - 1);  
        }  
    }  
  
    // =====  
    // Add in background  
    // =====  

```



```

double time = 365;
double bins = 80;
double totalbackground = 3530*(time/365);
double backgroundperbin = totalbackground/bins;
double bkgrnderrorperbin = sqrt(backgroundperbin);

TH1F * blah20 = new TH1F("blah20","blah20",80,-1.0,1.0);
TF1 * blah3 = new TF1("blah3", "50",-1.0,1.0);

TRandom3 rr;
rr->SetSeed(0);

double __bkgrndsample = rr.Gaus(totalbackground, sqrt(totalbackground));
double __bkgrndsampleperbin=__bkgrndsample/bins;

for (int i = 0; i < __bkgrndsample; i++){
    double w = blah3->GetRandom();
    blah20->Fill(w);
}

cosplot ->Add(blah20);
cosplot_ ->Add(blah20);

// -----

// -----
// Fit the signal and background, add them to plot
// -----

TF1 * signalfit      = new TF1("signalfit",      "[0]+[1]*exp([2]*x)",
    -1.0,1.0);
TF1 * backgroundfit  = new TF1("backgroundfit",  "[0]",
    -1.0,0.0);

cout << "-----\n";
cout << "Signal + Background fitting parameter table\n";
cout << "-----\n\n";

TFitResultPtr q_ = cosplot->Fit("signalfit", "SR0");

cout << "\n-----\n\n";

cout << "-----\n";
cout << "Background fitting parameter table\n";
cout << "-----\n\n";

TFitResultPtr p_ = cosplot->Fit("backgroundfit", "SR+0"); // "0" means dont bkgrd
    plot fit right now

cout << "\n-----\n\n";

TF1 * bkggroundline  = new TF1("bkggroundline",  "[0]",
    -1.0,1.0);
TF1 * sigandbakline  = new TF1("sigandbakline",  "[0]+[1]*exp([2]*x)",
    -1.0,1.0);
TF1 * sigOnly        = new TF1("sigandbakline",  "[0]*exp([1]*x)",
    -1.0,1.0);

bkggroundline->SetParameter(0, backgroundfit->GetParameter(0));

```

```

backgroundline->SetParError (0, backgroundfit->GetParError (0));

sigandbakline->SetParameter(0, signalfit->GetParameter(0));
sigandbakline->SetParameter(1, signalfit->GetParameter(1));
sigandbakline->SetParameter(2, signalfit->GetParameter(2));
sigandbakline->SetParError (0, signalfit->GetParError (0));
sigandbakline->SetParError (1, signalfit->GetParError (1));
sigandbakline->SetParError (2, signalfit->GetParError (2));

sigOnly->SetParameter(0, signalfit->GetParameter(1));
sigOnly->SetParameter(1, signalfit->GetParameter(2));
sigOnly->SetParError (0, signalfit->GetParError (1));
sigOnly->SetParError (1, signalfit->GetParError (2));

// -----

// -----
// Calculate statistical significance
// -----

// -----
// Loop and find cos(theta) cut that results in largest sigma
// -----
//
// store this value, then later we will calculate the average
// turns out this is 0.74
//

TGraph * conf = new TGraph();
int qq = 0;

for (double vv = 0.0; vv < 0.99; vv += 0.01){

    double lowerbound = 0.0 + vv;
    double upperbound = 1.0;

    double SigIntegral      = sigandbakline->Integral(lowerbound, upperbound);
    double SigIntegralError = sigandbakline->IntegralError(lowerbound,
        upperbound, sigandbakline->GetParameters(), q->GetCovarianceMatrix()->
        GetMatrixArray());

    double BkgrdIntegral      = bkggroundline->Integral(lowerbound, upperbound);
    double BkgrdIntegralError = bkggroundline->IntegralError(lowerbound,
        upperbound, bkggroundline->GetParameters(), p->GetCovarianceMatrix()->
        GetMatrixArray());

    double SigMinusBkgrdIntegral      = SigIntegral - BkgrdIntegral;
    double SigMinusBkgrdIntegralError = sqrt(pow(SigIntegralError,2) + pow(
        BkgrdIntegralError,2));

        // Add signal error and background error in quadrature,
        // divide signal by this
    double confidence = SigMinusBkgrdIntegral/(sqrt(pow(BkgrdIntegralError,2)+
        pow(SigMinusBkgrdIntegralError,2)));

    conf->SetPoint(qq, lowerbound, confidence);
    qq++;
}

int n_      = conf->GetN();
double * y_ = conf->GetY();
double * x_ = conf->GetX();

```

```

int locmax = TMath::LocMax(n_, y_);
int locmin = TMath::LocMin(n_, y_);
double max = x_[locmax];
double min = x_[locmin];

// Store the best cos theta cuts so we can calculate the average later
bestcosthetacuts.push_back(max);

//confidences.push_back(conf->Eval(max));

// -----

// -----
// Use the 0.74 cut to calculate the significance, store this value
// -----

double SigIntegral = sigandbakline->Integral(0.74,1);
double SigIntegralError = sigandbakline->IntegralError(0.74,1,sigandbakline->
  GetParameters(), q->GetCovarianceMatrix()->GetMatrixArray());

double BkgrdIntegral = bkgroundline->Integral(0.74,1);
double BkgrdIntegralError = bkgroundline->IntegralError(0.74,1,bkgroundline->
  GetParameters(), p->GetCovarianceMatrix()->GetMatrixArray());

double SigMinusBkgrdIntegral = SigIntegral - BkgrdIntegral;
double SigMinusBkgrdIntegralError = sqrt(pow(SigIntegralError,2) + pow(
  BkgrdIntegralError,2));

// Add signal error and background error in quadrature, divide signal by this
double confidence = SigMinusBkgrdIntegral/(sqrt(pow(BkgrdIntegralError,2)+pow(
  SigMinusBkgrdIntegralError,2)));

confidences.push_back(confidence);

// -----

// -----
// Fix the exponential slope parameter and recalculate
// -----

cout << "-----\n";
cout << "Exponential slope fixed fit\n";
cout << "-----\n\n";

TF1 * expofit = new TF1(" expofit ", "[0]+[1]*exp(3.4*x)", -2.0,0.0);
TFitResultPtr k_ = cosplot->Fit(" expofit ", "SR0");

double confidence_2 = expofit->GetParameter(1)/expofit->GetParError(1);
confidences_2.push_back(confidence_2);

cout << "\n\nY intercept = " << expofit->GetParameter(1) << " +/- " << expofit->
  GetParError(1) << "\n";
cout << "This results in a confidence of " << confidence_2 << " sigma\n\n";

cout << "-----\n";

// -----

// -----

```

```

// Difference between the two methods
// -----

double pcentDiff = fabs((((confidence-confidence_2)/confidence_2)*100);
pcentDiffs.push_back(pcentDiff);

cout << "\n\n% difference between method 1 and method 2 = " << pcentDiff << "%\n\n";

// -----

// -----

lower += 1517;
upper += 1517;

}

// =====

// =====
// Create histograms
// =====

TH1F * sigmahist = new TH1F("sigmahist", "blah", 16, 6, 14);
TH1F * sigmahist2 = new TH1F("sigmahist2", "blah", 16, 6, 14);
TH1F * pcentDiff_ = new TH1F("pcentDiff_", "blah", 40, 0, 18);

double asdf1[64] = {};
double asdf2[64] = {};

for (int ww = 0; ww < confidences.size(); ww++){

    cout << confidences[ww] << "\t" << confidences_2[ww] << "\t" <<
        pcentDiffs[ww] << "\n";
    sigmahist->Fill(confidences[ww]);
    sigmahist2->Fill(confidences_2[ww]);
    pcentDiff_->Fill(pcentDiffs[ww]);

    asdf1[ww] = confidences[ww];
    asdf2[ww] = confidences_2[ww];
}

sigmahist->Draw();
sigmahist->SetTitle("Sigma of sigmas (1 year) (Original method)");
sigmahist->GetXaxis()->SetTitle("#sigma");
sigmahist->GetYaxis()->SetTitle("Counts");

//TCanvas * c111 = new TCanvas("c111", "blah11", 800, 0, 800, 600);
sigmahist2->Draw("sames");
sigmahist2->SetTitle("Sigma of sigmas (1 year) (Y intercept method)");
sigmahist2->GetXaxis()->SetTitle("#sigma");
sigmahist2->GetYaxis()->SetTitle("Counts");

TLegend* leg = new TLegend(0.5, 0.3, 0.75, 0.5);
leg->AddEntry(sigmahist, "Without Calibration", "f");
leg->AddEntry(sigmahist2, "With Calibration", "f");

```

```

leg->Draw(" same");

TCanvas * c112 = new TCanvas(" c112", " blah12", 800, 0, 800, 600);
pcentDiff->Draw();
pcentDiff->SetTitle("% Diffs from Method 1 and 2");
pcentDiff->GetXaxis()->SetTitle("%");
pcentDiff->GetYaxis()->SetTitle(" Counts");

// =====

// Calculate average best cos(theta) cut
cout << "\n\n";
double thetacutsum = 0;
for (int z = 0; z < bestcosthetacuts.size(); z++){
    cout << bestcosthetacuts[z] << "\n";
    thetacutsum += bestcosthetacuts[z];
}
cout << "\n\nAverage best cos theta cut = " << thetacutsum/(bestcosthetacuts.
size()) << "\n";

}

```